(12) LEVEL II

NW

DNA 4545F

DYNAMIC BEHAVIOR OF AIRCRAFT MATERIALS

Effects Technology, Inc.
5383 Hollister Avenue
Santa Barbara, California 93111

28 February 1978

Final Report for Period 1 February 1977—31 December 1977

CONTRACT No. DNA 001-77-C-0103

THIS WORK SPONSORED BY THE DEFENSE NUCLEAR AGENCY
UNDER RDT&E RMSS CODE B342077464 N99QAXAE50501 H2590D.

Prepared for
Director
DEFENSE NUCLEAR AGENCY
Washington, D. C. 20305

Destroy this report when it is no longer needed. Do not return to sender.

PLEASE NOTIFY THE DEFENSE NUCLEAR AGENCY, ATTN: TISI, WASHINGTON, D.C. 20305, IF YOUR ADDRESS IS INCORRECT, IF YOU WISH TO BE DELETED FROM THE DISTRIBUTION LIST, OR IF THE ADDRESSEE IS NO LONGER EMPLOYED BY YOUR ORGANIZATION.

(18) DNA, SBIE

UNCLASSIFIED

SECURITY CLASSIFICATION OF THIS PAGE *(When Data Entered)*

(19) **REPORT DOCUMENTATION PAGE**

READ INSTRUCTIONS BEFORE COMPLETING FORM

1. REPORT NUMBER: DNA 4545F, AD-E300 446	2. GOVT ACCESSION NO.
3. RECIPIENT'S CATALOG NUMBER	
4. TITLE (and Subtitle): DYNAMIC BEHAVIOR OF AIRCRAFT MATERIALS (6)	5. TYPE OF REPORT & PERIOD COVERED (9): Final Report for Period 1 Feb 77—31 Dec 77
	6. PERFORMING ORG. REPORT NUMBER (14): ETI-CR78-485
7. AUTHOR(s) (10): Frederic A. Bick, Pamela Van Blaricum	8. CONTRACT OR GRANT NUMBER(s) (15): DNA 001-77-C-0103 new
9. PERFORMING ORGANIZATION NAME AND ADDRESS: Effects Technology, Inc., 5383 Hollister Avenue, Santa Barbara, California 93111	10. PROGRAM ELEMENT, PROJECT, TASK AREA & WORK UNIT NUMBERS (16): Subtask N99QAXAE505-01
11. CONTROLLING OFFICE NAME AND ADDRESS (11): Director, Defense Nuclear Agency, Washington, D.C. 20305	12. REPORT DATE: 28 February 1978
	13. NUMBER OF PAGES: 128 (17) L 75
14. MONITORING AGENCY NAME & ADDRESS *(if different from Controlling Office)* (12) 13 p.	15. SECURITY CLASS *(of this report)*: UNCLASSIFIED
	15a. DECLASSIFICATION DOWNGRADING SCHEDULE

16. DISTRIBUTION STATEMENT *(of this Report)*

Approved for public release; distribution unlimited.

17. DISTRIBUTION STATEMENT *(of the abstract entered in Block 20, if different from Report)*

18 SUPPLEMENTARY NOTES

This work sponsored by the Defense Nuclear Agency under RDT&E RMSS Code B342077464 N99QAXAE50501 H2590D.

19 KEY WORDS *(Continue on reverse side if necessary and identify by block number)*

Blast
Overpressure
Composite Materials
Aircraft
Dynamic Testing
Graphite Epoxy
Quartz Polyimide

20 ABSTRACT *(Continue on reverse side if necessary and identify by block number)*

Dynamic, high strain rate loading characterization of two composite materials that are being used today in the design of military and commercial aircraft was accomplished. Of particular concern was the response of such materials to nuclear blast and thermal environments. Primary emphasis is placed on the graphite epoxy designated AS/3501-6, as would be used in body or wing panels. Of secondary emphasis is the quartz polyimide designated F178/581, a radome material. Both materials were tested quasistatically and →

DD FORM 1 JAN 73 1473 EDITION OF 1 NOV 65 IS OBSOLETE

UNCLASSIFIED

SECURITY CLASSIFICATION OF THIS PAGE *(When Data Entered)*

405842

20. ABSTRACT (Continued)

namically (strain rates up to 18 inches/in/sec), and from -65°F to above resin cure temperature (Cure temperatures of 350°F for the graphite epoxy and 475°F for the quartz polyimide). Test results indicated that both materials were stronger under dynamic loads than quasistatic loads. Additionally, at elevated temperatures the responses were dramatically different with the dynamic properties exhibiting little or no degradation due to temperature effects, while quasistatic properties decreased significantly with temperature.

SUMMARY

This report describes the dynamic, high strain rate loading characterization of two composite materials that are being used today in the design of military and commercial aircraft. Of particular concern was the response of such materials to nuclear blast and thermal environments. Primary emphasis is placed on the graphite epoxy designated AS/3501-6,* as would be used in body or wing panels. Of secondary emphasis is the quartz polyimide designated F178/581,** a radome material. Both materials were tested quasistatically and dynamically (strain rates up to 18 inches/inch/sec), and from -65°F to above resin cure temperature [Cure temperatures of 350°F for the graphite epoxy and 475°F for the quartz polyimide].

This program was funded under Defense Nuclear Agency contract DNA001-77-C-0103. The Project Officer during the majority of the work was Major Dave Garrison, now reassigned. The Project Officer for the completion of the work was Captain Mike Rafferty. The period of performance was 15 February 1977 to 31 December 1977.

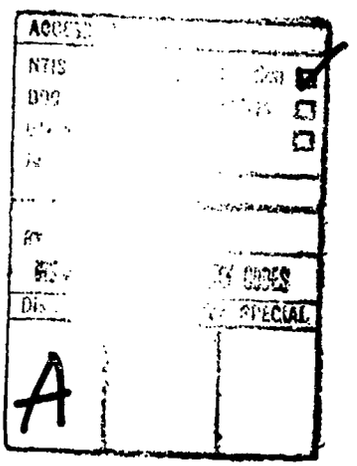

*Provided by Hercules Magnamite

**Provided by Brunswick

PREFACE

The authors thank Major Garrison for his guidance and support during the performance of this contract, and Captain Rafferty for his continuing interest. We also thank AVCO Systems Division and Kaman Avidyne personnel for many interesting and fruitful discussions. Also appreciated are the technical discussions with Boeing Co., Wichita Division and Air Force Weapons Laboratory personnel regarding past correlation studies on aircraft vulnerability.

Although not within the scope of this program, we thank S. C. Chou of Army Materials and Mechanics Research Center for performing high strain rate uniaxial tension and compression tests at Army Materials and Mechanics Research Center facilities. These tests were intended as an additional checkpoint on dynamic properties data.

Finally, special thanks go to Bob Globus of ETI for his many valuable suggestions during the course of the program, and to Jim Aleszka of ETI who carried the main burden for the work in the ETI Materials Testing Laboratory.

CONVERSION FACTORS FOR U.S. CUSTOMARY
TO METRIC (SI) UNITS OF MEASUREMENT

To convert from	To	Multiply by
mils	millimeters	0.0254
inches	centimeters	2.54
feet	meters	0.3048
miles	kilometers	1.6093
square inches	square centimeters	6.4516
square feet	square meters	0.0929
square miles	square meters	2,589,998.0
cubic inches	cubic centimeters	16.38706
cubic feet	cubic meters	0.0283
cubic yards	cubic meters	0.764555
gallons (U.S.)	liters	3.785
gallons (Imperial)	liters	4.542
ounces	grams	28.349
pounds	kilograms	0.454
tons (short)	kilograms	907.185
tons (long)	kilograms	1,016.047
pounds per foot	newtons per meter	14.59390
pounds per square inch	newtons per square centimeter	0.6894757
pounds per cubic inch	kilograms per cubic centimeter	27,679.90
pounds per square foot	newtons per square meter	47.88026
pounds per cubic foot	kilograms per cubic meter	16.0185
inches per second	centimeters per second	2.54
inch-pounds	meter-newtons	0.1129848
inch-kips	meter-kilonewtons	0.0001129848
Fahrenheit degrees	Celsius degrees or Kelvins[a]	5/9
kilotons	terajoules	4.183

[a]To obtain Celsius (C) temperature readings from Fahrenheit (F) readings, use C = (5/9) (F - 32). To obtain Kelvin (K) readings, use K = (5/9) (F - 32) + 273.15.

TABLE OF CONTENTS

LIST OF ILLUSTRATIONS

LIST OF ILLUSTRATIONS

(Continued)

LIST OF ILLUSTRATIONS

(Continued)

LIST OF ILLUSTRATIONS

(Continued)

LIST OF TABLES

LIST OF TABLES

(Continued)

1.0 INTRODUCTION

Composite materials such as graphite epoxies are being used in ever greater quantities on military aircraft. The time is not far off when this use will routinely include primary load carrying structures. A dramatic demonstration of this technology was shown in the November 14, 1977 (p. 21) issue of Aviation Week and Space Technology. The magazine photograph shows a supercritical composite wing made of graphite epoxy for the AV-8B Advanced Harrier V/STOL aircraft. This all composite wing will weigh 20% less than its predecessor and contribute to doubling the range and payload capability of the aircraft. Other aircraft, such as the F-14, 15, 16, 17, 18, A-10 close air support, and others, use composite materials to varying extents. In addition, there are major advanced concept studies, sponsored by organizations such as the Air Force Flight Dynamics Laboratory and NASA, that are investigating the means of using graphite epoxies extensively throughout airplanes. The objective is to design aircraft that explicitly exploit the advantages that composites offer relative to metals. With this increasing use of composite materials comes the need for understanding and characterizing their behavior under a variety of environmental and loading conditions.

This program was concerned with the manner in which properties of composite materials are experimentally obtained, and how they are used to predict the response of such materials in the dynamic nuclear blast and thermal environments. The objectives of this program were:

- Evaluate state of the art analytical and experimental techniques used in hardness assessments, and identify any limitations in performing dynamic hardness assessments.

- Establish the dynamic behavior of a composite material using the dynamic test procedures demonstrated by Effects Technology, Inc. during the "Vulnerability Assessment of Non-metallic Aircraft" Program,

Contract DNA001-76-C-0101.[1]

- Compare the static and dynamic behavior of composites, and identify the impact of using dynamic properties in a hardness evaluation.

Investigations into state of the art capabilities relied exclusively upon work that has been done with metallic structures. While many of the analytic tools available for analyzing or computing structural response contain subroutines or options for treating composite materials, they were developed for treating metals, which are generally considered to be isotropic. While the equations of motion apply universally, the constitutive relations for anisotropic composite materials can require the determination of up to 21 independent elastic constants. Many organizations are working on developing models for composites, and some are in operation. Current capabilities will drive design practices to conservative approaches, simply because the experiments required to determine the appropriate properties have not yet been performed. As a result, correlations are essentially nonexistent, except between different analytic models, or between models and data obtained from structurally simple experiments. Compounding the problem is a lack of community feeling as to what failure criteria are applicable. This is a difficult question, even for metallic structures, so it might be quite some time before the composites community has other than a very conservative approach to this problem.

Experiments were performed with three point bend, shear plug and limited deflection three point bend techniques to arrive at ultimate flexural strength, shear strength and degraded properties. Test temperatures

ranged from -65°F to 425°F for the graphite epoxy, and up to 500°F for the quartz polyimide. In general, dynamic strengths for both materials were greater than static strengths at all temperatures. Furthermore, at elevated temperatures, the graphite epoxy retained near room temperature flexural strength in the dynamic test, while the static flexural strength steadily degraded with increasing temperature. At room temperature, both static and dynamic failure modes were similar, initiating at the outermost fibers oriented parallel to the specimen's longest dimension. At elevated temperatures, the dynamic failure mode remained similar to the room temperature mode. The static test failure location changed from the tensile side of the beam specimen to the compressive side, and was a complex compressive shear buckling mode.

Currently the design community is outracing everyone else in the desire to get composites in the air. The resulting vacuum that has been and is being created leaves substantial room for a variety of studies leading toward a better understanding of how well and why composites work. This program looked into a small part of that total space and provides an indication of trends and where state of the art capabilities and shortcomings lie. It must be emphasized that the test results that will be presented in greater detail are for two particular materials and fabrication processes. Composite materials as a class present a remarkable range of properties and possibilities. The results obtained from any such program as this one depend upon fiber/matrix combinations and fabrication variables such as times at cure temperatures and pressures. The materials used in this program were selected as representative only because of the wide application they are receiving in airplane manufacturing. There are other fiber/matrix combinations in use and it should not be assumed that similar trends will be found. Nevertheless, the evidence indicates that composite materials are strain rate sensitive, both in mechanical properties and failure modes. To effectively use these materials in aerospace structures and systems, new types of tests and analyses need to be employed. It is in that way that more effective designs can be accomplished and greater surety in mission performance achieved.

2.0 AIRCRAFT VULNERABILITY ASSESSMENT STATE OF THE ART

2.1 INTRODUCTION

To arrive at a state of the art assessment it is necessary to identify four elements of the technology base. These are the analytic models, the test techniques, the available data base and correlation studies that have been performed using the other three elements. It was not the intent in this program to survey all structural response models that are used to analyze aircraft. Rather, those techniques that were developed specifically for aircraft vulnerability and hardness (V&H) assessments were examined. The same is true for experimental techniques, data and correlation studies. In general, it will be found that there are a select few techniques that have developed over a period of years that are peculiar to a particular technology area, and this is true for aircraft V&H studies.

The techniques that are needed can best be defined by describing an aircraft loading history such as is shown in Figure 1. If some arbitrary design allowable is chosen, then during takeoff and benign flight the loads can be represented as shown in (1) and (2) in the figure. A nuclear intercept event imposes a short time, dynamic load on the aircraft which potentially causes damage or degradation of load carrying capability. Depending upon the range to burst and yield, the magnitude of response and preconditioning of the material will vary. Specifically, the closer the burst, the greater the thermal pulse, and the closer in time that the air shock arrives at the aircraft in relation to the thermal pulse. This timing can be critical since the temperature of the structure will vary accordingly. Under these conditions the load allowable will be a function of the heating rate, the strain rate and the absolute temperature attained. After the initial response the material will cool and unload. Depending upon conditions, it can return to its original state, or have some degraded load carrying capability.

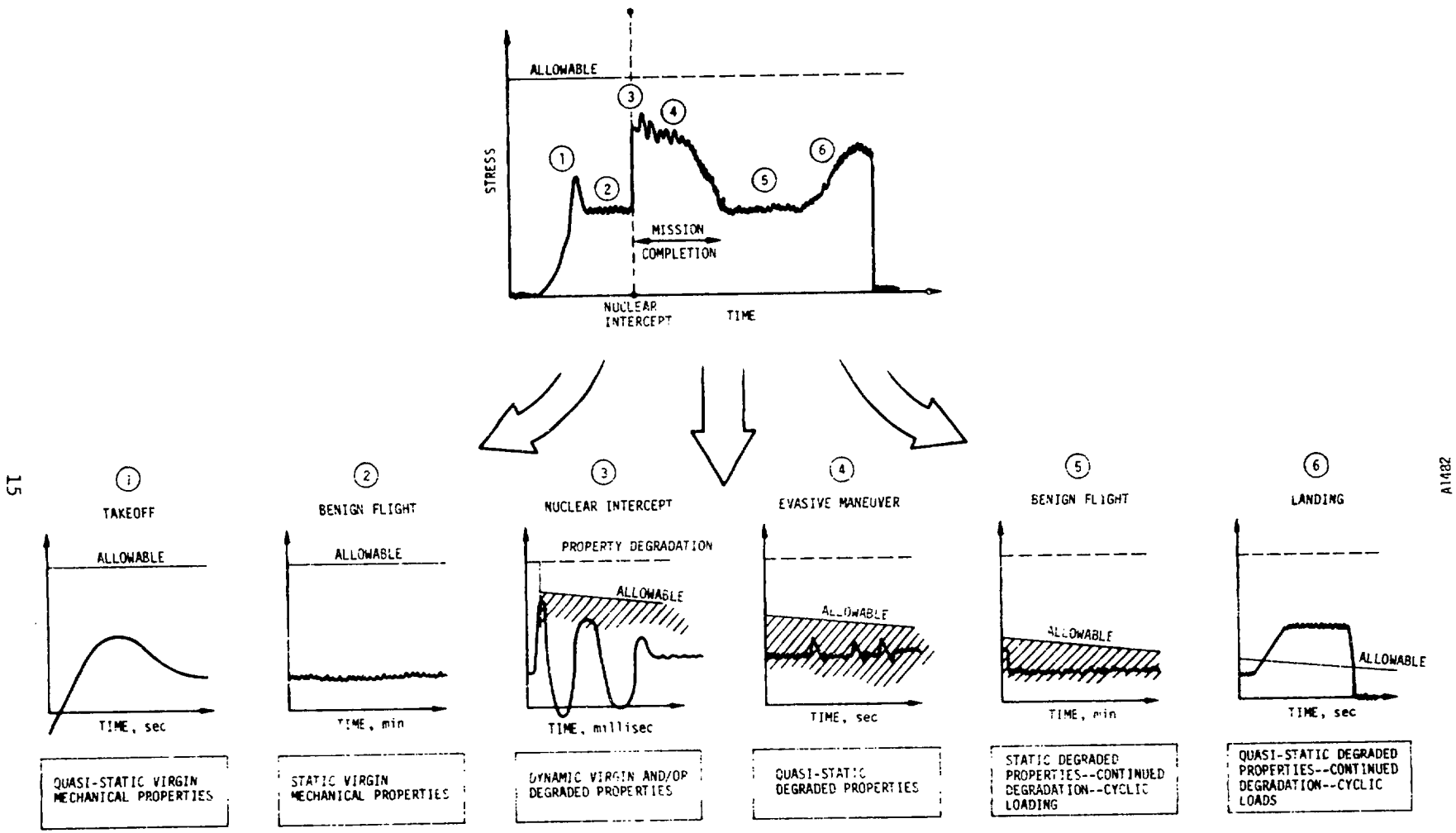

Figure 1. Aircraft Loading History

Fatigue can lead to further degradation as the mission continues. It is possible that at some later time in the flight the degraded load allowable will be exceeded, resulting in aircraft destruction. In fact, one study found that immediate aircraft destruction is an unlikely event for nonnuclear threats.[2] That study looked at the frequency of occurrence of various kill times. The ratio of 2 seconds, 15 seconds, 5 minutes and 30 minutes kills to each other was 1:3:8:15, where the 30 minutes to kill occurs 15 times more frequently than the 2 seconds to kill. This does not include "repair" kills where an aircraft is cannibalized after landing because it has been so severely damaged that in effect it could only survive one last landing.

An examination of Figure 1 reveals that a variety of material properties are required for analyzing the aircraft response and performance. Figure 2 presents this situation in greater detail. The types of test conditions are implied through the top tier of boxes, the types of properties and information desired in the second tier, and expected aircraft performance during and subsequent to an intercept in the third or bottom tier. By examining the mission and system requirements in this way it is possible to identify the types of tests and analyses required to calculate the response of an aircraft to a nuclear intercept. It is in this context that a technology state of the art assessment should be made. This program specifically addressed boxes 3 through 6 through experimental and analytical work, and the implications of having dynamically derived properties rather than statically or quasistatically derived properties.

To address the question of state of the art technology status, it is convenient to start with a testing methodology such as is shown in Figure 3. The important point of this figure is that the starting point for doing a test or analysis is not with indiscriminate use of the technology but with careful consideration of the system and the materials and structures making up the system. Imposed on this are the system

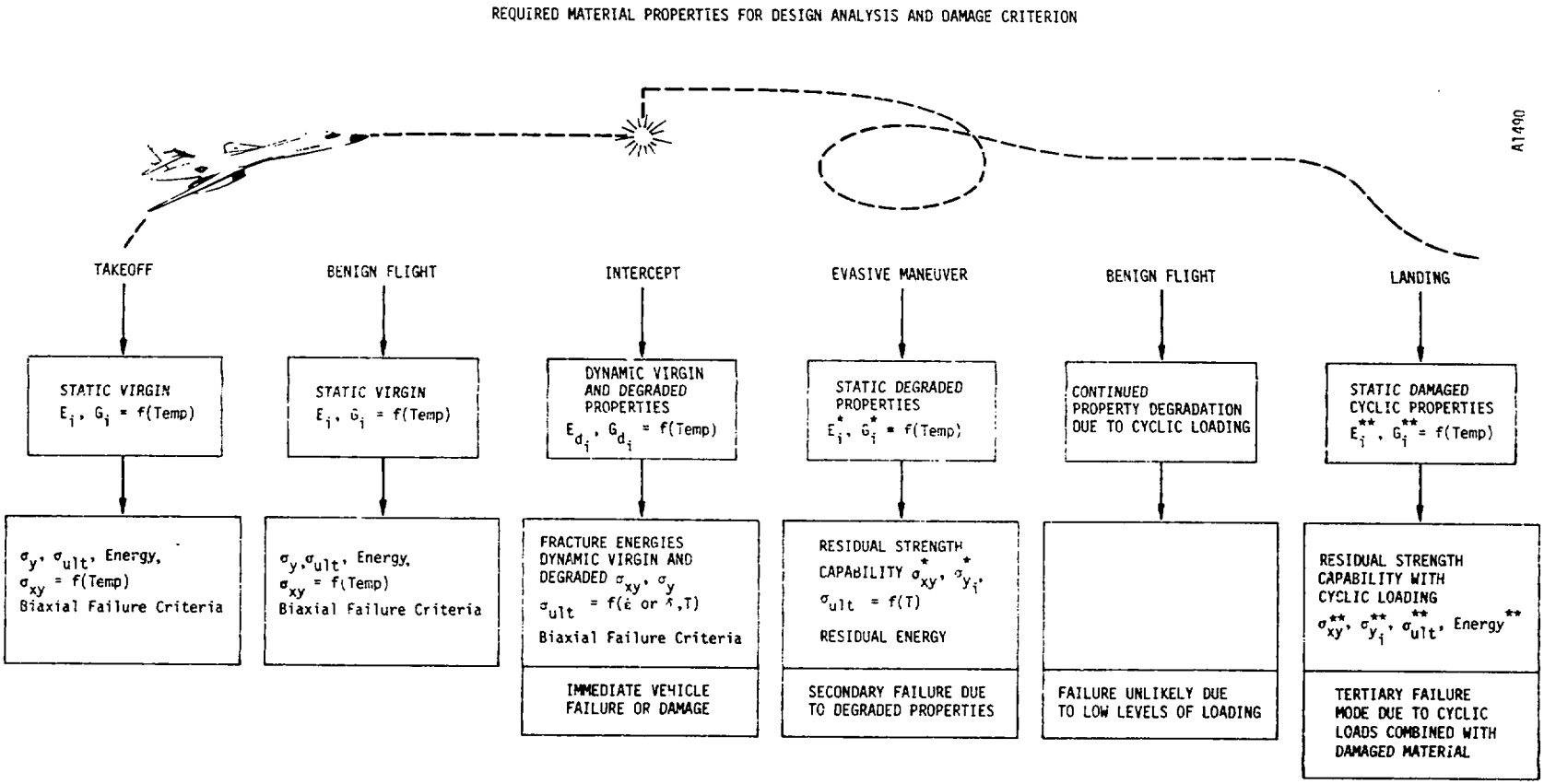

Figure 2. Required Material Properties for Design Analysis and Damage Criterion

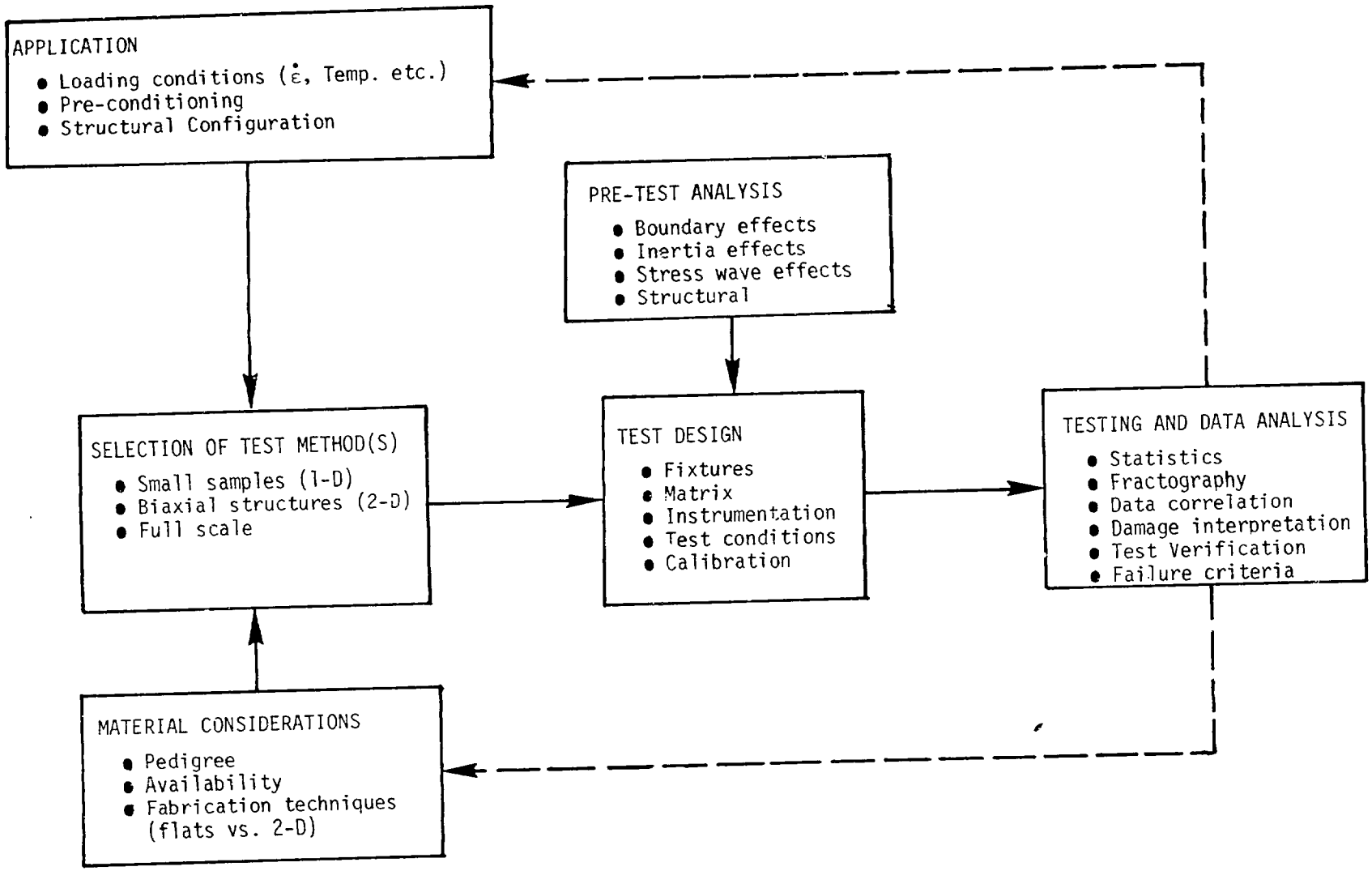

Figure 3. Composite Material Testing Methodology

considerations such as operational requirement(s) of interest. If these items are understood, then the required types of analysis and testing follow readily.

To determine the adequacy of the tools used for analysis and test, or better, for performing hardness assessments, it is necessary to perform correlations between different analytic techniques, analyses and tests, and different test techniques. Figure 4 illustrates this basic approach as it has been applied for overpressure response evaluation on existing aircraft, i.e., metal structures. The remainder of this section will examine two major correlation studies that have been performed and which substantially establish state of the art capabilities. Once this has been done for metal airplanes, the requirements for doing the same with composite structures will be examined and the state of the art capabilities for that class of materials will be outlined. The final part will be an outline of the types of correlations and data that are needed for credible nuclear hardness assessments to be possible for airplanes constructed of composite materials.

2.2 AVAILABLE CORRELATION STUDIES

A comprehensive evaluation of the KC-135A was completed by the Air Force Weapons Laboratory (AFWL) during the early 70's.[3] The primary emphasis was on analyzing the capabilities of the KC-135A when damaged by nuclear blast and thermal environments. Tests were performed on certain critical components to obtain damage thresholds using simulated overpressure and thermal environments. The primary tools used in the study were VIBRA for gust analysis, NOVA for overpressure analysis and TRAP for thermal analysis. These are discussed in Reference 4, and will not be discussed here.

This program arrived at hardness levels for the KC-135A, and an evaluation of its ability to complete a particular mission. The ulti-

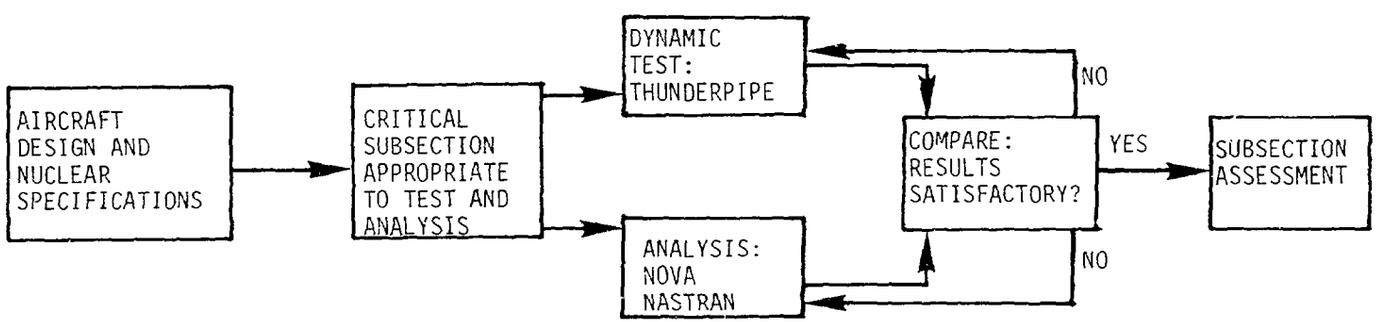

Figure 4. Aircraft Assessment - Metals

mate arbiter, however, appeared to be tests conducted at the DASACON Dahlgren, Virginia, shock tube facility, or rather the interpretation of those test results by Boeing Co., Wichita Division personnel. The problem that ultimately had to be met was that of damage vs. failure prediction. Damaged structures from the air shock tube were inspected by Boeing personnel who made a judgment, based upon experience, as to whether the incurred damage would affect the airplane performance, and if so, how much; specifically, could the tanker still fly and complete its mission.

The study was a very complete and detailed example of how a hardness assessment can be done, and used the start of the art technology then available. Detailed correlations, as is usually meant, did not appear to be performed. The primary purpose was to assess the KC-135A hardness, and that was done. A fair amount of analysis was performed with the purpose of bounding the problem rather than critiquing the models, or test techniques. It was probably the most complete hardness assessment of any aircraft performed to that time.

The second program was reviewed in draft form, so no report number was available. The program was "STRESNO" for "Structural Response to Simulated Nuclear Overpressure" and was performed by Boeing Co., Wichita, Kansas.[5] The program was truly a correlation study, using flat and curved aluminum panels as test pieces. The Thunderpipe Shock Tube at Sandia Laboratories, Albuquerque, New Mexico was the test facility for the experiments. Since overpressure loads were being considered, NOVA-2 was applied as the correlative analytic tool. A variety of gages was used in the experiments to measure temperature, air pressures, strains, displacements and accelerations.

Since the program was looking at a particular test facility and analytic model, and correlations between the two, the results and conclusions are very pertinent to this report. Briefly, some of the major

conclusions were:

- The NOVA-2 version used was not properly designed to analyze curved specimens under shock loadings. (NOVA has been revised to correctly treat this geometry.[6])

- The Sandia shock tube is a useful simulation technique. However, the long strings of primacord used to obtain the desired pulse positive phase duration results in a series of small detonations and produces a pressure pulse that is more ragged than desired.

- The NOVA-2 static analysis agrees with the static tests in strain, but not so well in displacement.

- Plastic response analysis capability varies from test specimen to test specimen.

- NOVA-2 predicted the proper critical free field overpressure for all specimens within 20%.

In examining these results, the following points need to be kept in mind. First, the test materials were aluminum, a well characterized aircraft structure material with years of history and experience in use for aircraft application. Second, failure prediction was not the correlation criterion, strain and displacement were. This avoids the failure criteria morass and concentrates on the initial step in the problem. Third, the test samples were structurally simple and tested in a manner analogous to the NOVA model geometry - unconnected panels subjected to an overpressure loading. As a result, the capabilities for calculating the free field overpressure environment and panel response to overpressure loading were established. This forms one part of a total capability for performing hardness assessments. It must be noted

that these tests did not include a simulation of a nuclear thermal pulse.

These two programs filled large gaps that existed in the aircraft nuclear hardness assessment community, but do not constitute a complete or exhaustive set. In fact, with the increasing use of composite materials in airplanes, it is necessary to reevaluate the specifics of the approach shown in Figure 4. The basic arrangement for an assessment remains as shown in Figure 3 and for correlation and assessment as shown in Figure 4, but the contents of the boxes change, in some cases quite substantially. Figure 5 is an expanded version that incorporates composite materials. In actuality, the first major impact occurs in subdividing the aircraft into critical subsections appropriate to test and analysis. Current composite design practices are based on a one-for-one substitutional basis - a composite panel replaces an aluminum panel. This approach is gradually changing and design approaches unique to composites are evolving. These new approaches will conceivably change what can be considered a critical independent subsection. For test purposes, the large air shock tubes will be as valid for composites as for metal structures testing. Environmental diagnostics will be comparable, as will other instrumentation requirements. The biggest perturbation will be in the analysis box, for reasons to be discussed shortly. At the present time, the correlation box is essentially an empty space - neither experiments nor analyses of any consequence have been performed with due consideration for mission and environmental requirements. The added set of boxes at the bottom of Figure 5 are a result of work that has been done in studies on composite materials for dynamic response characterization for non-nuclear environments. In general it is not expected that material models such as found in the current version of NOVA/DEPROP will be adequate for predicting the response of composite materials such as graphite epoxy. This statement must be tempered, however, by the reality of conservative design practices that tend to overpower any but the most unexpected responses.

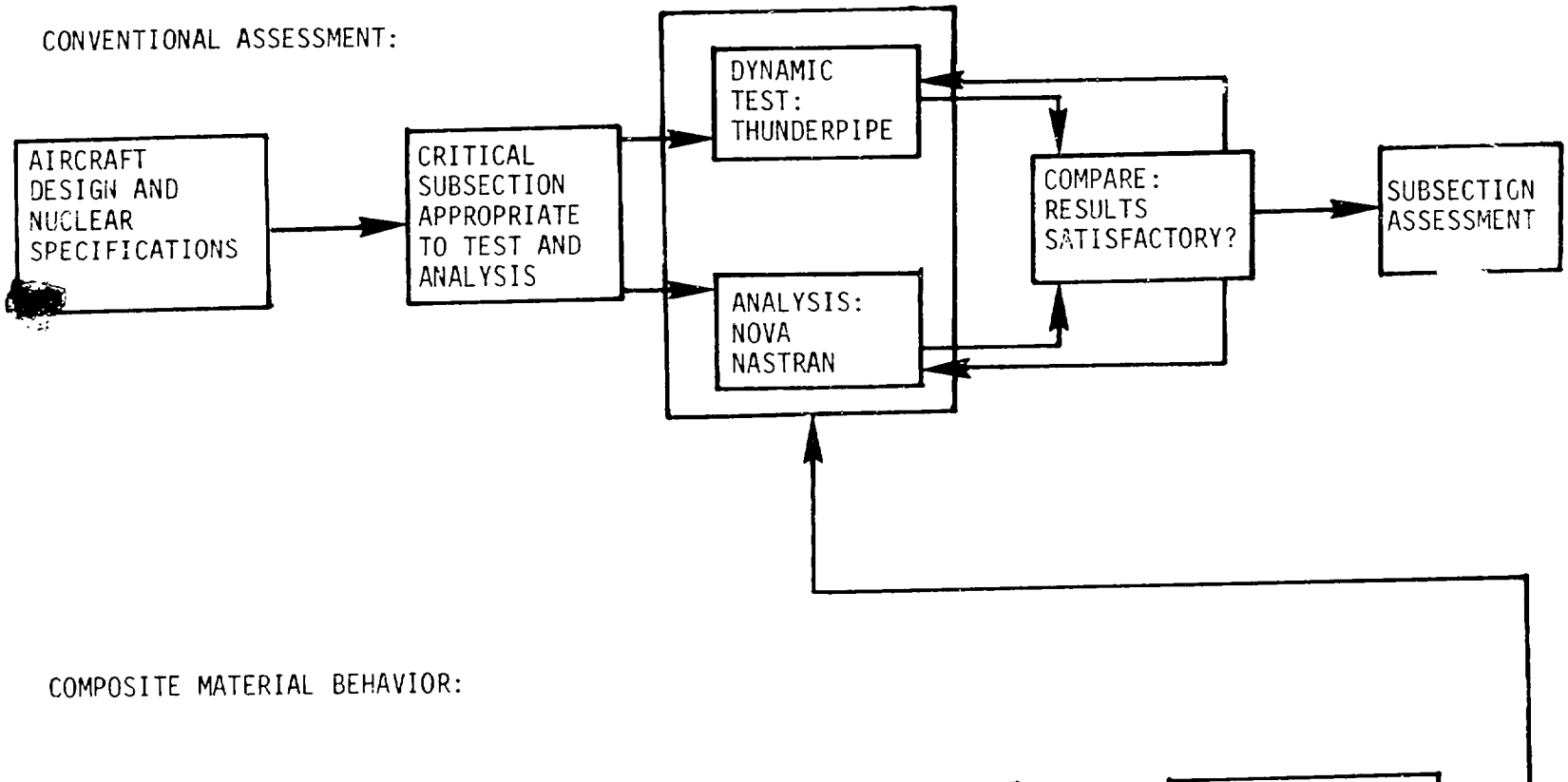

Figure 5. Aircraft Assessment - Composite Materials

2.3 COMPOSITE REQUIREMENTS

For an atmospheric burst at sufficient range from an airplane such that the airplane is not engulfed in the fireball, there are three principal environments that result in loads on the structure. The first to arrive is the thermal pulse, which results in a temperature rise in the material, depending upon properties such as absorptivity, emissivity, conductivity and boundary conditions. Of course, the greater the range, for a given weapon, the lower the fluence (energy per unit area) and the lower the amount of heat energy absorbed. It is this amount of energy absorbed that determines the final temperature to which the material is raised, which then establishes one of the initial conditions of the hardness assessment. Since the aircraft is under essentially a static load condition at this time, appropriate material properties would include static loads with heating rates, and static loads at elevated temperatures. At some time following the thermal pulse, depending upon range, the air shock arrives. Two types of loadings result from this blast. One is gust loading due to the air mass velocity behind the shock front. This results in low frequency responses such as wing bending. While the frequencies are low, the amplitudes of the loads can be extremely large, and can result in an overstressing of a component. Depending upon the time of arrival, the materials will have cooled somewhat from maximum front surface temperature. It is possible that the component will be uniformly heated to a significant temperature. Due to the low frequency nature of the gust loading, appropriate properties are quasistatically generated at the appropriate soak temperature. Also associated with the shock wave is the dynamic overpressure. This amounts to an additional few pounds per square inch loading on all surfaces of the aircraft, and induces high frequency vibrations. Such loadings can result in slight damage (panel dimpling), to moderate damage (panel rupturing), to severe damage (frame buckling). This is a dynamic response mode, so the appropriate properties should be generated under dynamic loading conditions, and with appropriate heating rates

and temperatures for the encounter geometry.

There is substantial evidence that is beginning to accumulate and appear in the literature that supports the need for considering both heating and strain rate effects, not only for composite materials, which clearly exhibit a strain rate dependence, but also for metals, which are generally thought of as being strain rate insensitive. Reference 7 contains an excellent compilation of strain and heat rate effects on the properties of aluminum, summarizing several sources of data over a range of heating times of 10^{-4} seconds to 10^{3} hours, and strain rates from the shock region into the static.

The data obtained in this program show a difference in properties dependent upon strain rate. The effect is even greater at elevated temperatures (up to resin cure) where the quasistatically measured properties steadily fall with increasing temperature, while the dynamically obtained properties do not show a significant decrease until the resin cure temperature is exceeded (350°F for AS/3501-6 graphite epoxy and 475°F for the quartz polyimide). For these particular materials, the implication is that for the dynamic response case, even at elevated temperatures, they are stronger than analyses based on quasistatic test results would indicate. Dynamic tests on other graphite epoxies have shown decreases in strength, which emphasizes the need for characterizing each material rather than relying upon general generic guidelines.

Table 1 summarizes the nuclear hardness assessment state of the art technology capability, wherein three terms must be defined:

Technology Gap - The technology required to generate this information does not currently exist.

Performance Gap - Attempts have been made to generate the data or information, but for various reasons, such as

improper experimental techniques or analytic models, it has not been successfully done.

Data Gap - All the tools exist to produce the data, perform the analysis, etc., but it has not been done.

With the reminder that for the most part correlations have not been done, the table is presented as an indicator of the types of data and tools that are needed to perform correlation studies. The table is not a complete listing, and only goes up to structural response of components. It also only addresses thermal and overpressure loadings since those were the primary concerns of the experimental part of this program.

In general, there is a data gap in all areas. There are several programs that are generating response data on composites, some at prodigious rates, but very few of these programs are addressing the particular requirements of nuclear hardness data. Those programs that are addressing nuclear hardness continue to be in support of metallic structures, which are still the predominant basis of aircraft structural components. The results of these studies indicate that the load producers, such as air blast tunnels, and the associated diagnostic instrumentation are generally adequate, at least for linear response. There is no reason to suspect that the same techniques would not be applicable to composites. There is a gap so far as testing complete aircraft, although drone helicopters have been exposed to the air blast generated by high explosive tests. Therefore, the hardness assessment accuracy is limited by the assessor's ability to extrapolate component effects to system operation. The largest apparent weaknesses are in the analytic tools such as NOVA/DEPROP that have rather simple models for treating orthotropic materials. Until correlation studies are performed, however, the magnitude of the weaknesses will not be known.

Table 1. Composite Materials Assessment Capability Gaps

PARAMETER	DATA GAP	PERFORMANCE GAP	TECHNOLOGY GAP	COMMENTS
Material Properties				
Quasistatic	Partial	No	No	Some Available/Required for analysis & design
Dynamic	Substantial	No	No	Little available, need is apparent.
Response				
Displacement	Yes	No	Partial	With exception of displacement measurements on large structures, no major experimental gaps exist.
Strain	Yes	No	Potential	
Damage	Yes	No	Potential	
Failure	Yes	No	Probable	Potentially serious gap exists without use of analytic model appropriate to composite materials.
				Severity of gaps cannot be evaluated since no adequate correlation studies have been performed.

3.0 DESCRIPTION OF EXPERIMENTS AND ANALYSES

3.1 TEST TECHNIQUES

3.1.1 General

All the composite material mechanical tests conducted in this contract were performed in the Materials Sciences Laboratory at ETI. Most specimens were tested in the three-point bend configuration. For this test the specimen is in the shape of a beam and is loaded at midspan while being simply supported at the ends. Static and dynamic tests at various temperatures were conducted on these specimens. Before testing some samples were either fatigue cycled or subjected to low blow tests. A series of three point bend tests was also conducted on material treated with a thermal protective coating applied by AVCO Systems Division and exposed in the Air Force Materials Laboratory Thermal Flash Facility. The remaining tests were shear plug tests. The shear plug configuration is a punch and die system requiring a square plate of material.

Static tests were conducted on a Tinius Olsen four range, 60,000 lb. capacity, electro-mechanical testing machine which has the capability to perform tension, compression and flexural tests. This machine is equipped with associated strain instrumentation and recorders for producing stress-strain and other pertinent data.

Dynamic tests were conducted with a Model 8000 Dynatup instrumented impact machine having a maximum capability of approximately 2000 ft-lb at an impact velocity of 15 ft/sec. The strain rate induced in the specimen is controlled through varying the specimen geometry and the drop height of the tup.

A detailed description of the test techniques, configurations and associated data reduction are presented in the remainder of this section.

A summary of the total test matrix is given in Appendix A.

3.1.2 Three Point Bend Tests

The three point bend specimen is loaded across the midspan and is simply supported at the ends. This configuration is advantageous due to its relative geometric simplicity and ease of testing. A representative load history is shown in Figure 6 where the response is partitioned into three regions, namely:

1. Pre-initial fracture
2. Initial fracture
3. Post-initial fracture.

Figure 7 illustrates the salient features of a dynamic three point bend test. The moving striker (tup) and specimen are shown immediately before impact and again at a later time during the final stages of fracture. A balanced-bridge strain gage system is imbedded in the tup to provide a direct measurement of the load-time history of the specimen during fracture. A representative oscilloscope trace is shown in the lower half of the figure.

Interpretation of the fracture data is relatively straightforward. Static and dynamic values of yield strength, fracture load and fracture energy as well as post-fracture material behavior may be obtained as shown in Figure 8. Energy values are a direct output of the Dynatup instrumentation whereas quasistatically, they must be measured from the load-deflection history. Values of quasistatic flexural modulus are obtained by direct measurement of the initial slope of the load history. Values of dynamic flexural modulus are obtained by a linear least squares fit through the initial portion of the oscilloscope trace.

Three parameters were identified as being appropriate for material characterization from a three point bending test. These are:

A1644

REGIONS

1 PRE-INITIAL FRACTURE
2 INITIAL FRACTURE
3 POST-INITIAL FRACTURE

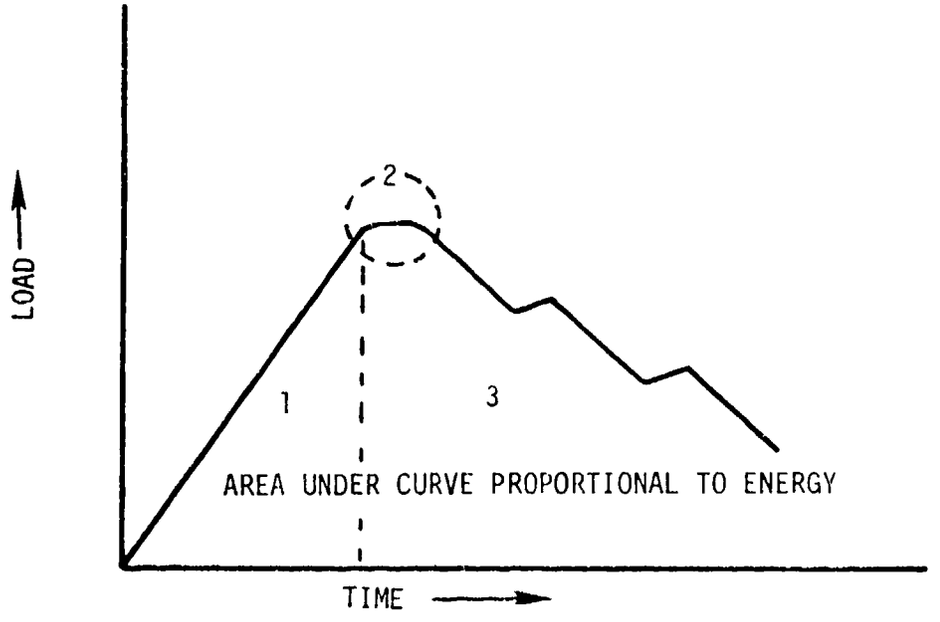

(PROPORTIONAL TO DEFLECTION, STRAIN)

Figure 6. Schematic of Load vs. Time Response History

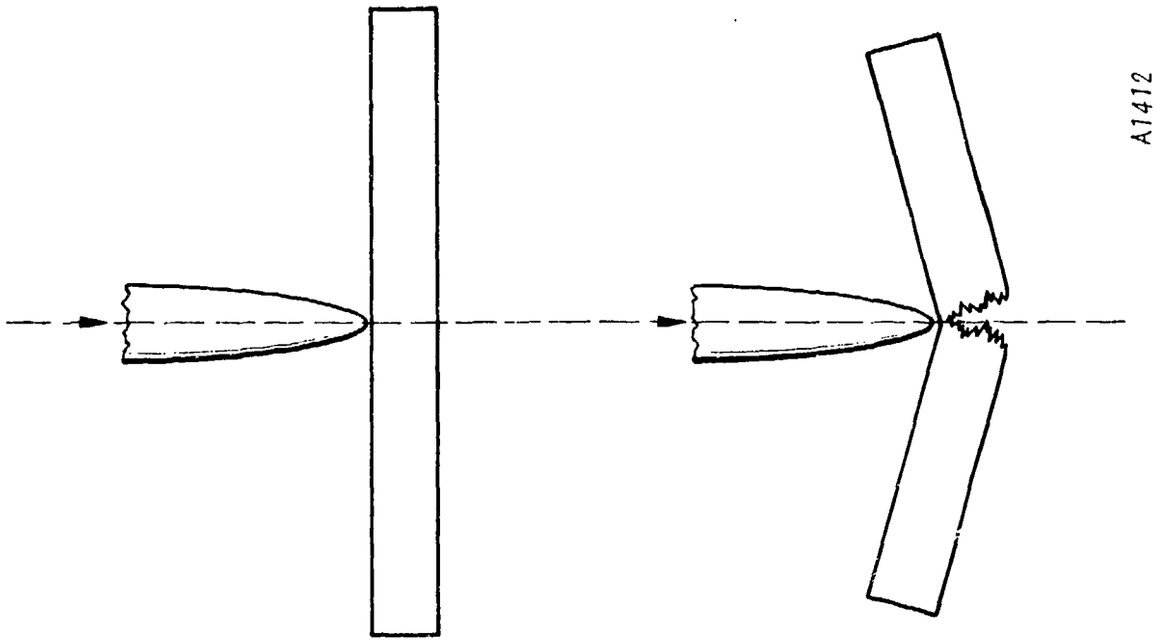

(A) SPECIMEN AND TUP ORIENTATION

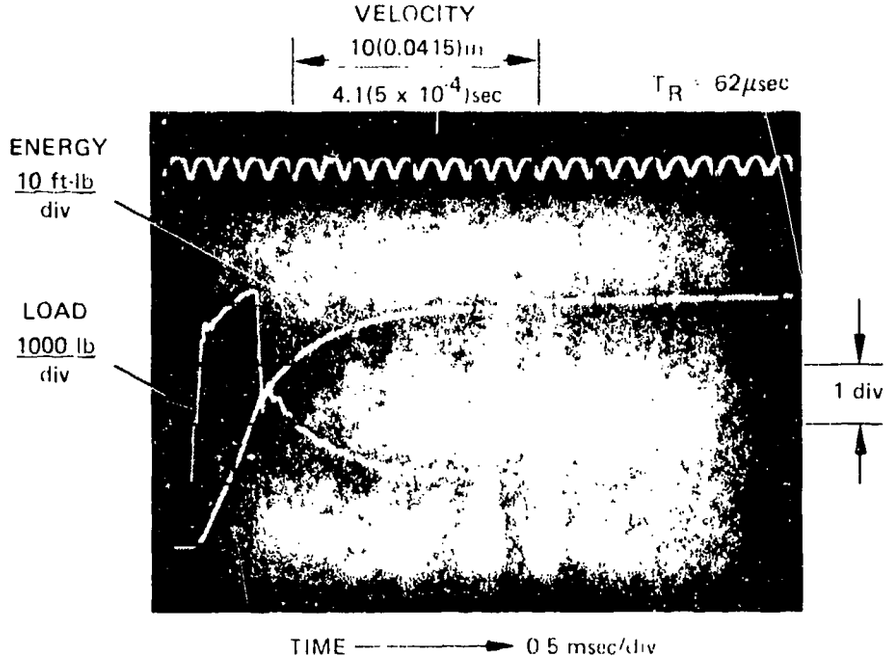

(B) LOAD-TIME AND ENERGY-TIME RECORDS

Figure 7. Dynamic Three-Point Bend Test

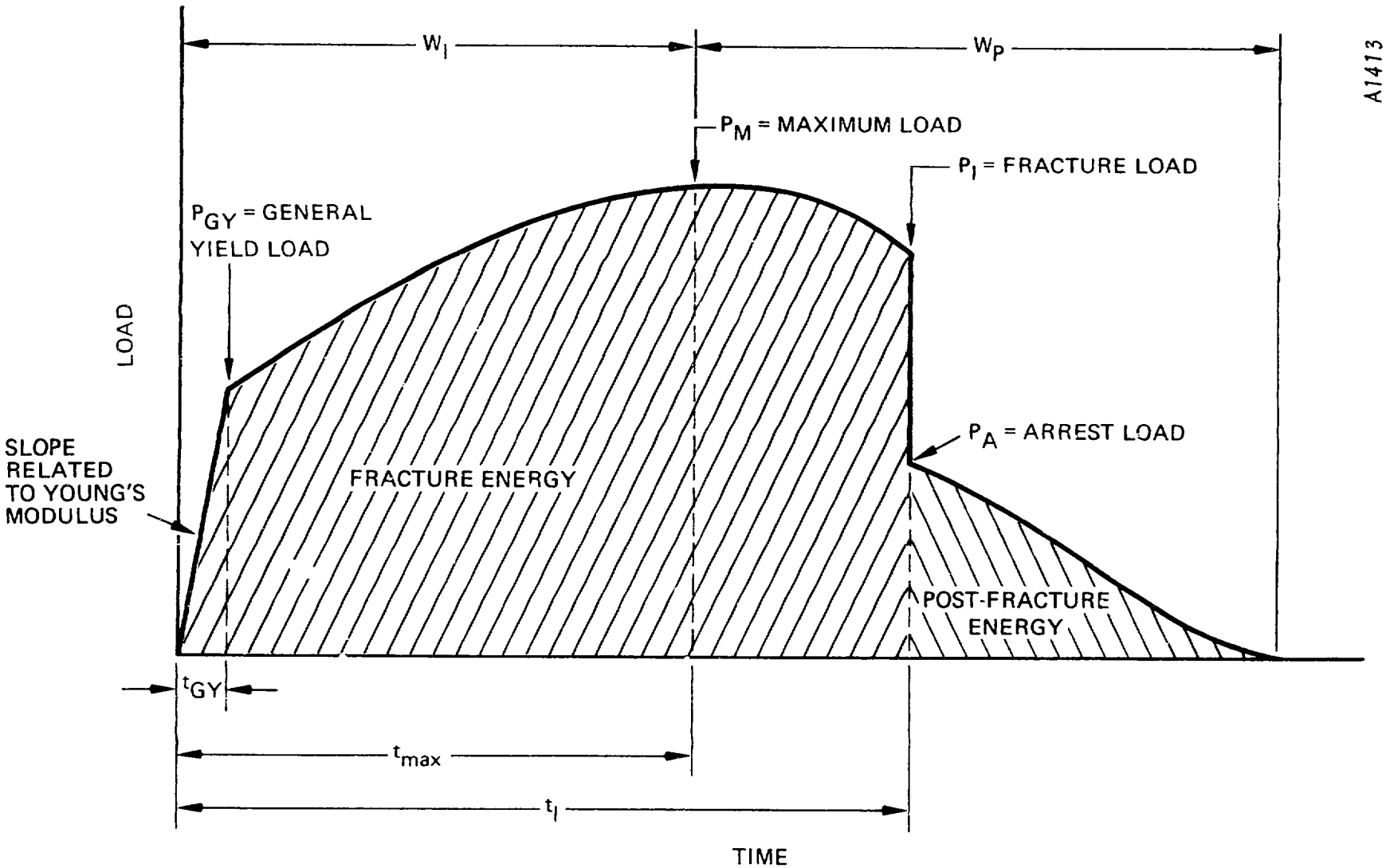

Figure 8. Idealized Load-Time Record from Three-Point Bend Test

1. Ultimate Flexural Strength $\equiv \sigma_{\substack{FLEX \\ ULT}} = \dfrac{1.5P_{MAX}\ell}{bh^2}$

Where P_{MAX} = maximum load

ℓ = span length

b = specimen width

h = specimen thickness

2. Energy Absorbed to Peak Load $\equiv \Delta E_o$

$$\Delta E_o = \int P dx \text{ (for static tests)}$$

where x = midspan displacement

and

$$\Delta E_o = \int P v dt \text{ (for dynamic tests)}$$

where v = tup velocity

t = time

3. Flexural Modulus = E_{flex}

In order to obtain an accurate value for the flexural modulus the compliance of the testing apparatus must be taken into account. The machine compliance, C_m, is calculated from tests performed on materials of known modulus such as aluminum. The compliance of such a beam specimen is given by

$$C_S = \frac{\ell^3}{4bh^3E}\left(1 + 1.2\ (E/G)\ \left(\frac{h}{\ell}\right)^2\right)$$

where E is Young's modulus and G is the transverse shear modulus. For specimens with a low thickness-to-length ratio, the second term on the right side, which is related to transverse shear deformation, may be neglected. The value of the total compliance, C_T, is obtained from the slope of the linear portion of the load-time curve since

$$C_T = C_S + C_m \bullet$$

The machine compliance, C_m, is now easily calculated since both C_T and C_S are known for the aluminum specimen.

Values of C_m for both the static and dynamic testing equipment were obtained and subsequently used in the calculations of flexural modulus in all tests in the following manner:

1. calculate C_T from a least squares fit to the digitized load-time output,

2. calculate $C_S = C_T - C_m$,

3. calculate flexural modulus where

$$E_{flex} = \frac{1}{C_S} \left(\frac{\ell^3}{4bh^3} \right)$$

and the $\left(\frac{h}{\ell}\right)^2$ term is essentially zero for the graphite epoxy beam specimens used in this program.

In the dynamic three point bend test the maximum strain occurs in the extreme fibers at the midspan and is given by

$$\varepsilon_{max} = \frac{6h}{\ell^2} \delta$$

where δ is the midspan displacement. The strain rate is given by

$$\dot{\varepsilon}_{max} = \frac{6h}{\ell^2} \dot{\delta}$$

where $\dot{\delta}$ is the velocity of the tup. The tup velocity is approximately

$$\dot{\delta} = \sqrt{2gH}$$

where H is the drop height and g is the gravitational constant. The maximum strain rate in a given specimen is then

$$\dot{\varepsilon}_{max} = \frac{6h}{\ell^2} \sqrt{2gH}.$$

Strain rates for the tests are shown in Table 2. Since frictional losses are associated with the falling mass, the actual impact velocity is about 10% less than calculated by using $\sqrt{2gH}$. The actual impact velocity is measured using a fiber optic system and this value is used to obtain the actual strain rate for the tests.

3.1.3 Fatigue Tests

Beam specimens were subjected to fatigue cycling using a Dynatup® Model 108 Precracker. Figure 9 shows the specimen configuration during cycling. The beam is clamped at one end, supported at midspan and loaded at the free end. A special holding fixture was designed to accommodate the specimen geometry in the precracker. The deflection imposed at the free end can be varied in order to achieve the desired stress at the middle of the beam. The specified midspan stress, σ, is related to the end deflection, δ, by

$$\sigma = \frac{24Eh}{7\ell^2} \delta$$

derived from beam theory and the method of superposition.

3.1.4 Low Blow Tests

Low blow testing involves striking the beam in the same manner as for conventional three point bend tests but by either limiting the available energy or by restricting the travel of the tup, the specimen is not failed. For the tests in this series, the stops in the drop tower were adjusted to limit the deflection of the beam. The purpose of

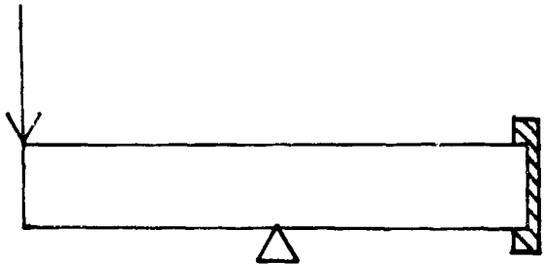

Figure 9. Fatigue Cycling Configuration.

Table 2. Calculated Strain Rates

MATERIAL	h (inch)	ℓ (inches)	H (inches)	$\dot{\varepsilon}$ (sec^{-1})
8-ply Graphite Epoxy	.045	1.6	1	2.9
16-ply Graphite Epoxy	.087	1.6	1	5.7
			10	17.9
32-ply Graphite Epoxy	.185	1.6	1	12.0
Quarts Polymide	.088	1.6	1	5.7
			10	18.1

low blow testing is to determine if deflections below those corresponding to ultimate load microscopically damage the beam such that its residual load carrying ability is degraded. Therefore, subsequent to the low blow tests the specimens were tested in three point bending, some statically and some dynamically.

3.1.5 Shear Plug Tests

The shear plug test configuration is shown in Figure 10. The apparatus is basically a punch and die system where the punch is driven by the tup. The specimen is a square of material three-quarters of an inch on a side. The shear strength, τ, of the material is determined from the relation,

$$\tau = \frac{P}{\pi D t}$$

where P is the peak load, D is the punch diameter and t is the thickness of the specimen.

3.1.6 Elevated Temperature Testing

The quasistatic elevated temperature tests were performed by installing a BEMCO Environmental Testing Chamber in the Tinius Olsen testing machine. This chamber permits static tests to be performed at temperatures between -300 and 1000 degrees Fahrenheit. Minor modifications were made to the existing Tinius Olsen testing equipment to enable three point bend tests to be conducted in this manner. The compliance of the modified apparatus was determined at the temperatures and load regimes appropriate to the tests.

The specimens used in the dynamic high temperature tests were heated in a Blue M Electric Company Lab-Heat muffle furnace. Specimens tested below 0°F were cooled in the BEMCO Environmental Testing Chamber.

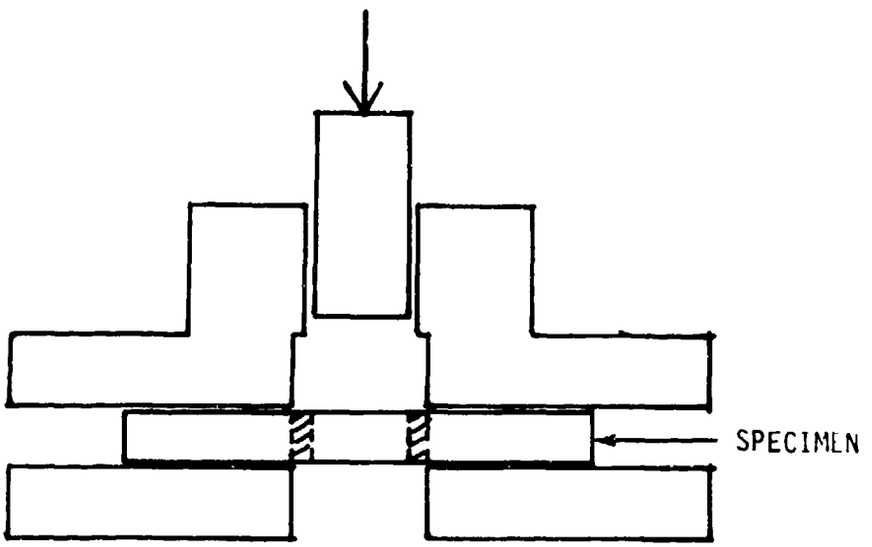

Figure 10. Shear Plug Test Configuration.

The tests were conducted by rapidly removing the test specimen from the oven and performing the dynamic three point bend test within five seconds of specimen removal. Thermocouples were installed on spare material to determine the temperature response of the samples during the five second interval. The maximum thermal gradients established in the specimens in the interval was 24° for specimens .044 inch thick and 11°F for specimens .085 inch thick. These gradients were felt to be tolerable for these tests.

Another aspect of the high temperature testing portion of the program involved exposing materials in the Thermal Flash Facility at the Air Force Materials Laboratory. The specimens were exposed at two temperatures - one below the cure temperature and one above. Thermocouples were mounted on the specimens to obtain the temperature distribution.

3.2 MATERIALS

3.2.1 Graphite Epoxy

Two graphite epoxies were used in this program. Both were supplied by Hercules Corporation and conformed to Northrop Aircraft Division specifications for aerospace grade material. AS/3501-6 graphite epoxy (AS fibers, 3501-6 resin) was obtained in 8 and 16-ply unidirectional configuration and in 8 and 16-ply layed-up configurations of $[\pm 45/0/90]_s$ and $[\pm 45/0/90]_{2s}$, respectively. Graphite epoxy, designated AS/3501-5 (available from another program),consisted of 32 plies in the configuration $[\pm 45/0/90]_{4s}$. Nominal ply thickness is .0052 inch. The cure temperature of the material was 350°F. Unidirectional room temperature, static properties of AS/3501-6 as provided by McDonnell-Douglas Astronautics Company (MDAC) are shown in Table 3.

Table 3. Room Temperature, Unidirectional Properties of AS/3501-6 Graphite Epoxy - MDAC

PROPERTY	TENSION	COMPRESSION
$E_{0°}$ (10^6 psi)	20.8	18.6
$E_{90°}$ (10^6 psi)	1.9	2.0
$T_{0°}$ (10^3 psi)	273.5	279.6
$T_{90°}$ (10^3 psi)	9.5	38.9

G_{12} = 0.85X10^6 psi

ν = 0.2 to 0.25

$E_{0°}$ ≡ Modulus, parallel to fibers

$E_{90°}$ ≡ Modulus, perpendicular to fibers

$T_{0°}$ ≡ Ultimate Strength, parallel to fibers

$T_{90°}$ ≡ Ultimate Strength, perpendicular to fibers

α_{12} ≡ in-plane shear modulus

ν ≡ Poisson's ratio

3.2.2 Quartz Polyimide

The second material tested was quartz polyimide, a radome material, consisting of 581 quartz fabric reinforcement impregnated with F178 resin. This material was fabricated by the Brunswick Corporation. Nominal thickness for the nine plies was 0.09 inch. The cure temperature of the material was 475°F. Static properties provided by Hexcel Aerospace are given in Table 4.

3.2.3 Specimen Geometries

All three point bend specimens had a span length (distance between supports) of 1.6 inches. Nominal width was 0.35 inch. The width and thickness of each specimen was measured to the nearest .001 inch prior to actual testing and the measured value was used in subsequent data reduction. The thickness of the shear plug specimens was also measured.

3.3 ANALYTIC TECHNIQUES

3.3.1 General

Although the scope of this program did not permit detailed analytical studies of the response of an aircraft fabricated with composite materials, a limited amount of analyses were carried out. These analyses are described in the remainder of this section.

3.3.2 AC-3

The computer code AC-3 was used to generate analytical predictions of flexural modulus and failure loads which were compared with experiment. AC-3 uses plane stress laminated plate theory to calculate the stresses and strains for any layer of a laminate. The applied stress and moment resultants are used to calculate mid-plane strains

Table 4. Quartz Polyimide Properties Supplied by Hexel Aerospace

Property \ Temperature	Room Temperature	350°F*	500°F*
Flexural Strength (10^3 psi)	85.0	65.0	56.0
Compressive Strength (10^3 psi)	63.0	45.0	35.0
Tensile Strength (10^3 psi)	60.0	58.0	58.0
Flexural Modulus (10^6 psi)	3.6	3.2	3.1
Compressive Modulus (10^6 psi)	4.1	3.6	3.3
Tensile Modulus (10^6 psi)	4.0	3.6	3.5

* Specimens maintained at this temperature ½ hour prior to testing.

and curvatures from which the strains in each layer may be determined. The stresses are then calculated from the strains by using the lamina constitutive relations. The yield strength criteria used in AC-3 are:

$$\frac{\sigma_1}{F_1} \leq 1 \qquad \text{(fiber)}$$

$$\frac{\sigma_2}{F_2}^2 + \frac{\sigma_6^2}{F_6} \leq 1 \qquad \text{(Matrix)}$$

where σ_1, σ_2 and σ_6 are the lamina longitudinal, transverse and shear stresses, respectively, and F_1, F_2 and F_6 are the corresponding lamina strengths. AC-3 also calculates the margin of safety which is defined as the factor by which the stress ratios must be multipied in order that the lamina reach the incipient failure condition, that is, the equalities are obtained. A complete listing of AC-3 is given in Volume II of the Air Force Advanced Composites Design Guide.

The flexural modulus is given approximately [8] by

$$E_{flex} = \frac{12}{h^3 D_{11}^{-1}}$$

where h is the specimen thickness and D_{11}^{-1} is the first element of the inverted D-matrix, the matrix of flexural constants calculated by AC-3 where

$$D_{ij} = \frac{1}{3} \sum_{k=1}^{n} \overline{Q}_{ij}^{k} (h_k^3 - h_{k-1}^3); \; i, j = 1, 2, 6$$

The $\overline{Q}_{ij}$ are elements of the reduced stiffness matrix and n is the number of layers in the laminate.

3.3.2 In-Plane Shear Modulus Determination

The in-plane shear modulus of a unidirectional laminate may be

determined if the Young's modulus parallel (0°), perpendicular (90°) and 45° to the fibers and the major Poisson's ratio are known.[9] These quantities are denoted by E_{11}, E_{22}, E_{45} and υ_{12}. The shear modulus, G, using the transformation equation for the uniaxial stiffness of an orthotropic material, is given by

$$\frac{1}{G} = \frac{4}{E_{45}} - \frac{1 - \upsilon_{12}}{E_{11}} - \frac{1 - \upsilon_{21}}{E_{22}}$$

where the minor Poisson's ratio is given by the reciprocal relation

$$\frac{\upsilon_{12}}{\upsilon_{21}} = \frac{E_{11}}{E_{22}}$$

The quantities E_{11}, E_{22} and E_{45} may be determined by tensile, compressive or flexure tests on specimens of the proper orientation while υ_{12} can be determined by means of two-element strain rosettes on a 0° specimen.

4.0 GRAPHITE EPOXY TEST RESULTS AND ANALYTICAL CORRELATIONS

Results of the three point bend tests on graphite epoxy are presented in this section. The results of three-point bend tests on fatigued, low blow tested and Thermal Flash Facility tested specimens are also given. Shear plug test results will conclude this section.

4.1 UNIDIRECTIONAL MATERIAL THREE-POINT BEND TESTS

Table 5 summarizes the results of the quasistatic and dynamic three point bend tests on 8-ply unidirectional graphite epoxy oriented at 0°, that is, the fibers are oriented at 0° to the longitudinal axis of the specimen. Static tests on 45° and 90° specimens were also performed using a very sensitive load scale. In spite of this, the peak loads were too low to be accurately determined, thus preventing further data reduction. No dynamic tests on the 45° and 90° specimens were carried out due to the low loads expected. From the limited data presented in Table 5, it can be seen that the ultimate flexural strength and energy to peak load decrease with temperature and increase with strain rate for the 0° specimens.

The next five figures summarize the results of the static and dynamic tests conducted on 0°, 45°, and 90° orientations of 16-ply unidirectional AS/3501-6 graphite epoxy. The magnitude of the error bands denotes standard deviation of the test parameter in all figures. The variation of ultimate flexural strength and flexural modulus with temperature for the 0° orientation is shown in Figures 11 and 12, respectively. The flexural strength decreases with temperature both quasistatically and dynamically with dynamic values higher than quasistatic at all temperatures. From Figure 12 the quasistatic flexural modulus decreases with temperature. The dynamic flexural modulus also tends to decrease with increasing temperature although the 250° value is 12% higher than the room temperature value. Figure 13 shows that

Table 5. Results of Three Point Bend Tests on 0° 8 Ply Unidirectional Graphite Epoxy

TEST CONDITION	ULTIMATE FLEXURAL STRENGTH (ksi)	ENERGY TO PEAK LOAD (in-lb)	FLEXURAL MODULUS (10^6 psi)
Static, R.T.	269.7 ± 12.8	7.9 ± .4	14.5 ± .9
Static, 250°F	233.5 ± 10.2	5.5 ± .4	14.7 ± 1.3
Dynamic, R.T.	335 ± 19.1	8.3 ± .9	13.41 + 1.3

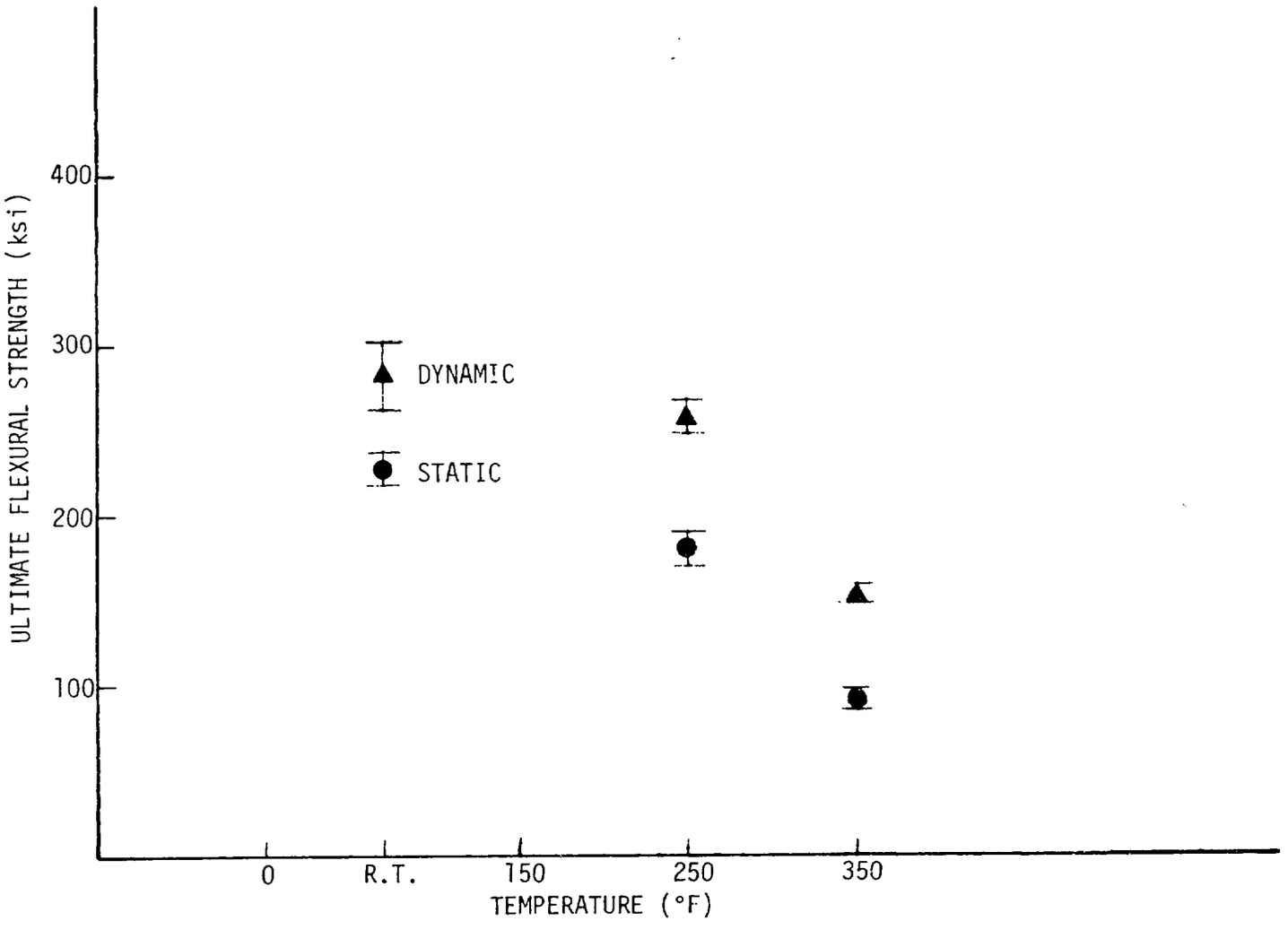

Figure 11. Ultimate Flexural Strength vs. Temperature
0° 16 ply Unidirectional.

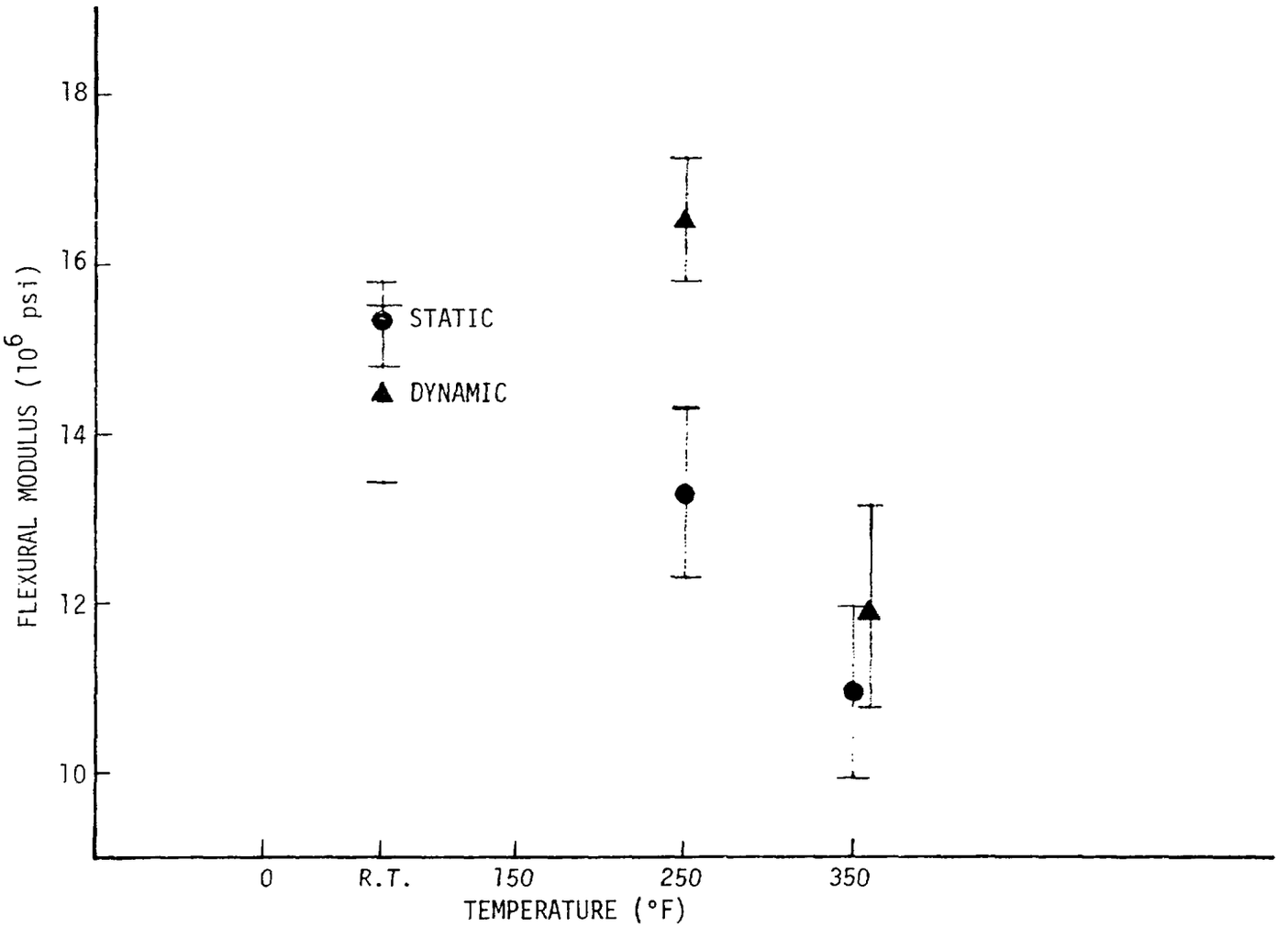

Figure 12. Flexural Modulus vs. Temperature - 0° 16 ply Unidirectional Graphite Epoxy Static and Dynamic.

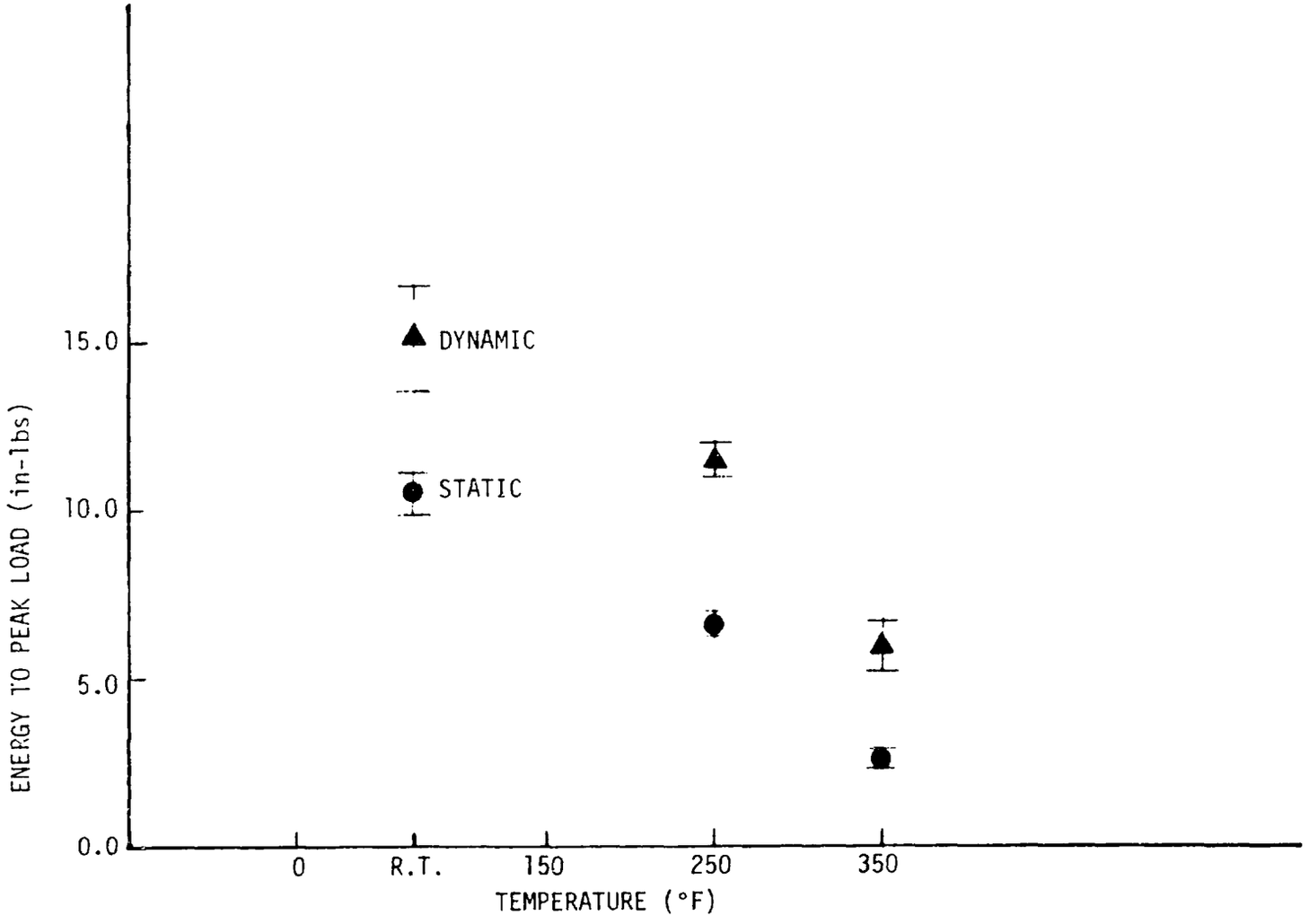

Figure 13. Energy to Peak Load vs. Temperature for 16 ply 0° Graphite Epoxy.

the energy to peak load increases with strain rate, and decreases with temperature.

Figures 14 and 15 summarize the results of tests on 45° and 90° 16-ply unidirectional graphite epoxy. Quasistatically, flexural strength and modulus decreased with temperature. Dynamically, flexural strength decreased with temperature for the 45° specimens but did not change significantly for the 90° specimens. Dynamic high temperature modulus values were not available because the loads were too low to trigger the transient recording apparatus. Dynamic ultimate flexural strength increased for the 45° specimens at all testing temperatures. Values of ultimate flexural strength did not vary significantly between quasistatic and dynamic tests for 90° specimens. From the room temperature data on Figure 15, no difference between the quasistatic and dynamic room temperature flexural moduli is apparent. Values of energy to peak load for the 45° and 90° specimens were less than 1 in-lb. Such low values cannot be accurately determined; therefore they will not be presented.

Table 6 shows the results of the flexural modulus correlation study carried out for unidirectional graphite epoxy. The MDAC values are the average of the reported tensile and compressive moduli in Table 3. The 350°F MDAC values were obtained by scaling the room temperature values according to 350° data appearing in Vol. I of the Air Force Advanced Composites Design Guide for intermediate strength graphite filaments such as AS fibers in an epoxy resin qualified for continuous 350°F service. This implies that the cure temperature exceeded 350°F. The cure temperature for the graphite epoxy used in this program was approximately 350°F which accounts for its choice as a test temperature. In general, graphite epoxy demonstrates drastic changes in properties at its cure temperature. The differences between the experimental and MDAC scaled 350° moduli can most probably be attributed to differences in the cure temperatures of the two materials.

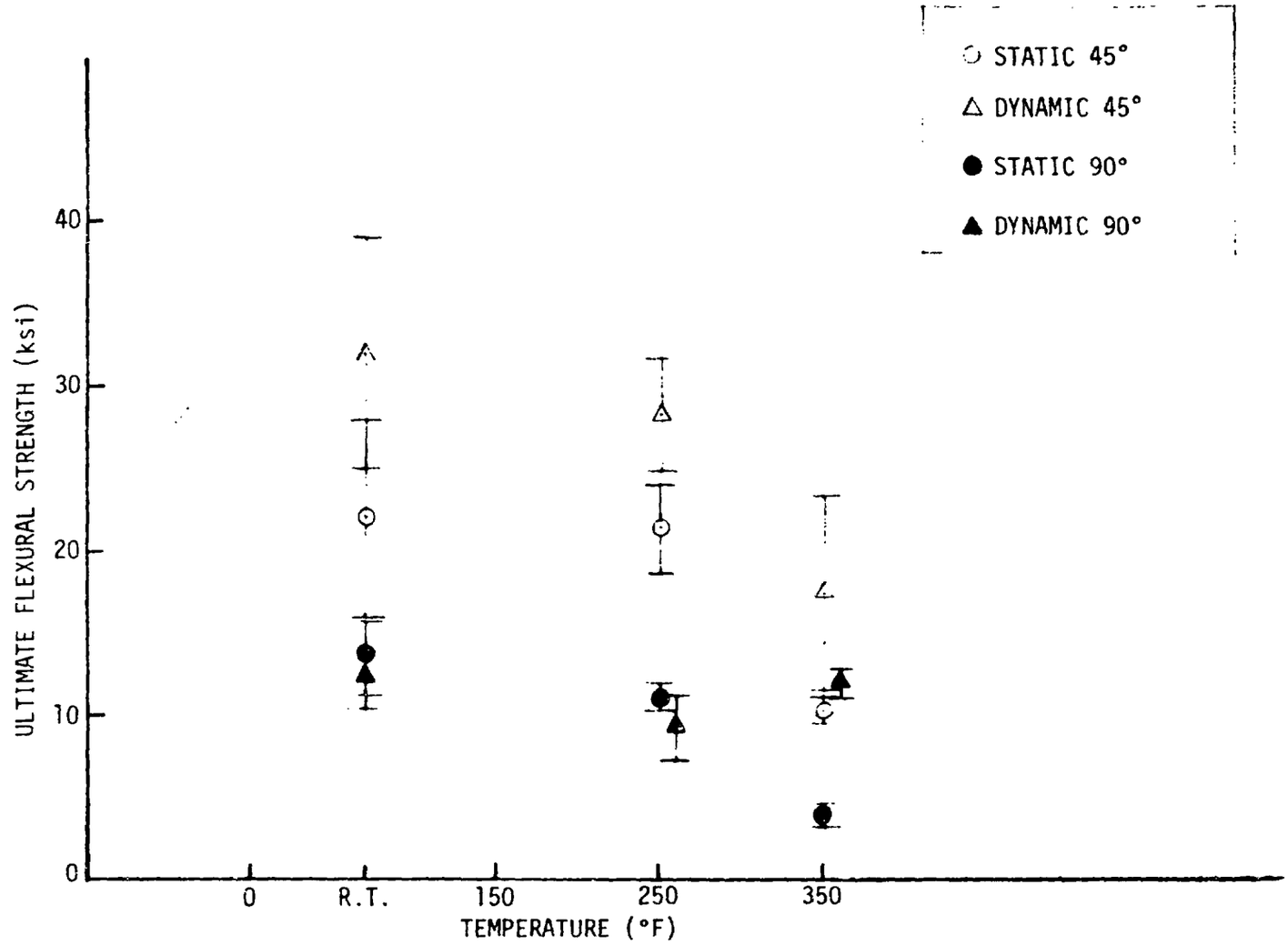

Figure 14. Ultimate Flexural Strength vs. Temperature 45° and 90° 16 ply Unidirectional.

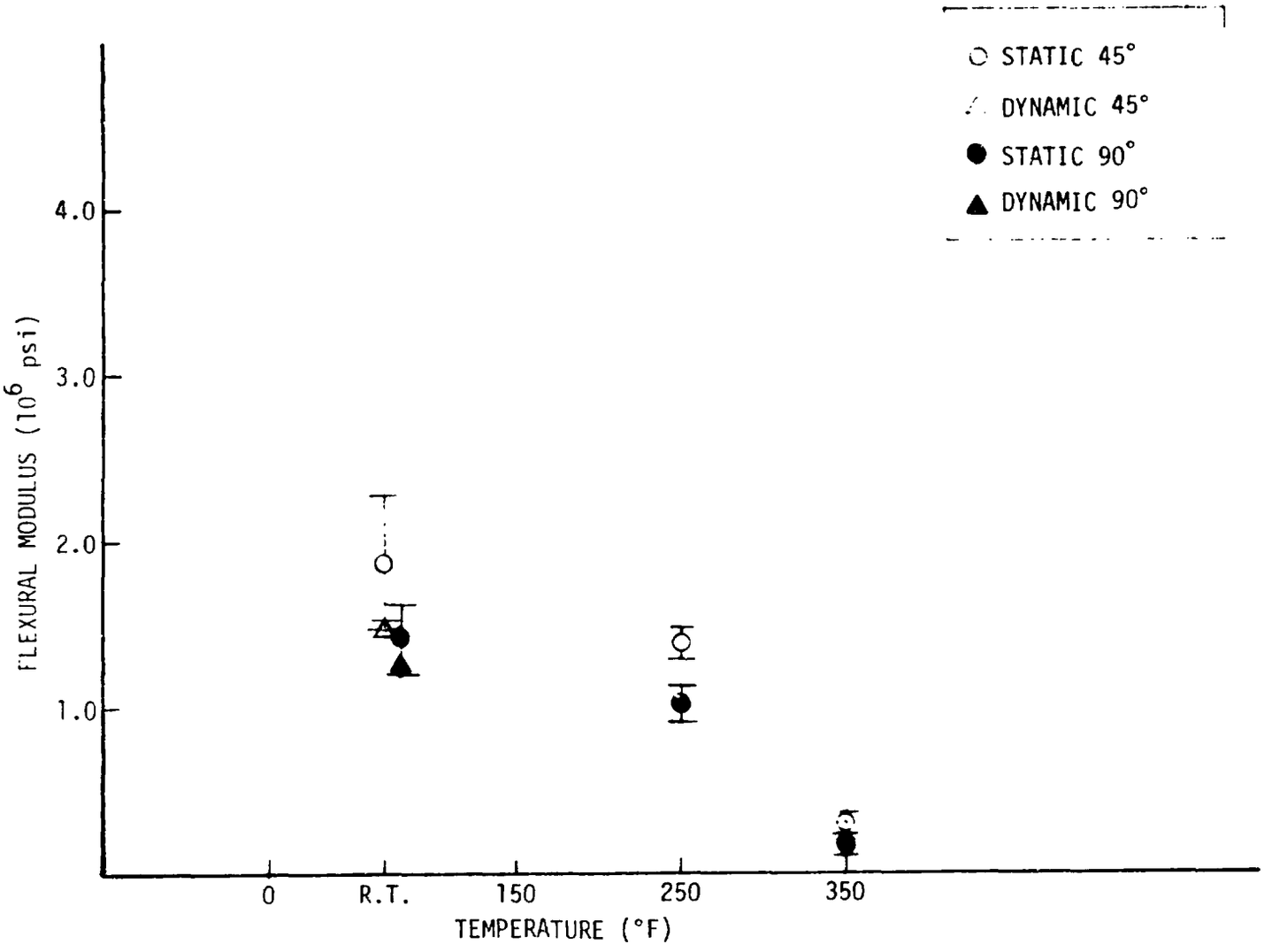

Figure 15. Flexural Modulus vs. Temperature - 45° and 90° 16 ply Unidirectional.

Table 6. Graphite Epoxy Flexural Modulus Correlation Study

ORIENTATION	EXPERIMENTAL QUASI STATIC (RT/350°F) 10^6 psi	EXPERIMENTAL DYNAMIC (RT/350°F) 10^6 psi	MDAC (RT/350°F) 10^6 psi
0°	15.5/10.9	14.5/11.9	19.7/18.6*
90°	1.4/0.2	1.2/----	2.0/1.2

*SCALED VALUES

Table 7 gives values of the calculated and experimentally obtained in-plane shear modulus. MDAC property values are included for comparison and the agreement between them is good.

4.2 SYMMETRIC 8, 16, AND 32-PLY THREE-POINT BEND TESTS

Figures 16 through 19 give the results of three point bend tests on $[\pm 45/0/90]_s$ AS/3501-6 graphite epoxy for the 0° and 90° orientations. The results appear somewhat anomalous relative to the remainder of the data, particularly where the room temperature dynamic strength is less than the quasistatic room temperature strength. While various mechanisms can be proposed to explain this, it must also be noted that in the context of the standard deviations, the behavior is not inconsistent.

Figures 20 through 27 give the results of three point bend tests on $[\pm 45/0/90]_{2s}$ AS/3501-6 graphite epoxy. Figures 20 and 21 show that the ultimate flexural strengths and flexural moduli increase with strain rate for the 0° and 90° orientation of the specimens. Figures 22 through 25 show how the quasistatic values of ultimate flexural strength and modulus decrease as the temperature increases. Dynamically, the flexural strength does not vary significantly with temperature while the flexural modulus decreases with temperature. Figures 26 and 27 show the variation of energy to peak load with temperature. Quasistatically, E_{MAX} decreases with temperature while dynamically E_{MAX} does not vary significantly. At elevated temperatures dynamic values of E_{MAX} are greater than quasistatic values.

Figures 28 through 33 summarize the test results for $[\pm 45/0/90]_{4s}$ AS/3501-5 graphite epoxy. At room temperature no strain rate effects were apparent. Quasistatic values of ultimate strength and flexural modulus decreased with temperature while dynamic values remained fairly constant. The energy to peak load did not vary with temperature quasistatically but increased dynamically.

Table 7. In-Plane Shear Modulus from 0°, 45°, 90° Tests of Unidirectional Material, R.T. Properties

Property \ Material	8 ply Static	16 ply Static	16 ply Dynamic	MDAC
$E_{0°}$ (E_{11}) 10^6psi	14.49	15.36	14.46	19.7
$E_{90°}$ (E_{22}) 10^6psi	1.5	1.39	1.25	1.95
$E_{45°}$ 10^6psi	2.21	1.88	1.75	N.A.
ν_{12}	.25	.25	.25	.25
ν_{21}	.0259	.0226	.0216	.0247
G 10^6psi	.902	.727	.689	.85

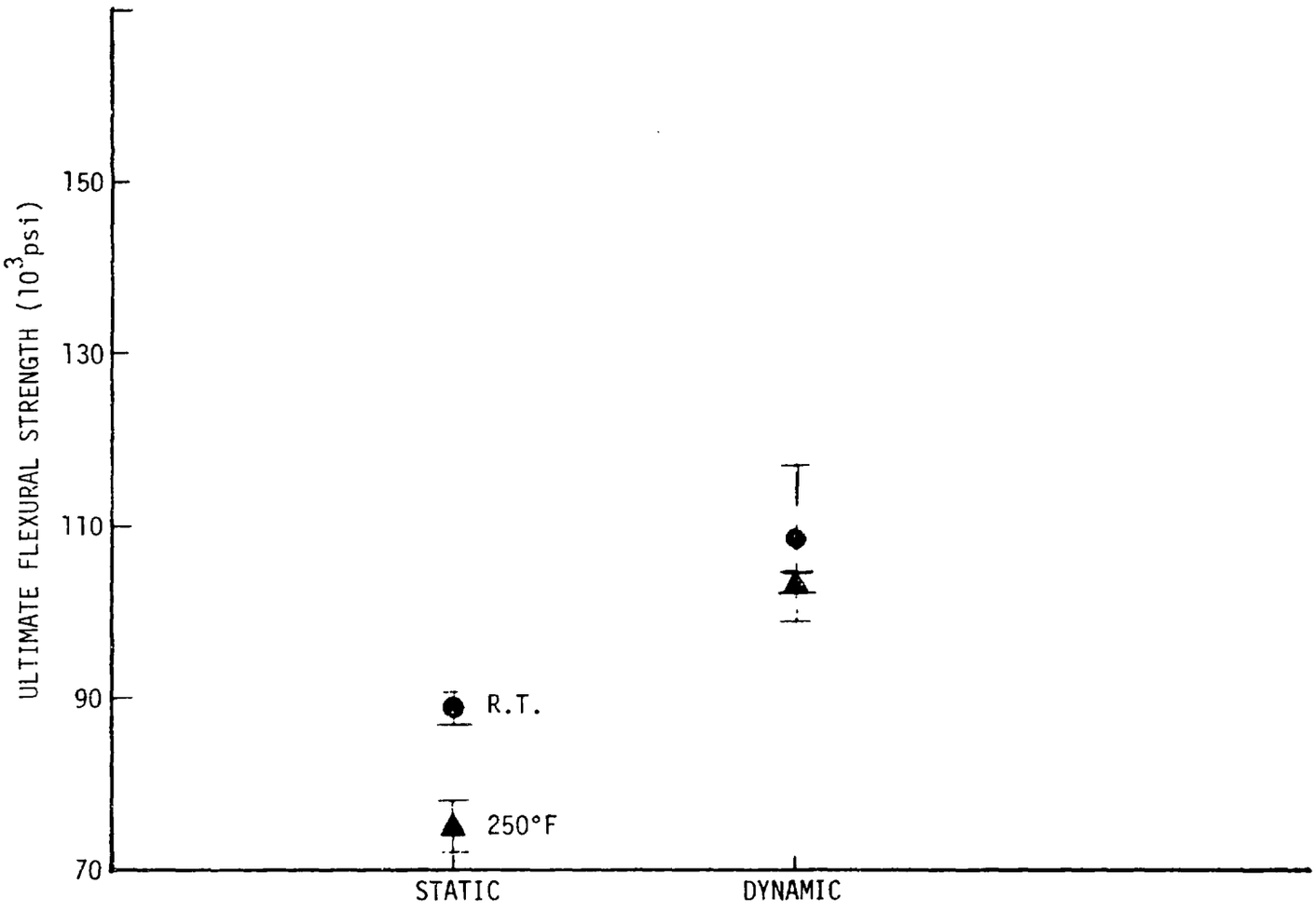

Figure 16. Ultimate Flexural Strength vs. $\dot{\epsilon}$ for $[\pm 45/0/90]_s$ Graphite Epoxy, 0° Orientation.

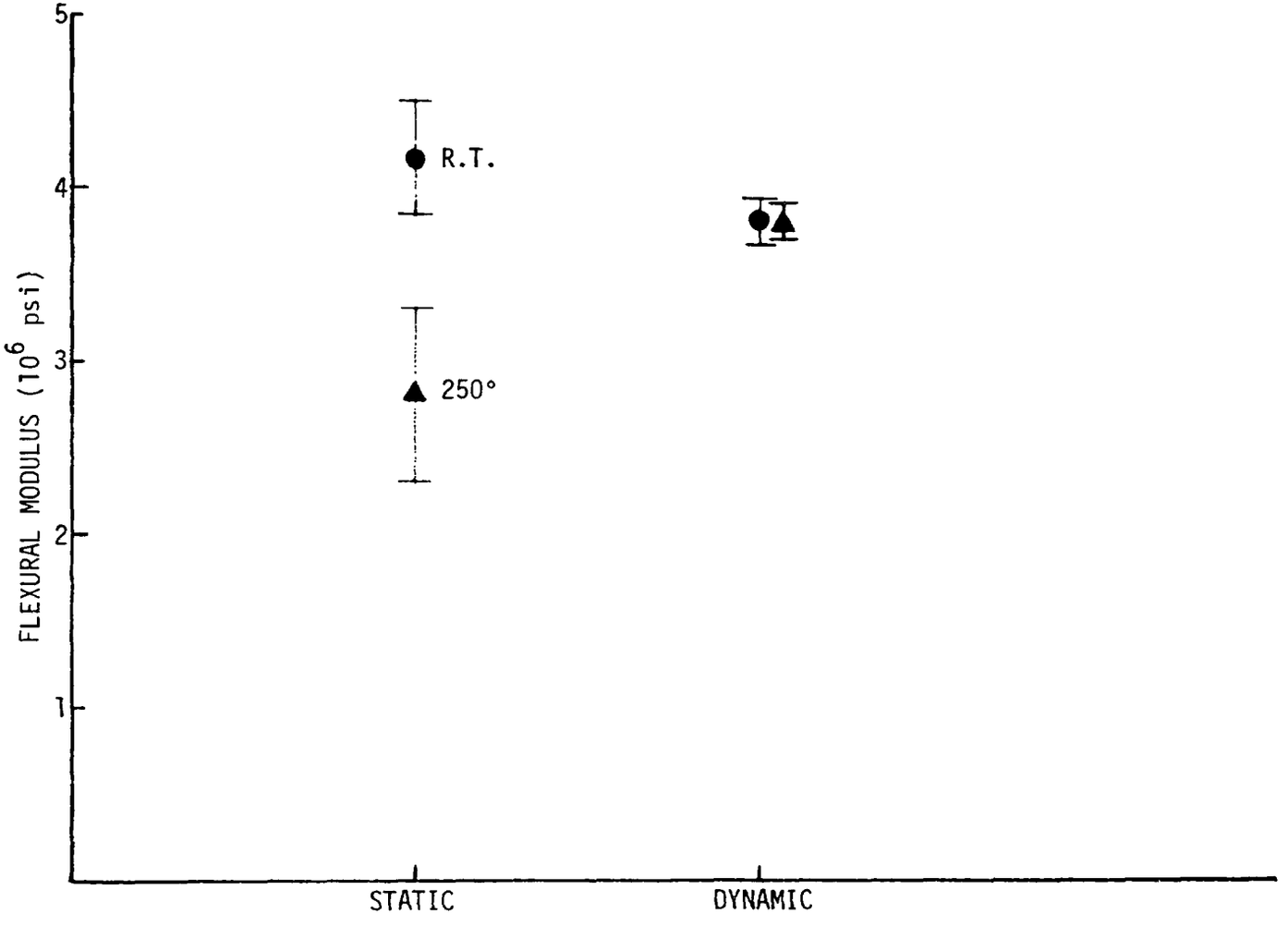

Figure 17. Flexural Modulus vs. $\dot{\epsilon}$ for $[\pm 45/0/90]_s$ Graphite Epoxy, 0° Orientation.

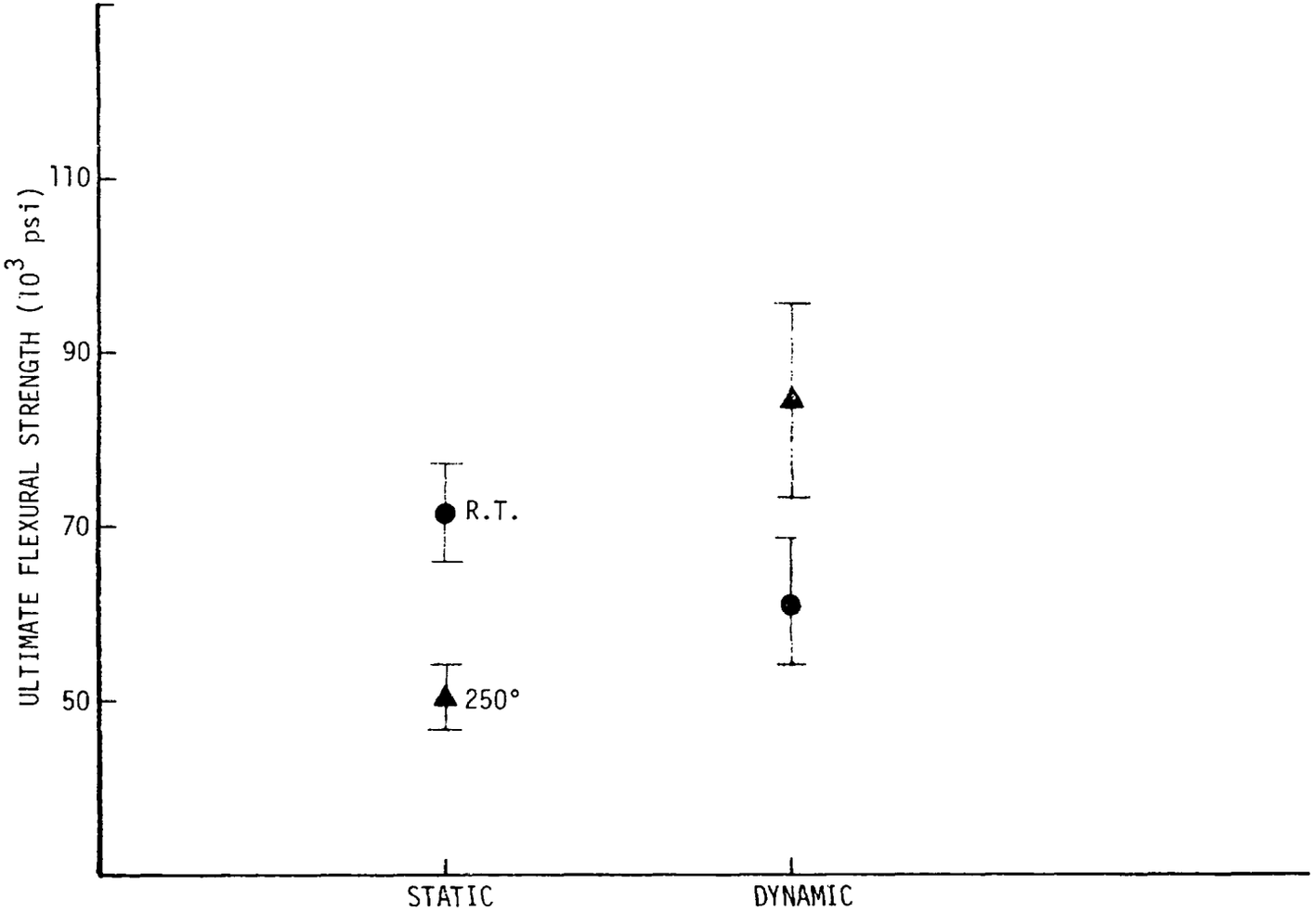

Figure 18. Flexural Strength vs. $\dot{\epsilon}$ for $[\pm 45/0/90]_s$ Graphite Epoxy, 90° Orientation.

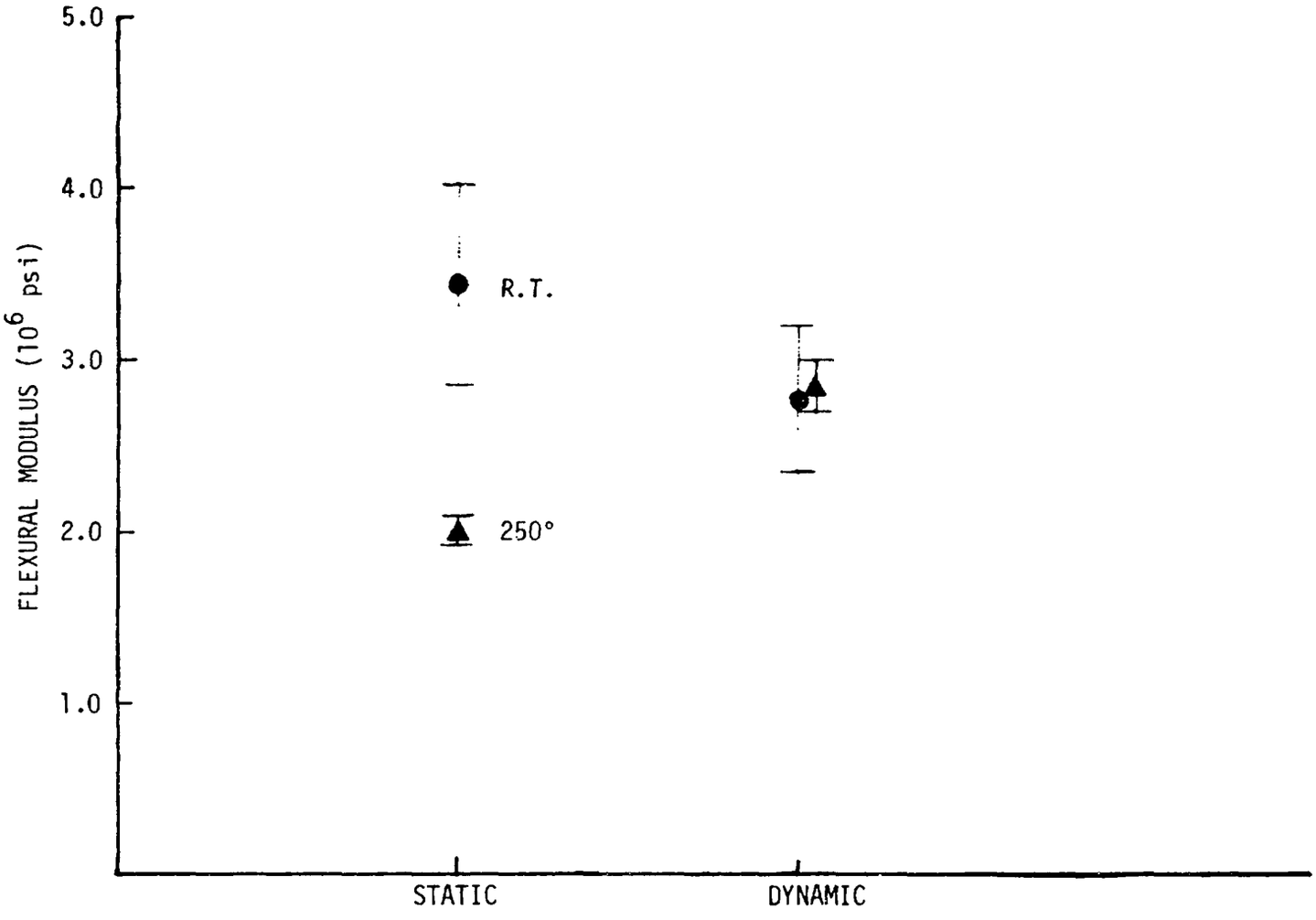

Figure 19. Flexural Modulus vs. $\dot{\varepsilon}$ for $[\pm 45/0/90]_s$, 90° Orientation.

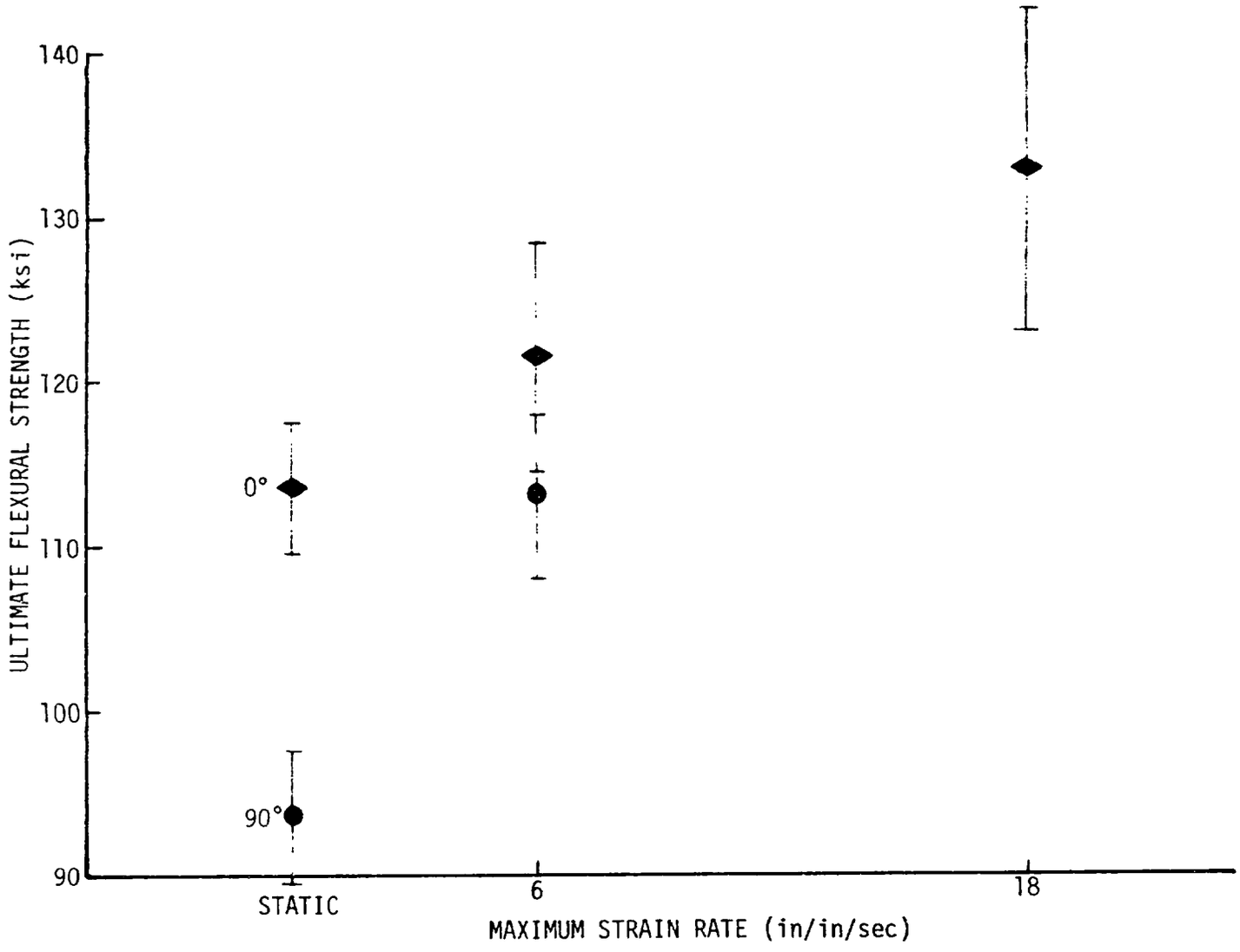

Figure 20. Ultimate Flexural Strength vs. Strain Rate - $[\pm 45/0/90]_{2s}$, R.T., 0° and 90°.

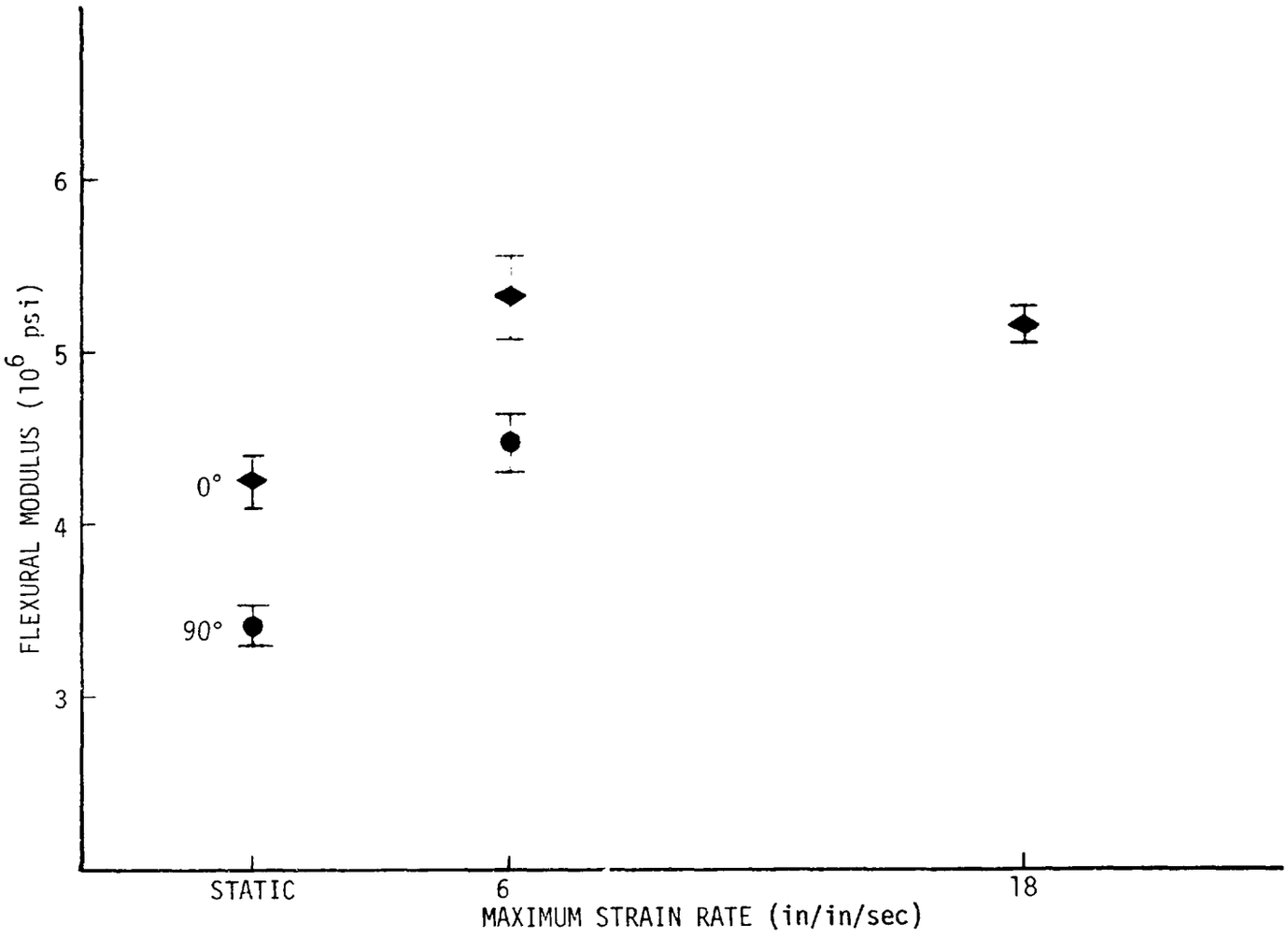

Figure 21. Flexural Modulus vs. Strain Rate $[\pm 45/0/90]_{2s}$, R.T., 0° and 90°.

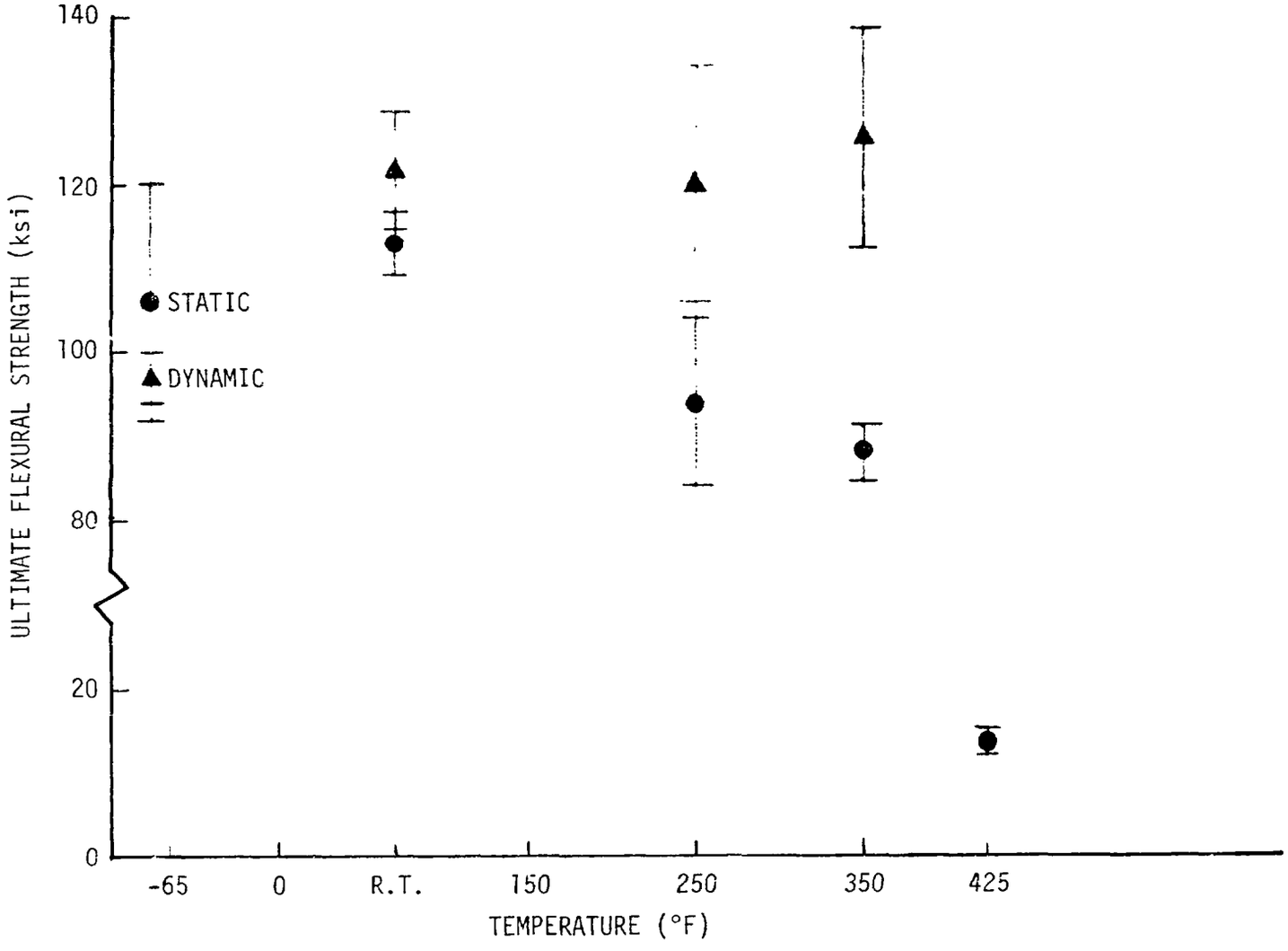

Figure 22. Ultimate Flexural Strength vs. Temperature, $[\pm 45/0/90]_{2S}$, 0°, Static and Dynamic.

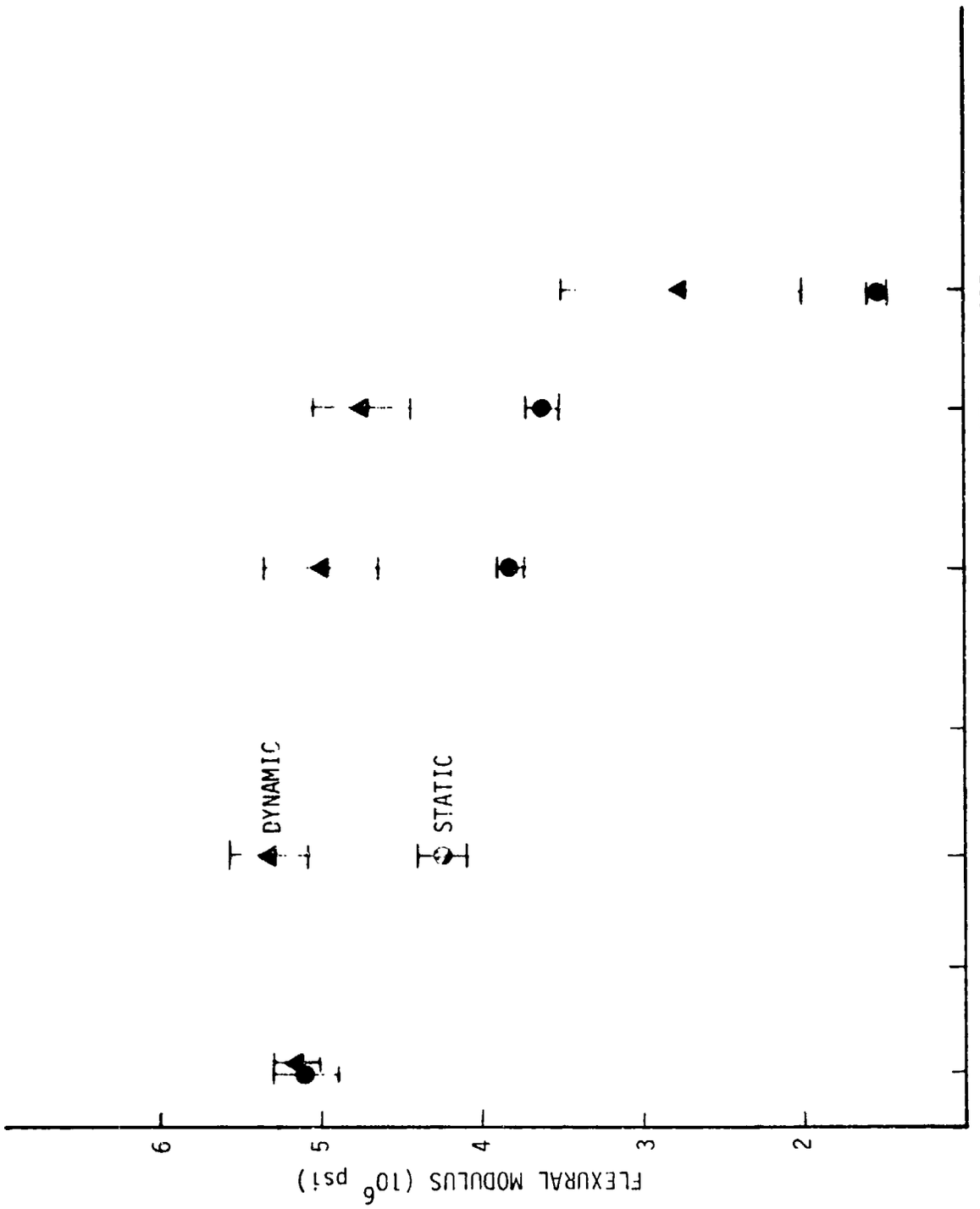

Figure 23. Flexural Modulus vs. Temperature $[\pm 45/0/90]_{2S}$, 0°, Static and Dynamic

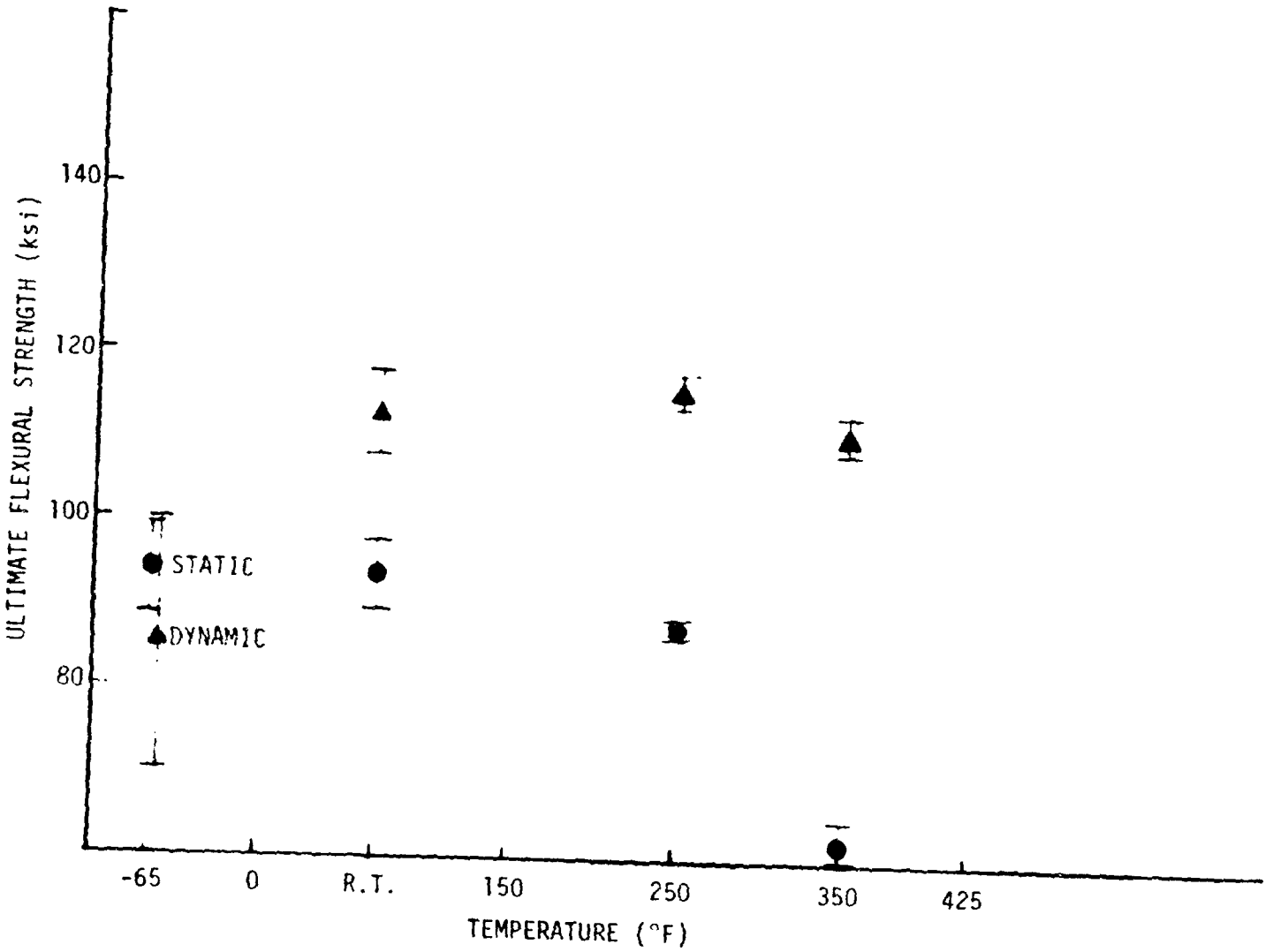

Figure 24. Ultimate Flexural Strength vs. Temperature, $[+45/0/90]_{2S}$, 90°, Static and Dynamic.

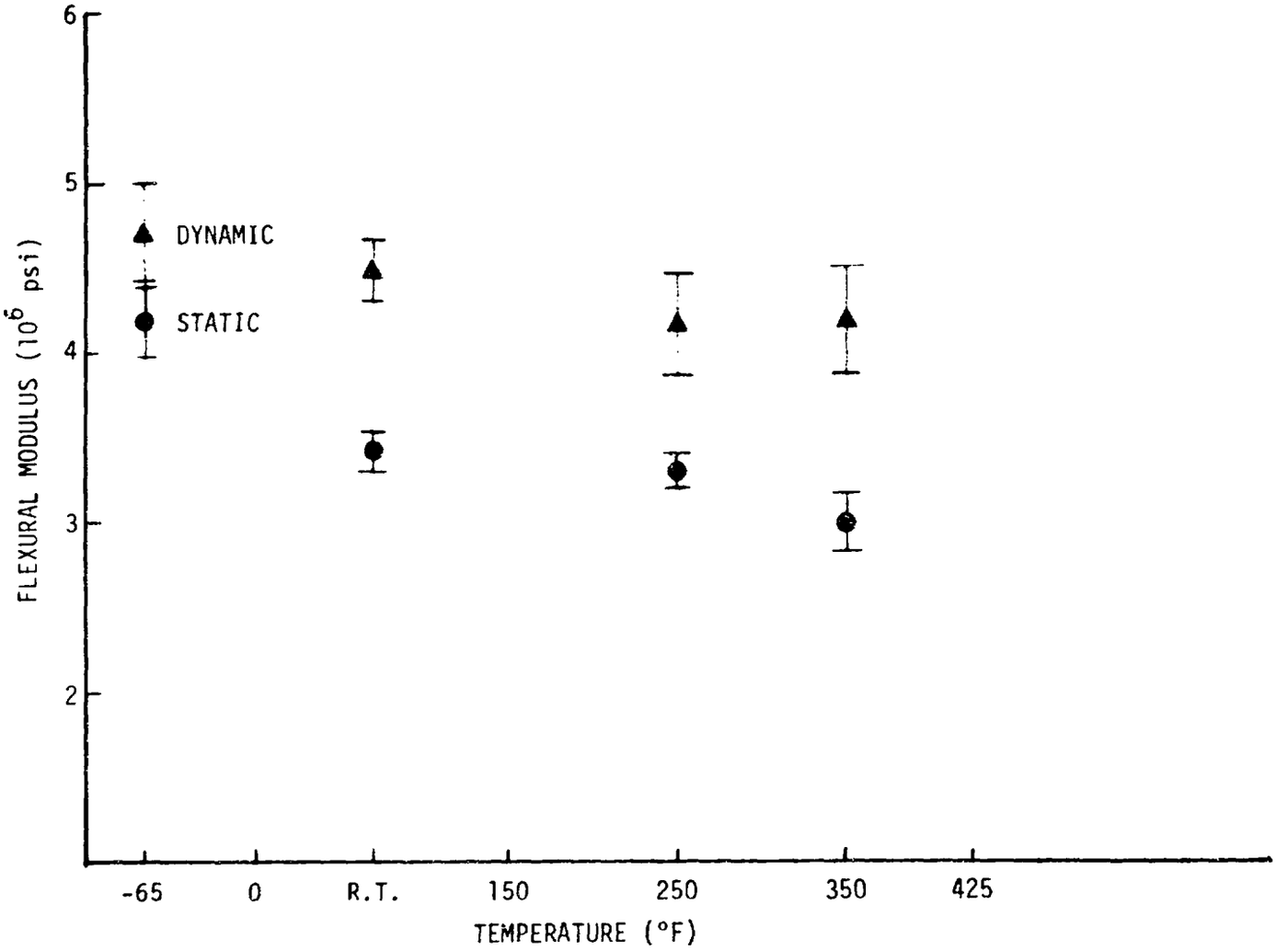

Figure 25. Flexural Modulus vs. Temperature, $[+ 45/0/90]_{2S}$, 90°, Static and Dynamic.

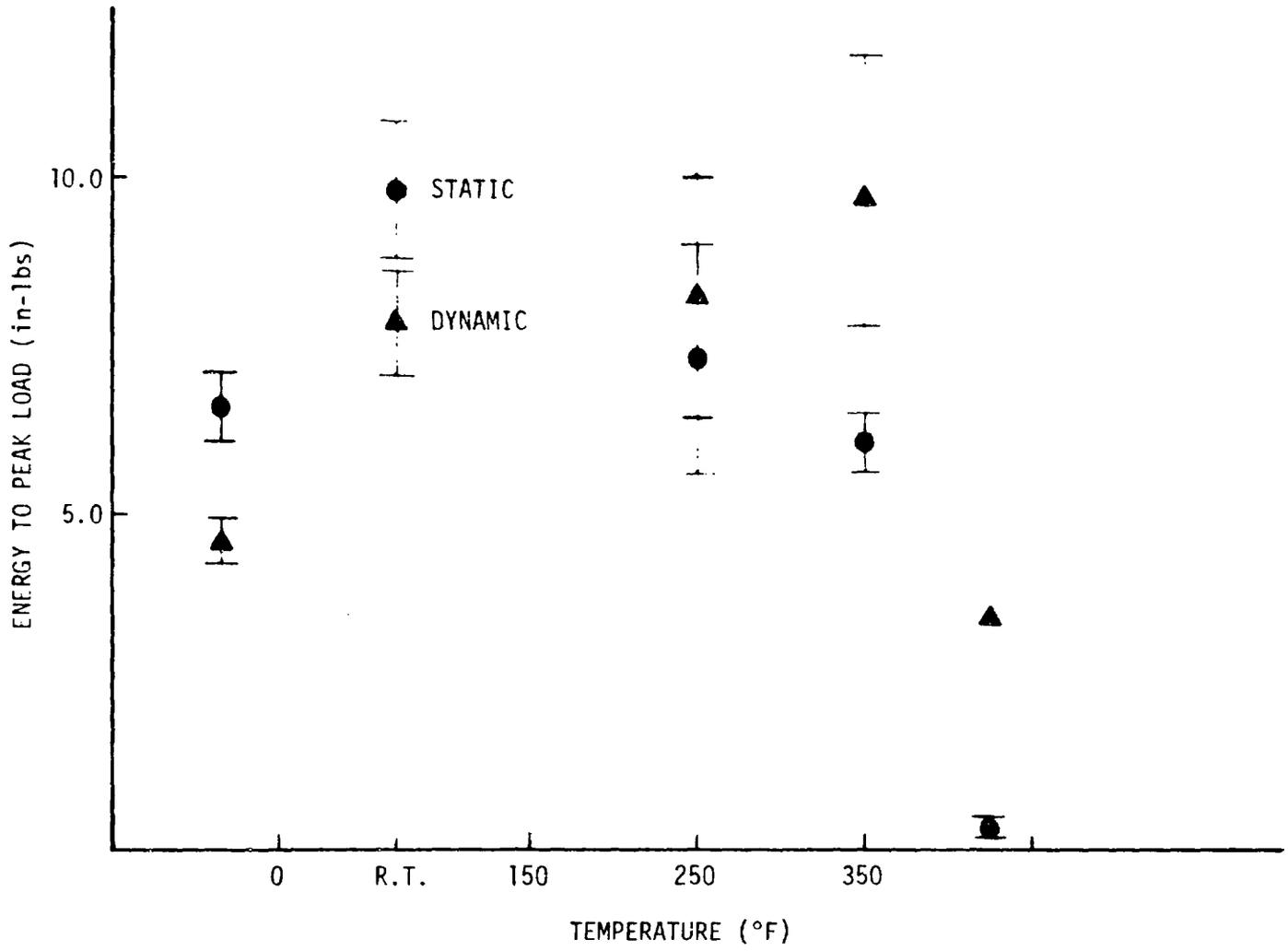

Figure 26. Energy to Peak Load vs. Temperature for $[\pm 45/0/90]_{2S}$ Graphite Epoxy, 0° Orientation.

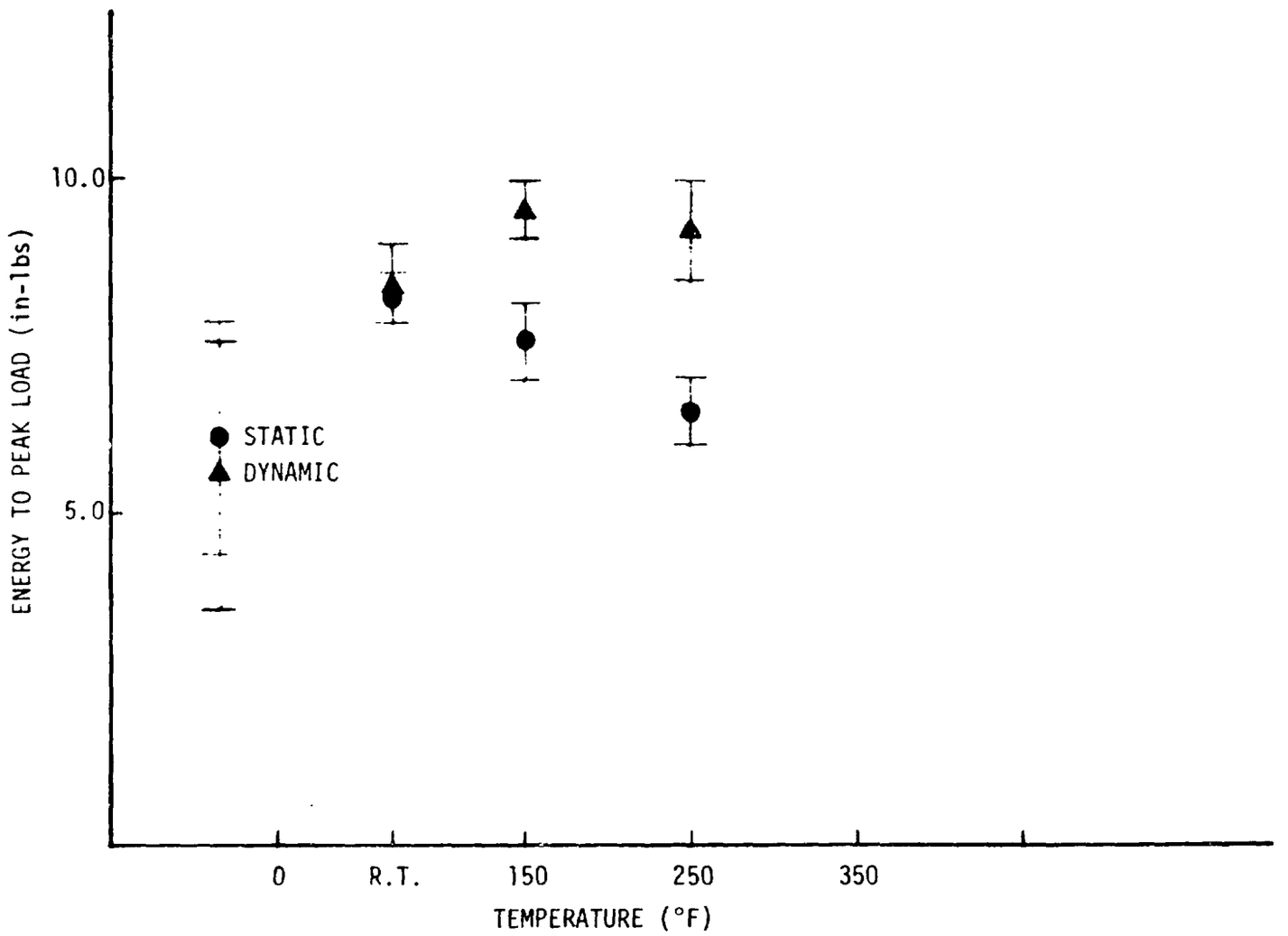

Figure 27. Energy to Peak Load vs. Temperature $[\pm 45/0/90]_{2S}$ Graphite Epoxy, 90° Orientation.

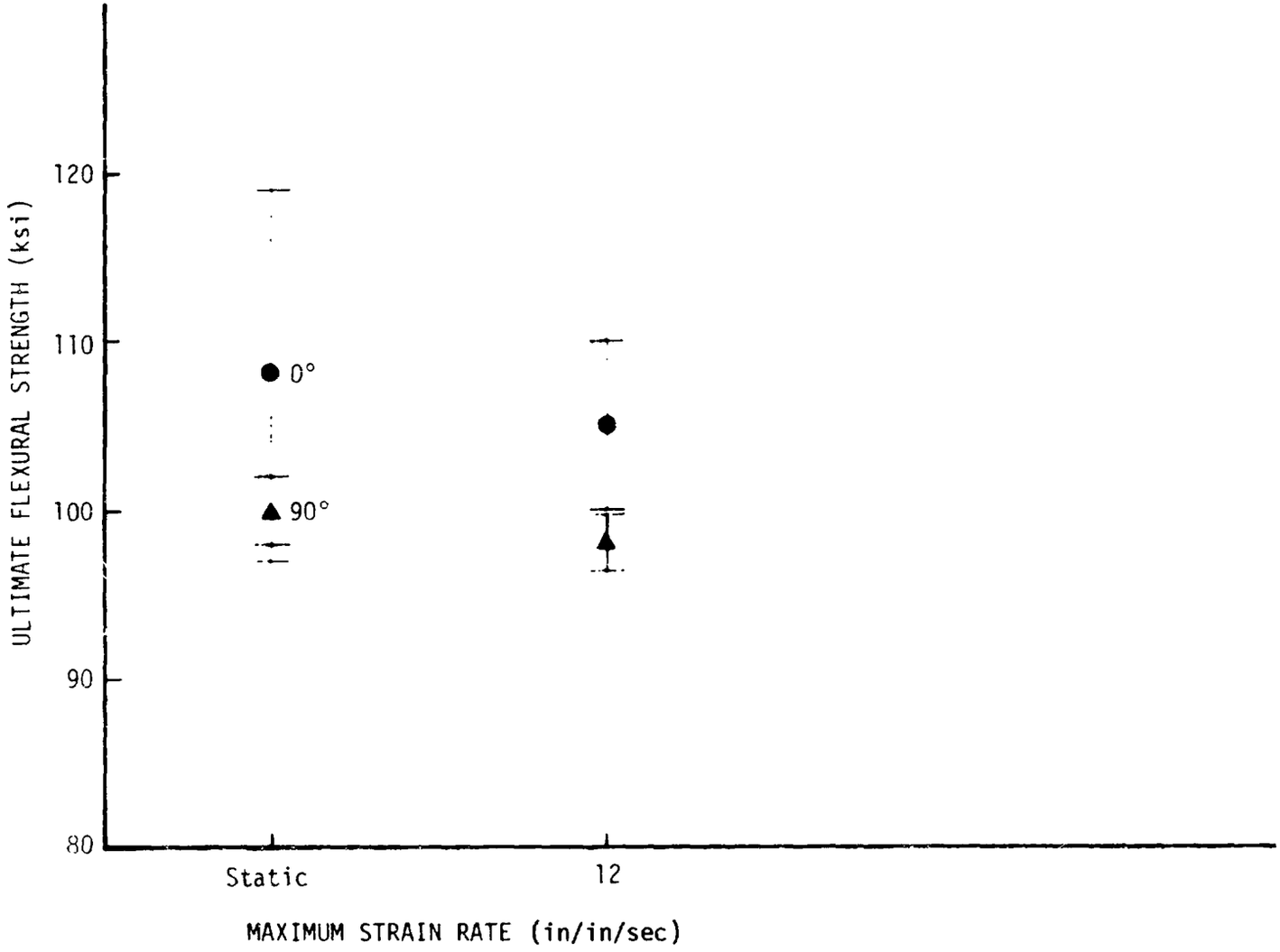

Figure 28. Ultimate Flexural Strength vs. Strain Rate for 32 ply $[+ 45/0/90]_{4S}$, Room Temperature.

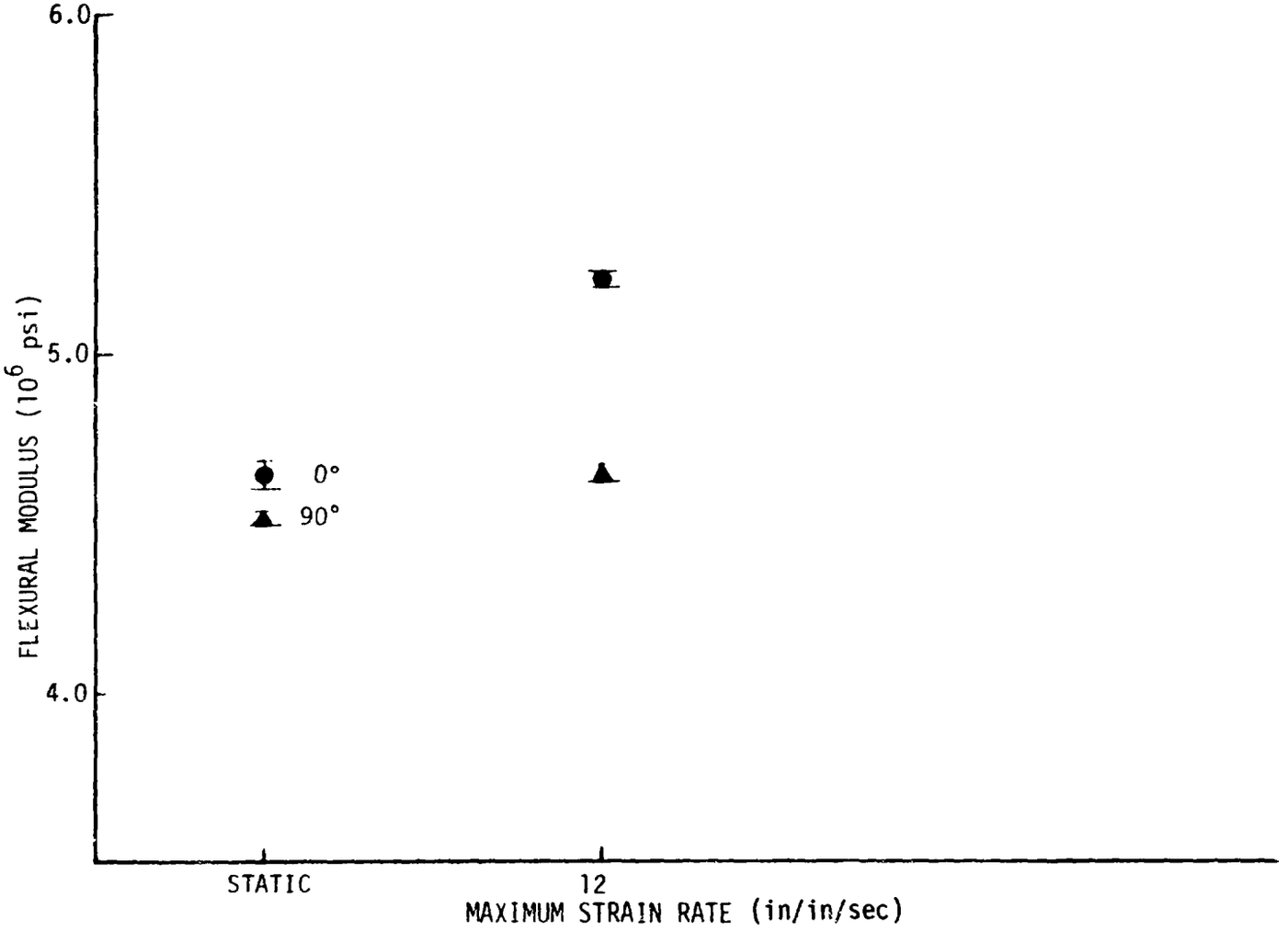

Figure 29. Flexural Modulus vs. Strain Rate for 32 ply $[\pm 45/0/90]_{4s}$, Room Temperature.

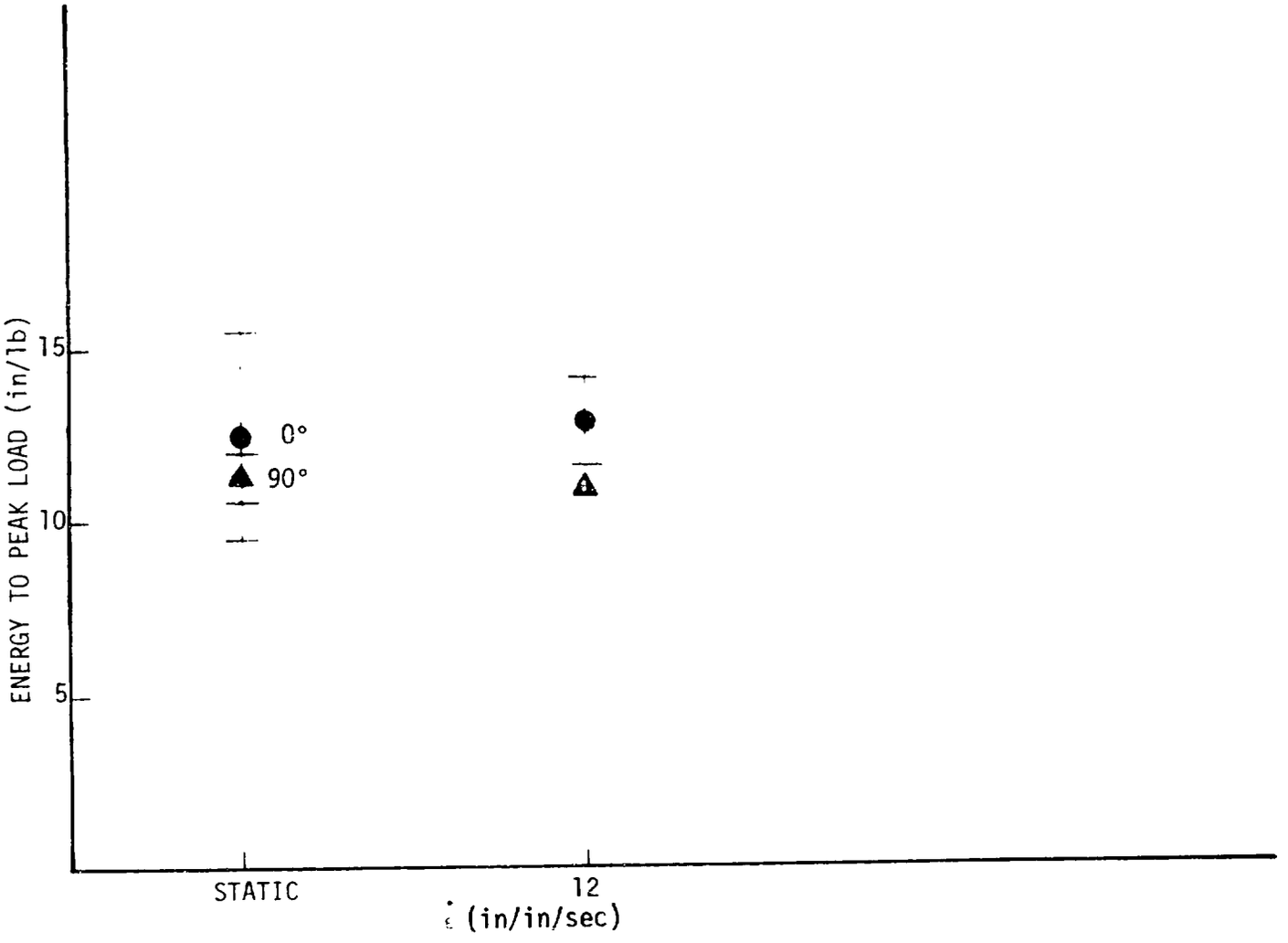

Figure 30. Energy to Peak Load vs. Strain Rate for $[\pm 45/0/90]_{4s}$, Graphite Epoxy, Room Temperature.

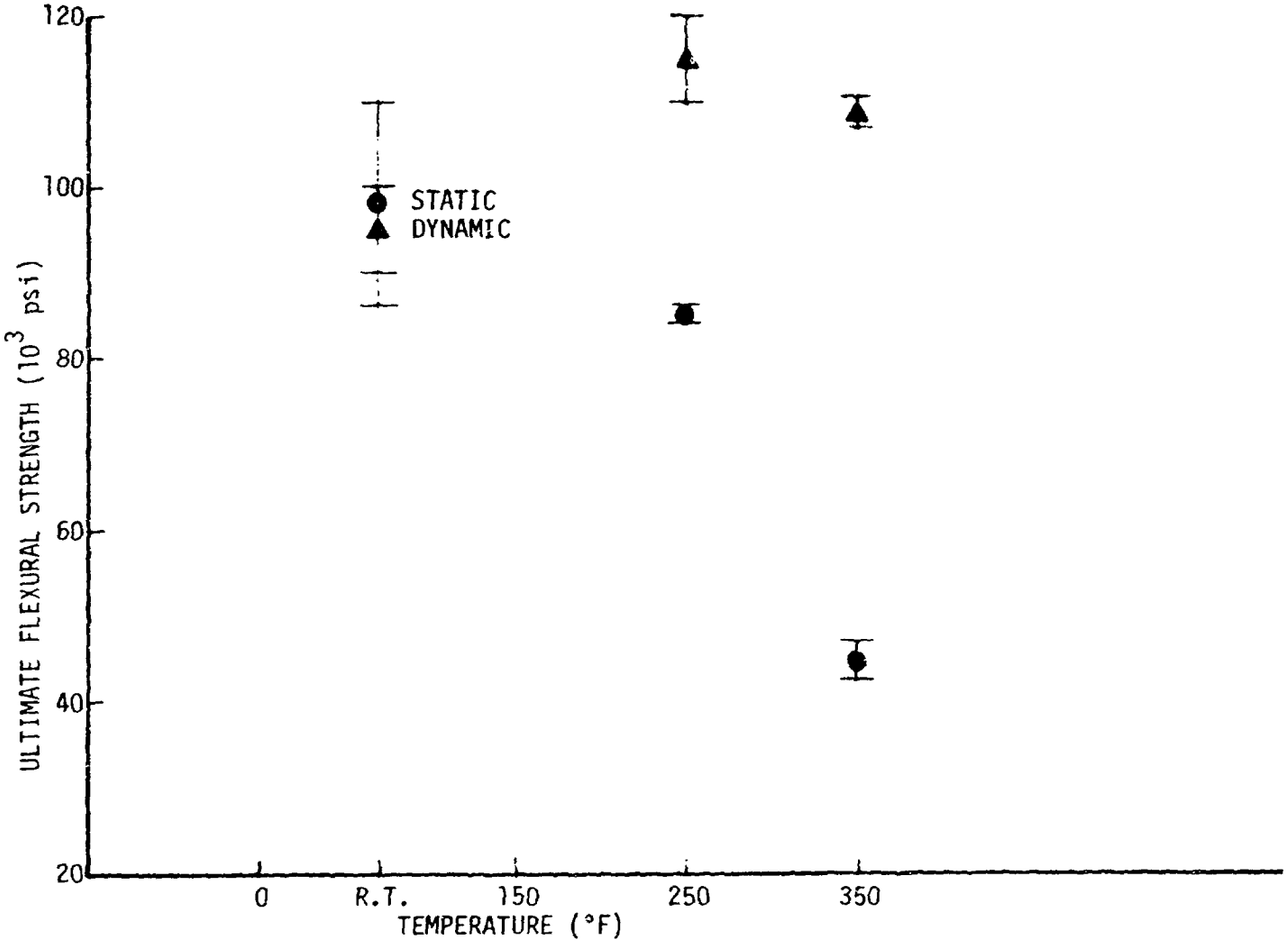

Figure 31. Ultimate Flexural Strength vs. Temperature for $[\pm 45/0/90]_{4s}$ Graphite Epoxy, 0° Orientation.

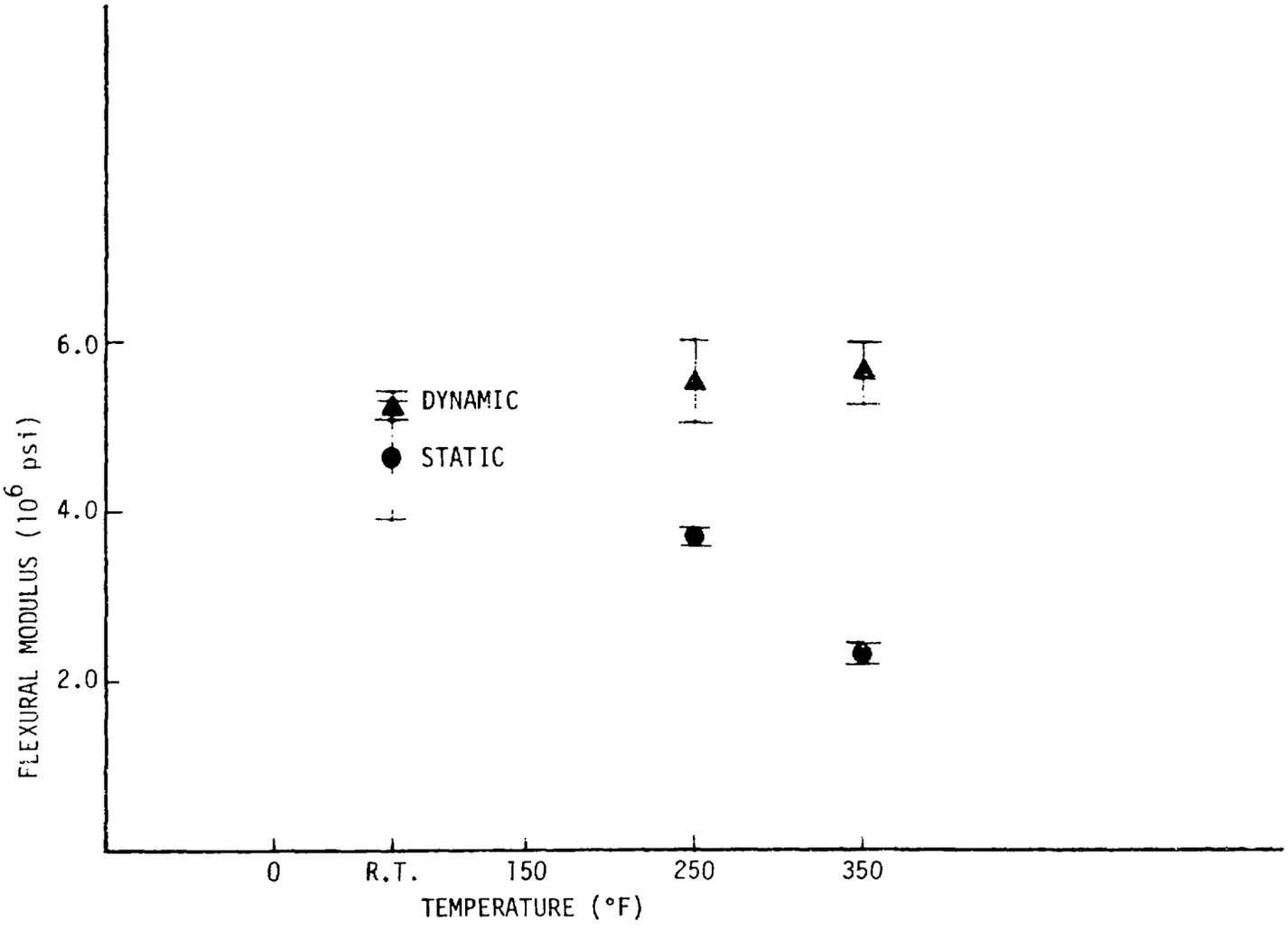

Figure 32. Flexural Modulus vs. Temperature for 0° $[+45/0/90]_{4s}$ Graphite Epoxy.

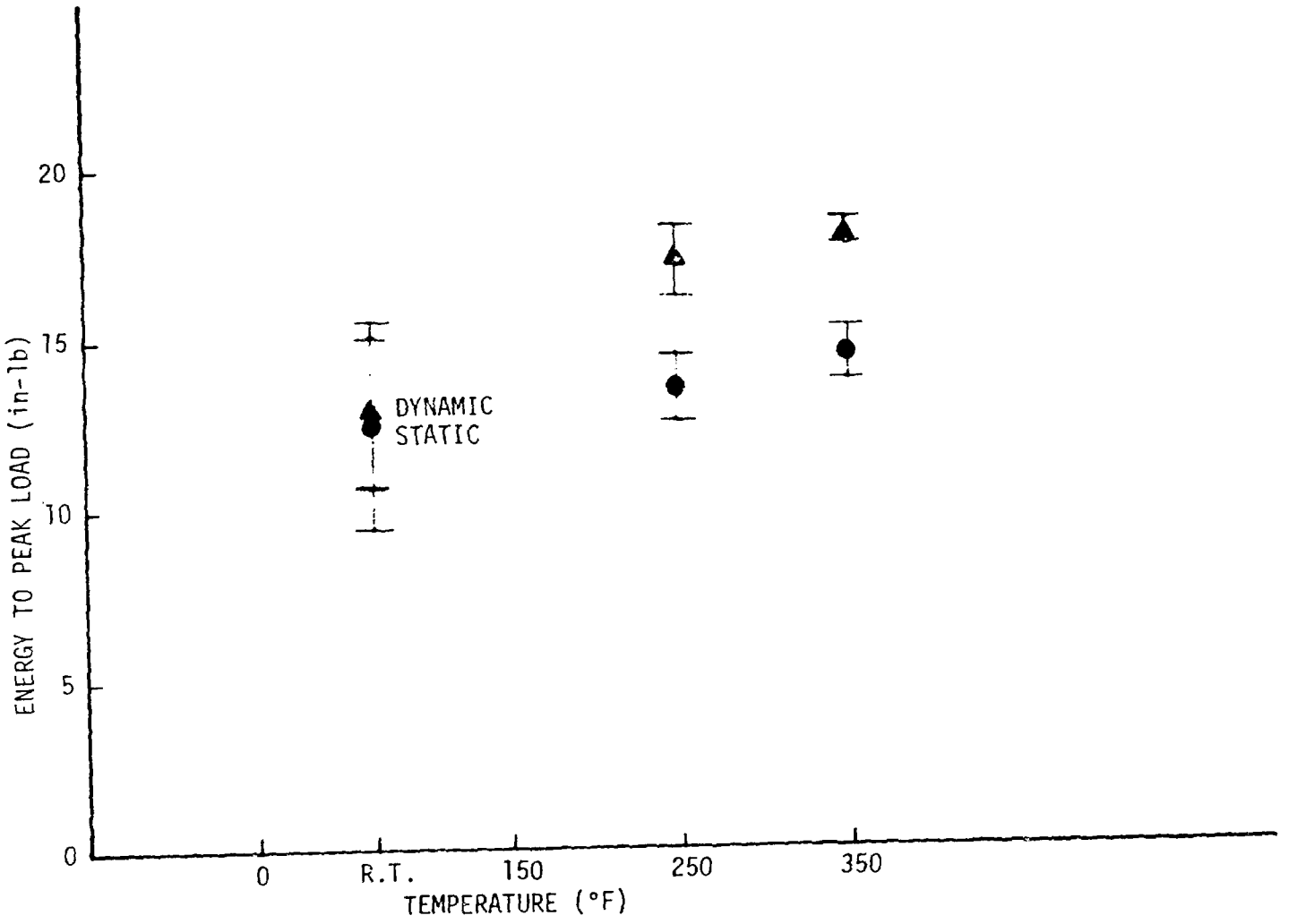

Figure 33. Energy to Peak Load vs. Temperature for $[+45/0/90]_{4s}$ Graphite Epoxy, 0° Orientation.

Comparisons between analytical predictions of flexural modulus and failure loads with experiment were made using the computer code AC-3. Load conditions corresponding to a unit load were used so that the calculated margins of safety could be directly interpreted as failure levels. Unidirectional ply properties given in Table 6 were used to calculate laminate values of flexural modulus. (The results of the flexural modulus correlation study are given in Table 8 and 9 for $[\pm 45/0/90]_{2s}$ and $[\pm 45/0/90]_{4s}$ graphite epoxy respectively.) The difference between the theoretical flexural modulus and the test derived values could be due to anisotropic material property coupling caused by the length to width ratio of the specimens. Similar results are reported in Reference 7. For these specimens the length to width ratio was 4.6 and from Reference 7, a moderate to severe coupling effect may be expected.

Experimental static properties and MDAC ultimate strengths were used with AC-3 to compare yield and failure loads with experimental values. Static experimental results were used because the yield point can be more accurately determined from the static load trace than from the dynamic trace. Table 10 presents the results of this study for $[\pm 45/0/90]_{2s}$ AS/3501-6 graphite epoxy. The loads to yield are in good agreement for both the 0° and 90° specimens while the peak loads predicted analytically are higher than the experimental values. This is expected due to the nature of the model. Specifically, once yield has occurred the model has no mechanism for accounting for load redistributions. If an extreme outer layer yields, it can be removed in the model and a reduced thickness material can be treated. In this case, however, the yield occurs at an inner fiber (the 0° oriented fibers), so that it cannot be removed. Therefore, the agreement between analysis and experiment on yield is reasonable, but from that point on the model should predict higher peak loads than the experiment shows. Table 11 presents the results of a similar study for AS/3501-5 $[\pm 45/0/90]_{4s}$ graphite epoxy. It is important to remember that 1) no unidirectional AS/3501-5 was tested in this program, so, for this analysis, the experimentally obtained AS/3501-6 unidirectional properties

Table 8. Flexural Modulus Correlation Study for $[\pm 45/0/90]_{2S}$ Graphite Epoxy

0° ORIENTATION

	QUASISTATIC (RT/350°F) 10^6 psi	DYNAMIC (RT/350°F) 10^6 psi	MDAC (RT/350°F) 10^6 psi
CALCULATED	5.58/3.63	5.39/--	6.84/5.81
TEST	4.26/3.74	5.33/4.75	---

90° ORIENTATION

	QUASISTATIC (RT/350°F) 10^6 psi	DYNAMIC (RT/350°F) 10^6 psi	MDAC (RT/350°F) 10^6 psi
CALCULATED	4.75/2.99	4.59/--	5.83/4.85
TEST	3.41/2.98	4.47/4.18	---

Table 9. Flexural Modulus Correlation Study for $[\pm 45/0/90]_{4S}$ Graphite Epoxy

0° ORIENTATION

	QUASISTATIC (RT/350°F) 10^6 psi	DYNAMIC (RT/350°F) 10^6 psi	MDAC (RT/350°F) 10^6 psi
CALCULATED	6.00/3.92	5.69/--	7.48/6.49
TEST	4.64/2.34	5.23/5.63	---

90° ORIENTATION (RT only)

	QUASISTATIC 10^6 psi	DYNAMIC 10^6 psi	MDAC 10^6 psi
CALCULATED	5.5	5.21	6.85
TEST	4.51	4.64	----

Table 10. Comparison of Analytical and Experimental Results for $[\pm 45/0/90]_{2s}$ Graphite Epoxy using 'scaled' MDAC ultimate strengths for 350° results

0° ORIENTATION

	AC-3 (RT/350°)	EXPERIMENT (RT/350°)
P yield Static (lb)	77.1/45.2 (1)	65.5/51
P max (lb)	171 (2) /139 (2)	126.3/104
E flex (10^6 psi)	5.58/3.63	4.22/3.74

(1) Matrix failure bottom 45° ply
(2) Fiber failure extreme 0° ply

90° ORIENTATION

	AC-3 (RT/350°)	EXPERIMENT (RT/350°)
P yield Static (lb)	60.2 (3) /39.1 (5)	68/60
P max (lb)	177.3 (4) /64.2 (6)	113.6/96.6
E flex (10^6 psi)	4.75/2.39	3.41/2.98

(3) Matrix failure bottom 0° ply
(4) Fiber failure extreme 90° ply
(5) Matrix failure bottom 45° ply
(6) Fiber compression failure top 0° ply

Table 11. Comparison of Analytical and Experimental Results for AS/3501-5 $[\pm 45/0/90]_{4s}$ Graphite Epoxy Using 'Scaled' MDAC AS/3501-6 Ultimate Strengths for 350° Result

0° ORIENTATION

	AC-3 (RT/350°)	EXPERIMENT (RT/350°)
P Yield Static (lb)	270(1)/204(3)	370/170
P max (lb)	600(2)/227(4)	483/225
E Flex (10^6 psi)	6.00/3.92	4.64/2.34

(1) Matrix failure bottom 90° ply
(2) Fiber failure bottom 0° ply
(3) Matrix failure bottom 45° ply
(4) Fiber failure top 0° ply

90° ORIENTATION (RT only)

	AC-3	EXPERIMENT
P Yield Static (lb)	226(5)/ --	303/ --
P max (lb)	592(6)/ --	454/ --
E flex (10^6 psi)	5.5/ --	4.51/ --

(5) Matrix failure bottom 90° ply
(6) Fiber failure bottom 0° ply

angles measured with respect to long axis of specimen

were used, 2) no ultimate strengths for AS/3501-5 were available so the AS/3501-6 MDAC properties were used, 3) the MDAC room temperature ultimate strengths were scaled to 350°F as described previously and any differences in cure temperatures would not be accounted for.

4.3 FATIGUE AND LOW BLOW TESTS

Three point bend specimens of AS/3501-6 graphite epoxy in the $[\pm 45/0/90]_{2s}$ configuration were fatigue cycled using a maximum free end deflection of 0.050 inch. The corresponding midspan stress was calculated to be 18,000 psi, which is approximately 20% of the ultimate stress. Specimens were subjected to 10^6 cycles which was felt to be a reasonable number of cycles for these tests. Two specimens were then tested quasi-statically to failure and the strength ratio of cycled to non-cycled material was 1.07. For a specimen cycled and then tested dynamically the strength ratio was 0.9. After cycling, still another specimen was subjected to limited deflections corresponding to 40% and 80% of the peak load and the strength ratio was 1.02. Such results imply that graphite epoxy is not sensitive to flexural fatigue. Similar results are shown in Reference 10 which also reports no reduction in strength in notched speciments that were subsequently cycled at 80% of static ultimate.

Low blow tests also resulted in no strength reduction. One specimen, subjected to deflections corresponding to 40% and 80% of peak load showed a strength increase of 9%. Another specimen subjected to the dynamic loading sequence of:

1. Deflection corresponding to 40% of peak load three times;
2. Deflection corresponding to 80% of peak load three times;
3. Failed

exhibited a strength increase of 4%. The coefficient of variation for the strength of material not subjected to limited deflection testing was 5% so the increases noted above are not significant.

4.4 THERMAL FLASH FACILITY SPECIMEN TEST RESULTS

Two 4.0" x 4.5" panels of $[\pm 45/0/90]_{2s}$ graphite epoxy had a .020 inch thick sheet of cork-silicone bonded to one surface by AVCO and were exposed in the AFML thermal flash facility. One flat was exposed at a temperature below the cure temperature and one above. One thermocouple was attached to the specimen front surface but under the cork-silicone, and five to the back surface. The temperature distribution across the back surface was not uniform due to a slight air flow in the test facility which is present only to clear debris injected by the specimen. The specimen designated E1 was exposed below cure temperature. The exposed surface reached 610°F and the average rear surface temperature was 284°F. Thermocouple data for specimen E2 exposed above the graphite epoxy cure temperature have not yet been received. Specimens were cut from these panels and as much of the thermal protective coating as possible was removed. The specimens were then tested at room temperature, quasi-statically and dynamically, some with the coated side in tension and others with the non-coated side in tension. Table 12 gives the results of these tests and compares them with virgin, or unexposed specimens. No significant differences in strength, absorbed energy or modulus were observed.

4.5 SHEAR PLUG TEST RESULTS

Shear plug tests were performed on 16-ply unidirectional and $[\pm 45/0/90]_{2s}$ AS/3501-6 graphite epoxy. Figures 34 and 35 summarize the results of these tests. For both configurations the maximum shear strength decreased with temperature and increased slightly for dynamic loading conditions.

4.6 VALIDITY OF DYNAMIC DATA

The validity of using a static analysis for analyzing the dynamic

Table 12. Comparison of Virgin and Thermal Flash Specimen Test Results for Graphite Epoxy

$\dot{\varepsilon}$	Specimen	Ultimate Flexural Strength (10^3psi)	Energy to Peak Load (in lb.)	Flexural Modulus (10^6psi)
Static	Unexposed	114 ± 4	9.9 ± 1.0	4.3 ± .20
Static	E1-UCSI	107 ± 8	9.6 ± 1.3	3.9 ± .2
Static	E1-CSI	109 ± 3	10.5 ± .6	4.0 ± .2
Static	E2-UCSI	110 ± 3	10.1 ± 1.1	4.0 ± .1
Static	E2-CSI	114 ± 7	11.1 ± 1.2	3.8 ± .4
Dynamic	Unexposed	122 ± 7	7.9 ± .7	5.3 ± .3
Dynamic	E1-UCSI	113 ± 7	11.0 ± 2	5.0 ± .1
Dynamic	E1-CSI	124 ± 8	9.1 ± .8	5.7*
Dynamic	E2-UCSI	129 ± 4	9.7 ± 1.3	5.0
Dynamic	E2-CSI	122 ± 6	8.9 ± 1.1	5.5*

* calculation done for one specimen only

UCSI uncoated side impacted
CSI coated side impacted

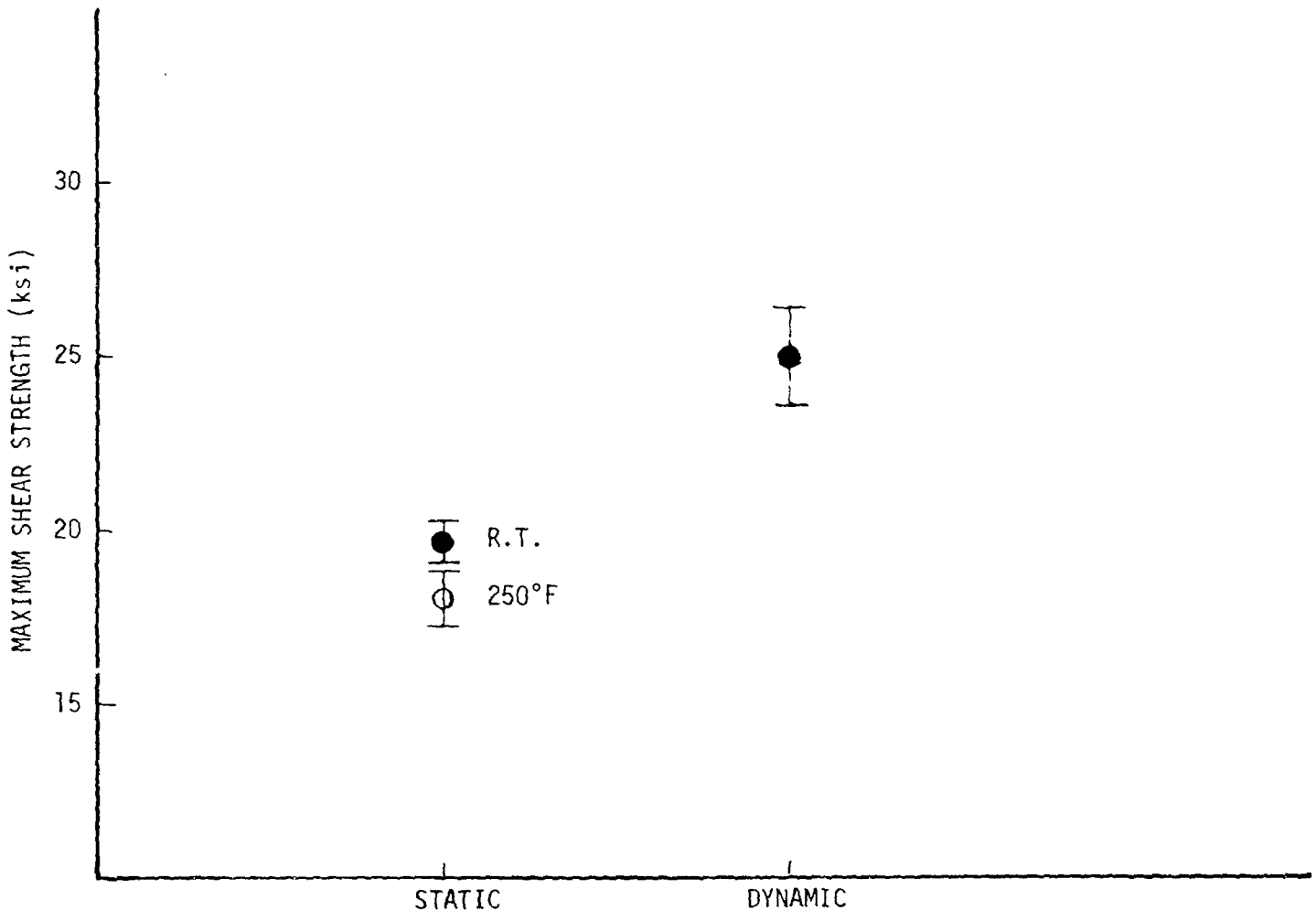

Figure 34. 16 ply Unidirectional Graphite Epoxy Shear Plug Test Results.

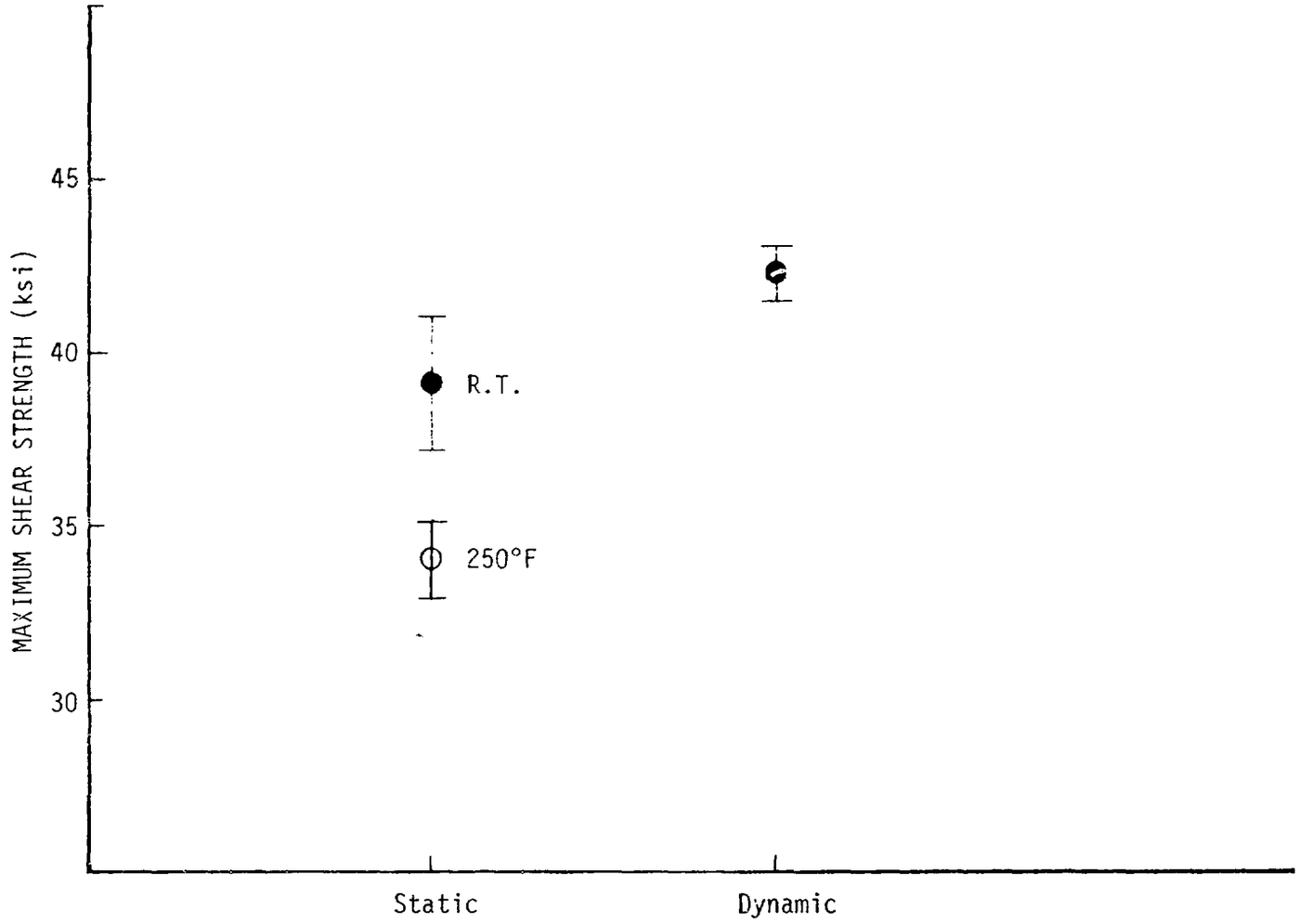

Figure 35. $[\pm 45/0/90]_{2S}$ Graphite Epoxy Shear Plug Test Results.

three point bend test has, in the past, been questioned. The question arises because of the possibility that dynamic loading conditions could induce higher bending modes that would invalidate the static analysis techniques. In order to verify the linearity of the response of a specimen undergoing dynamic loading, four specimens were instrumented with strain gages and subjected to dynamic three point bend tests. Each strain gage was mounted in the center of the specimen so as to be as nearly as possible under the point of impact. The output from the strain gage was compared to the theoretical strain in the extreme fibers at midspan given by

$$\varepsilon_{Theoretical} = \frac{1.5\ P\ell}{E\ bh^2}$$

where P is the load and E is the modulus obtained from the load-time trace.

Two of the specimens in this investigation were 16-ply unidirectional graphite epoxy with a 0° orientation. A representative strain-time output is shown in Figure 36. Note that the strain is linear to failure and that no higher order modes are apparent. Comparisons of theoretical and experimental results are given in Figures 37 and 38. The theoretical strain, given by the crosshatched region, was calculated using the nominal test determined modulus with the coefficient of variation of the Young's modulus for this material obtained in previous tests. The slight deviation of the experimental line from the theoretical region may be due to an offset of the strain gage from the exact impact location. Again the linearity of the results is obvious thus confirming the applicability of a static analysis.

The remaining two specimens were 16-ply graphite epoxy in the twice symmetric configuration or $[\pm 45/0/90]_{2s}$ lay-up. A representative strain gage output is shown in Figure 39. The linearity of the strain response is again apparent. Figures 40 and 41 show that the experimental and theoretical results are in good agreement.

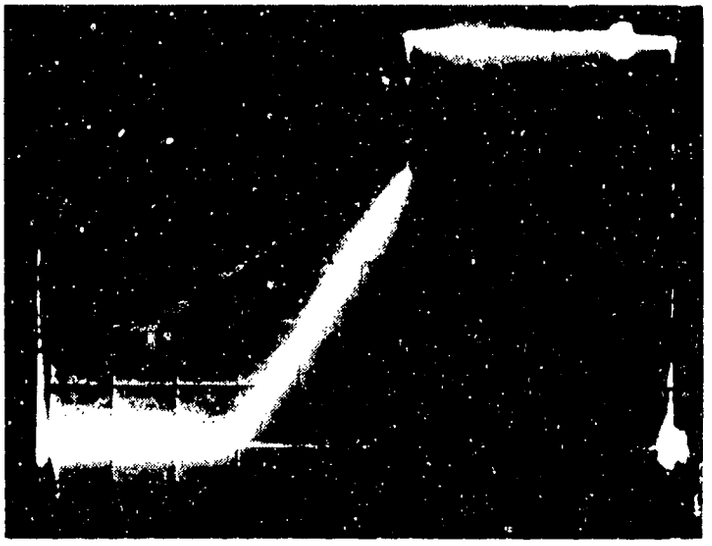

Figure 36. Strain-Time Output from Strain Gage for 16 Ply Unidirectional Graphite Epoxy, 0° Orientation.

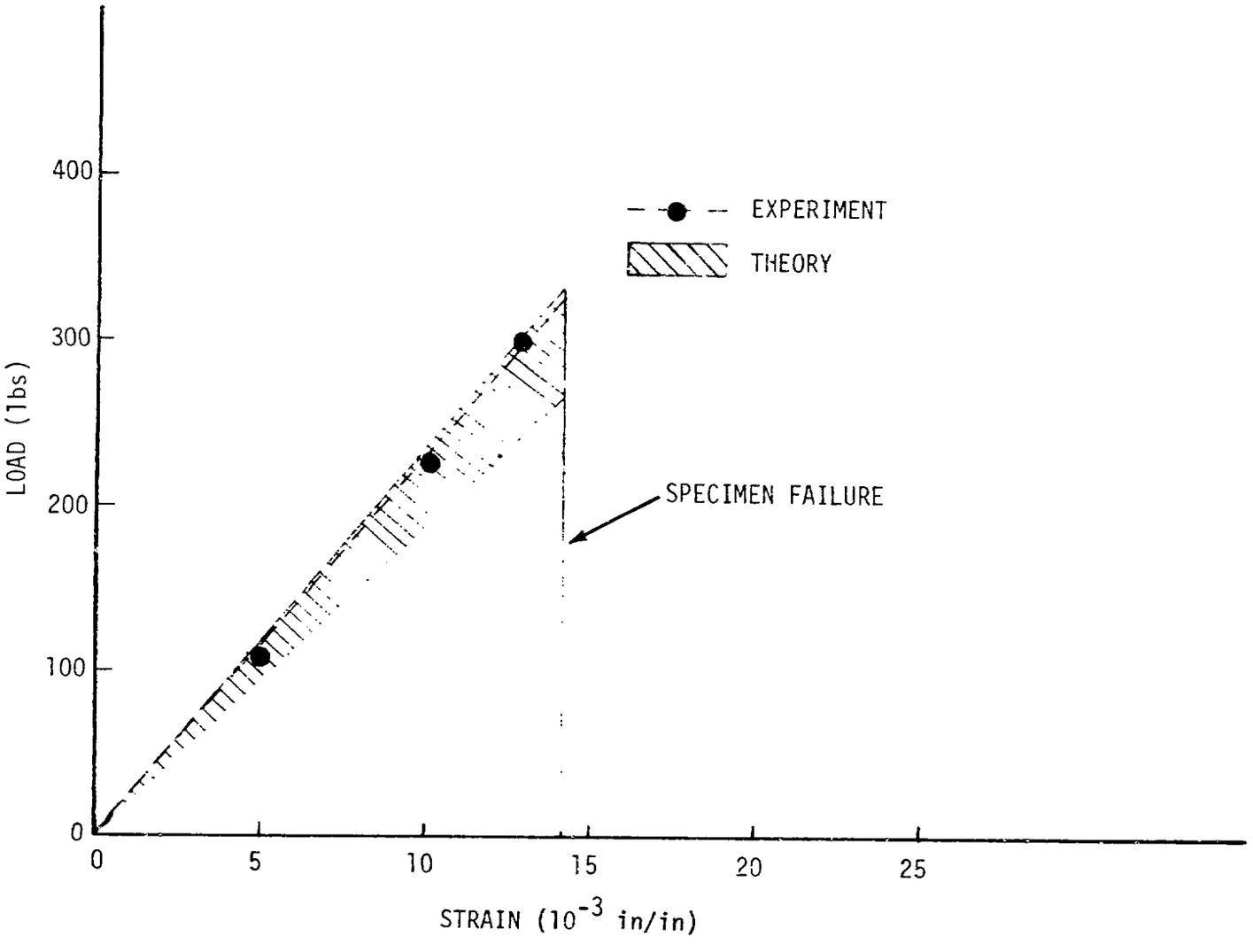

Figure 37. Comparison of Theoretical and Experimental Results for Strain-Gaged Graphite Epoxy 16 ply Unidirectional 0° Specimen.

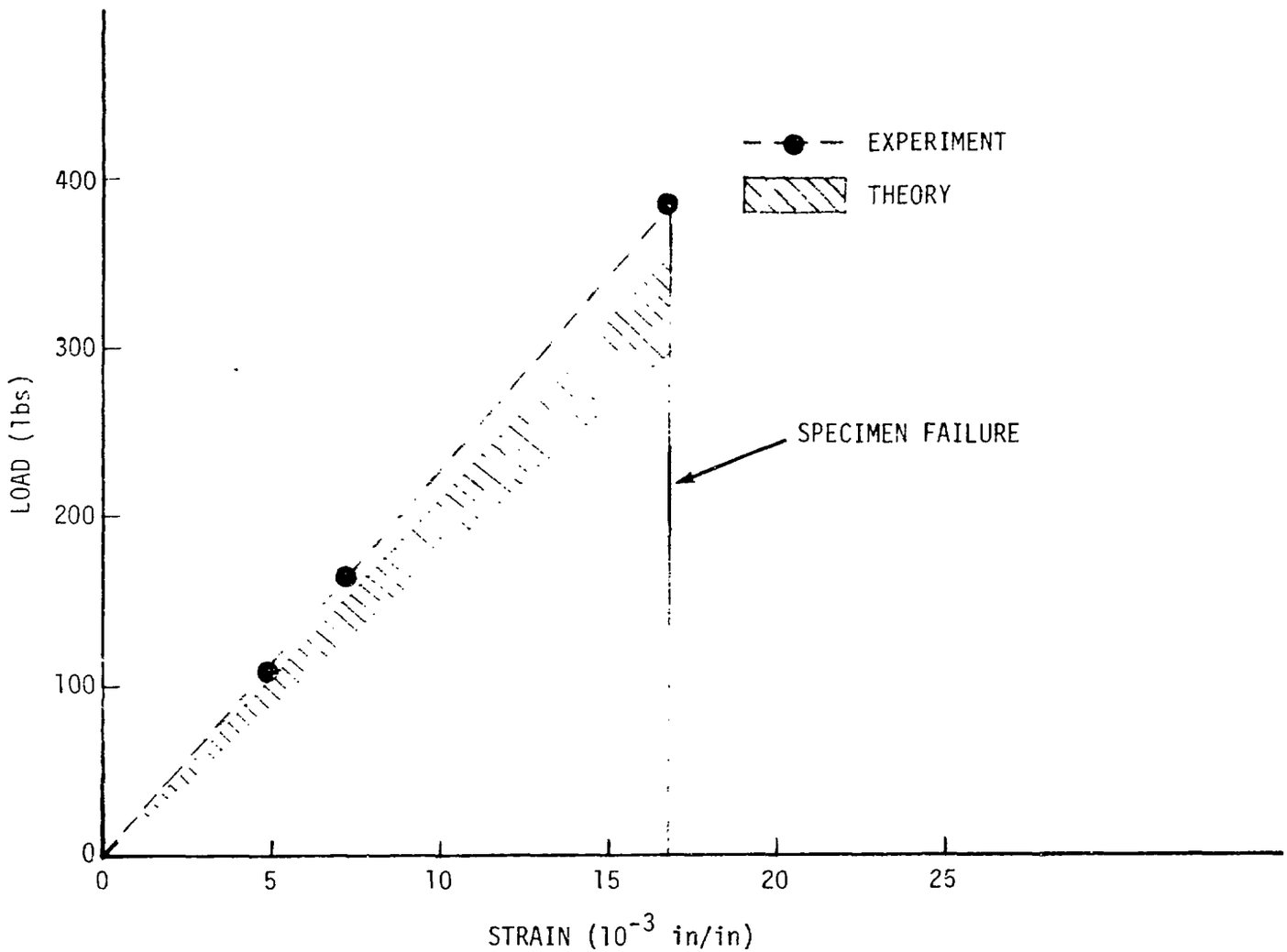

Figure 38. Comparison of Theoretical and Experimental Results for Strain-Gaged Graphite Epoxy 16 ply Unidirectional 0° Specimen.

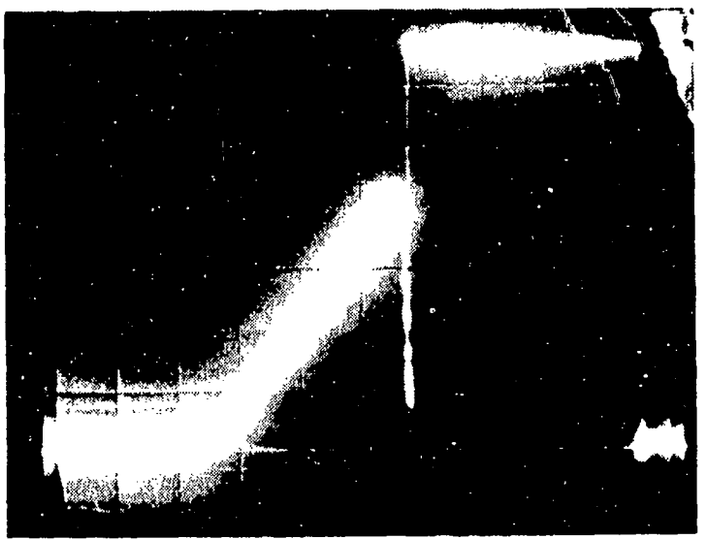

Figure 39. Strain-Time output from Strain Gage for $[\pm 45/0/90]_{2S}$ Graphite-Epoxy, 0° Orientation.

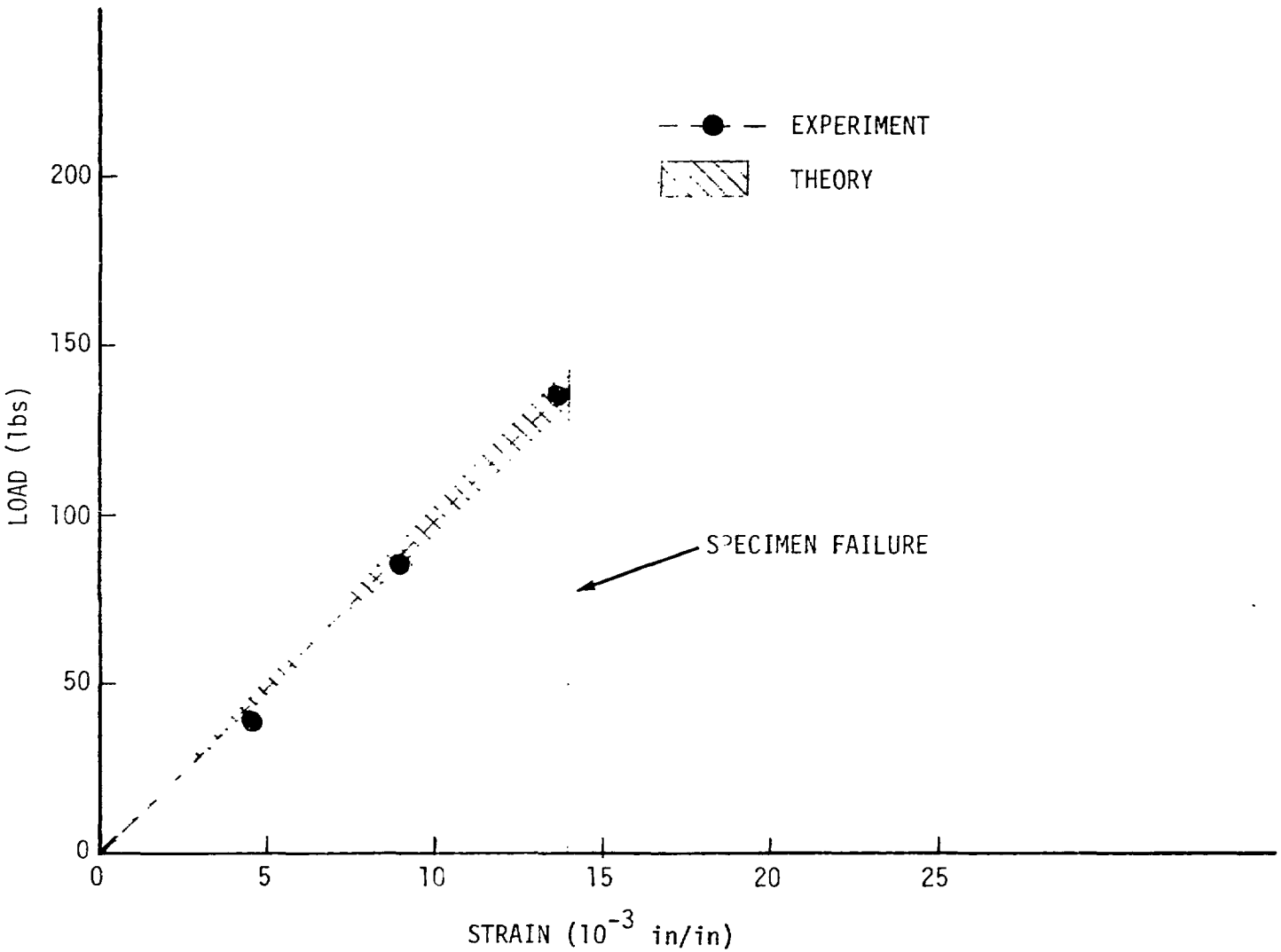

Figure 40. Comparison of Theoretical and Experimental Results for Strain-Gaged Graphite Epoxy $[\pm 45/0/90]_{2S}$ Specimen.

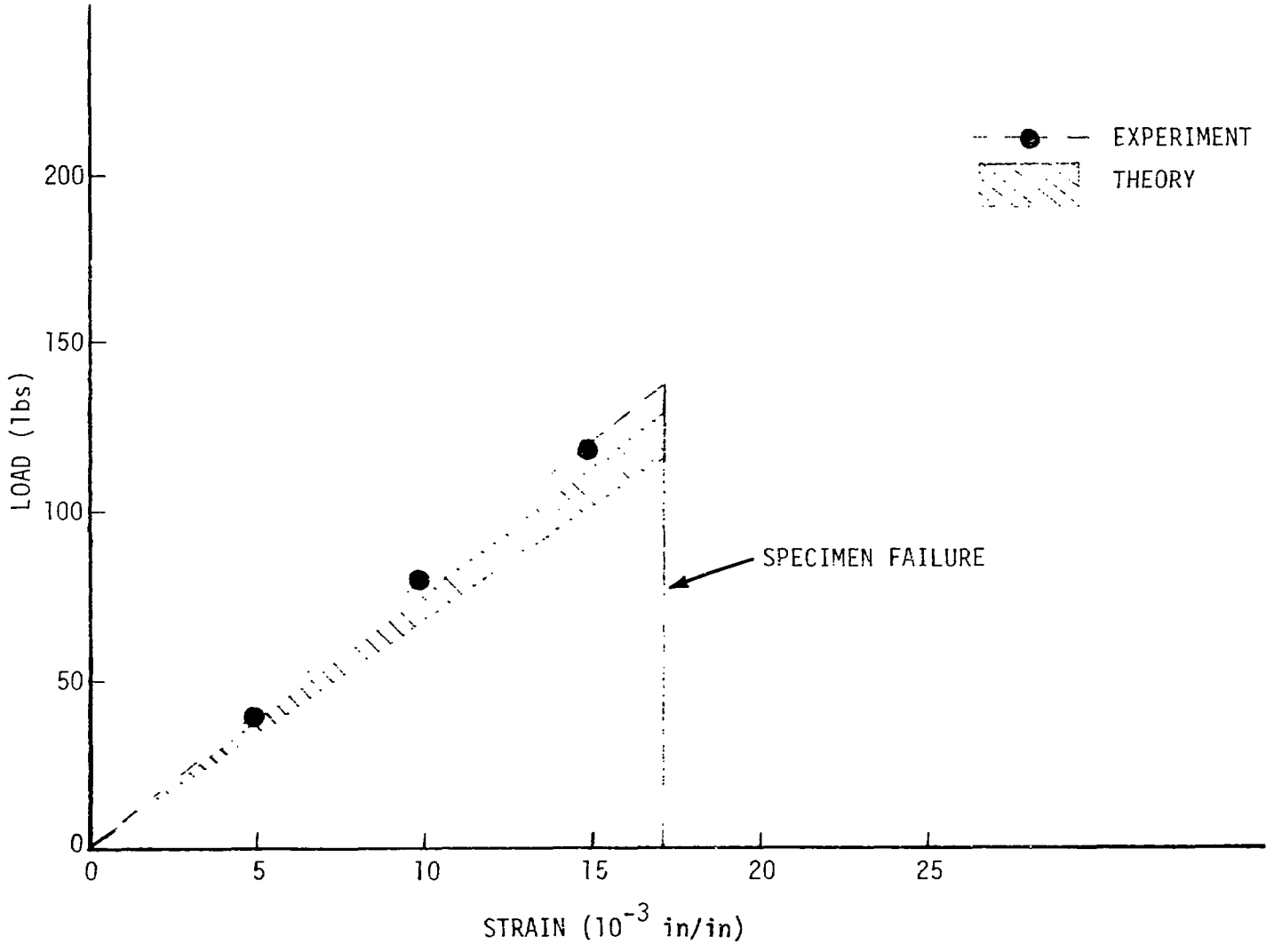

Figure 41. Comparison of Theoretical and Experimental Results for Strain-Gaged Graphite Epoxy $[\pm 45/0/90]_{2S}$ Specimen.

5.0 QUARTZ POLYIMIDE TEST RESULTS

Results of three point bend tests on F178/581 virgin quartz polyimide material and on material which was tested in the Thermal Flash Facility are presented in this section.

Figures 42, 43 and 44 summarize room temperature test results for ultimate flexural strength, flexural modulus and energy to peak load, respectively, as a function of strain rate for the warp and fill directions. Ultimate flexural strength and energy to peak load increased with strain rate in both the warp and fill directions. Experimental results indicate slightly more strength and energy absorption capability in the warp direction than in the fill direction. No strain rate effects were apparent for the flexural modulus except at the highest strain rate where the flexural modulus in the warp direction increased 22% over its quasistatic value. The next six Figures, 45 through 50, summarize the results of elevated temperature tests on warp and fill specimens at both quasistatic and dynamic loading rates. These test results indicate a decrease in flexural strength, flexural modulus and energy absorption capability with increasing temperature both quasistatically and dynamically. The tendency for the flexural strength and flexural modulus of quartz polyimide to decrease with temperature is also evident from Table 13, where experimentally obtained properties are compared to the properties supplied by Hexcel Aerospace. It can be seen that the experimental property values exhibit a sharper decline with temperature than the Hexcel values.

Two 4.0" x 4.5" flats of quartz polyimide were exposed in the AFML Thermal Flash Facility. Prior to testing one surface of each flat was coated with a .020 inch thick sheet of cork silicone, a proposed thermal protective substance. The cure temperature of the quartz polyimide was approximately 475°. One flat, E3, was exposed at a temperature less than the cure temperature. A thermocouple measurement on the exposed

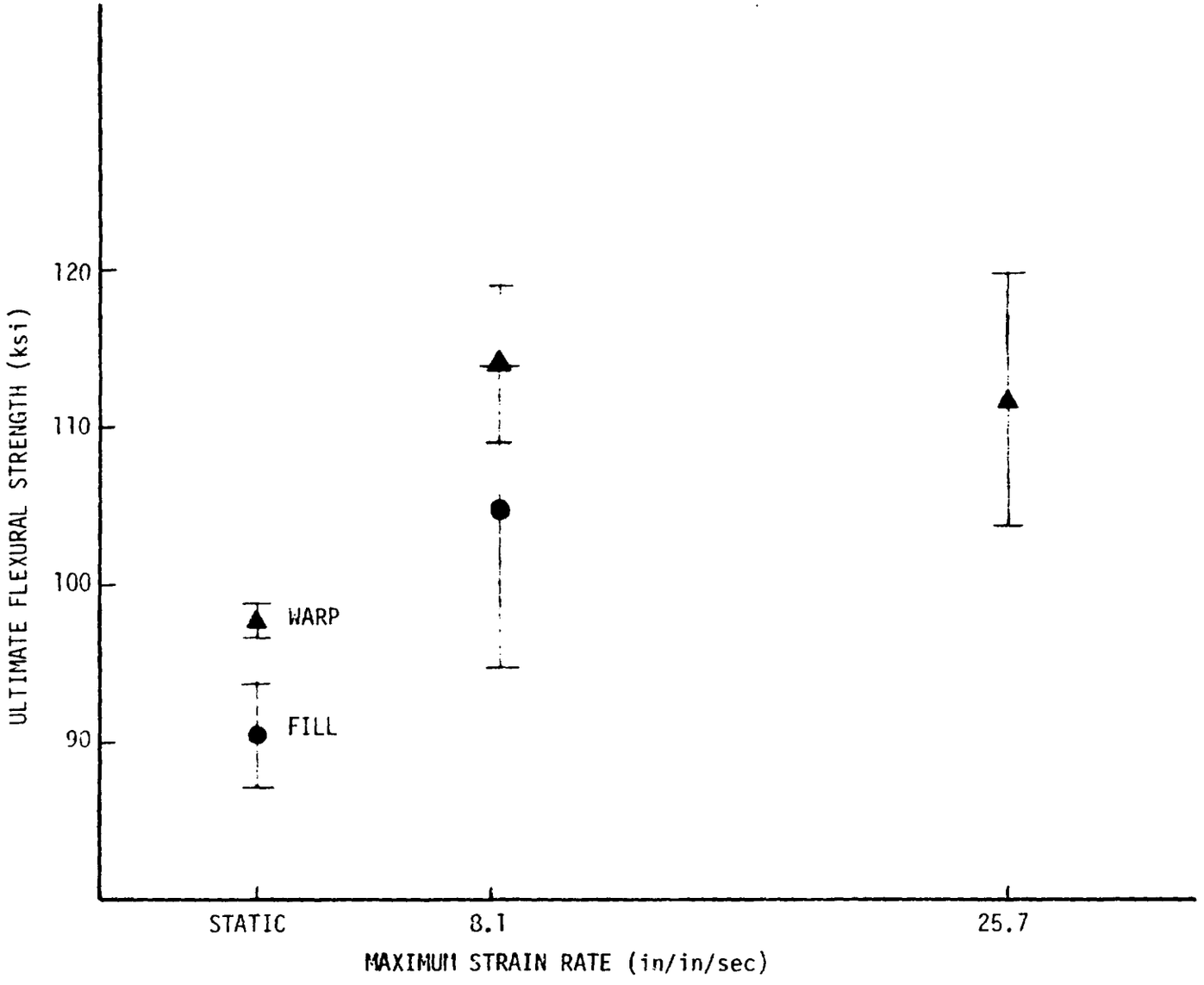

Figure 42. Ultimate Flexural Strength vs. Strain Rate-Quartz Polyimide, Room Temperature.

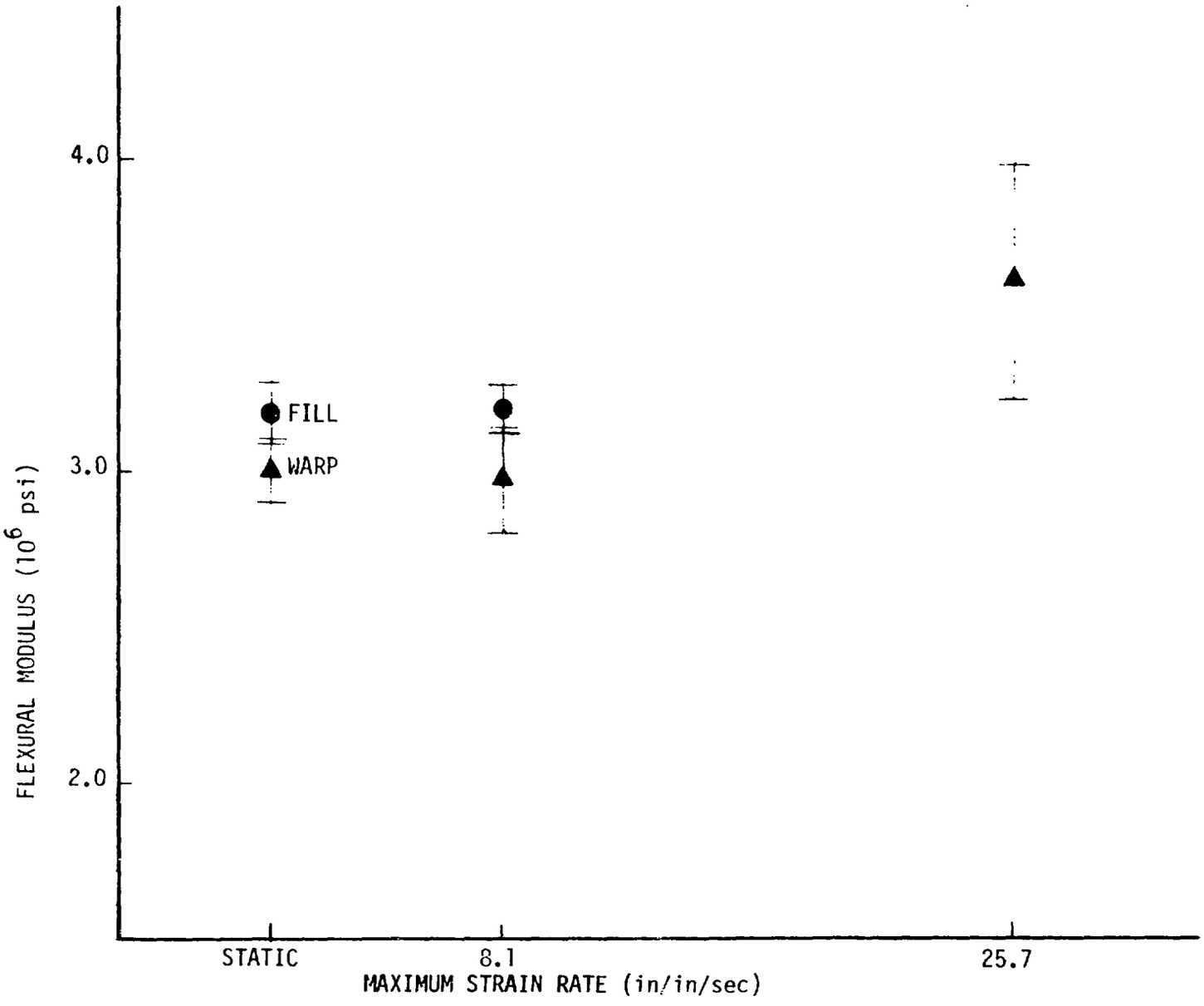

Figure 43. Flexural Modulus vs. Strain rate-Quartz Polyimide, Room Temperature.

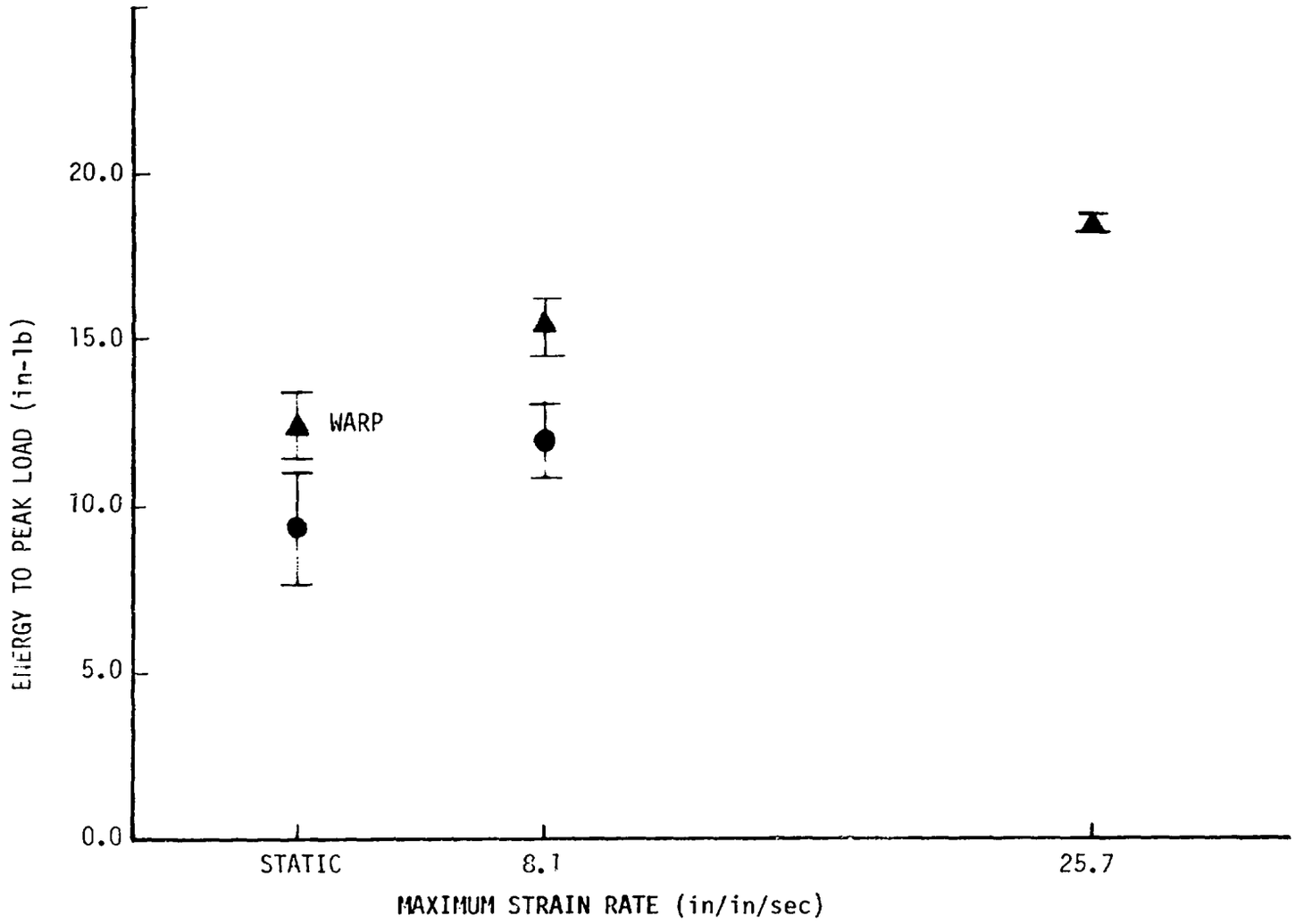

Figure 44. Energy to Peak Load vs. [illegible] for Room Temperature Quartz Polyimide Tests.

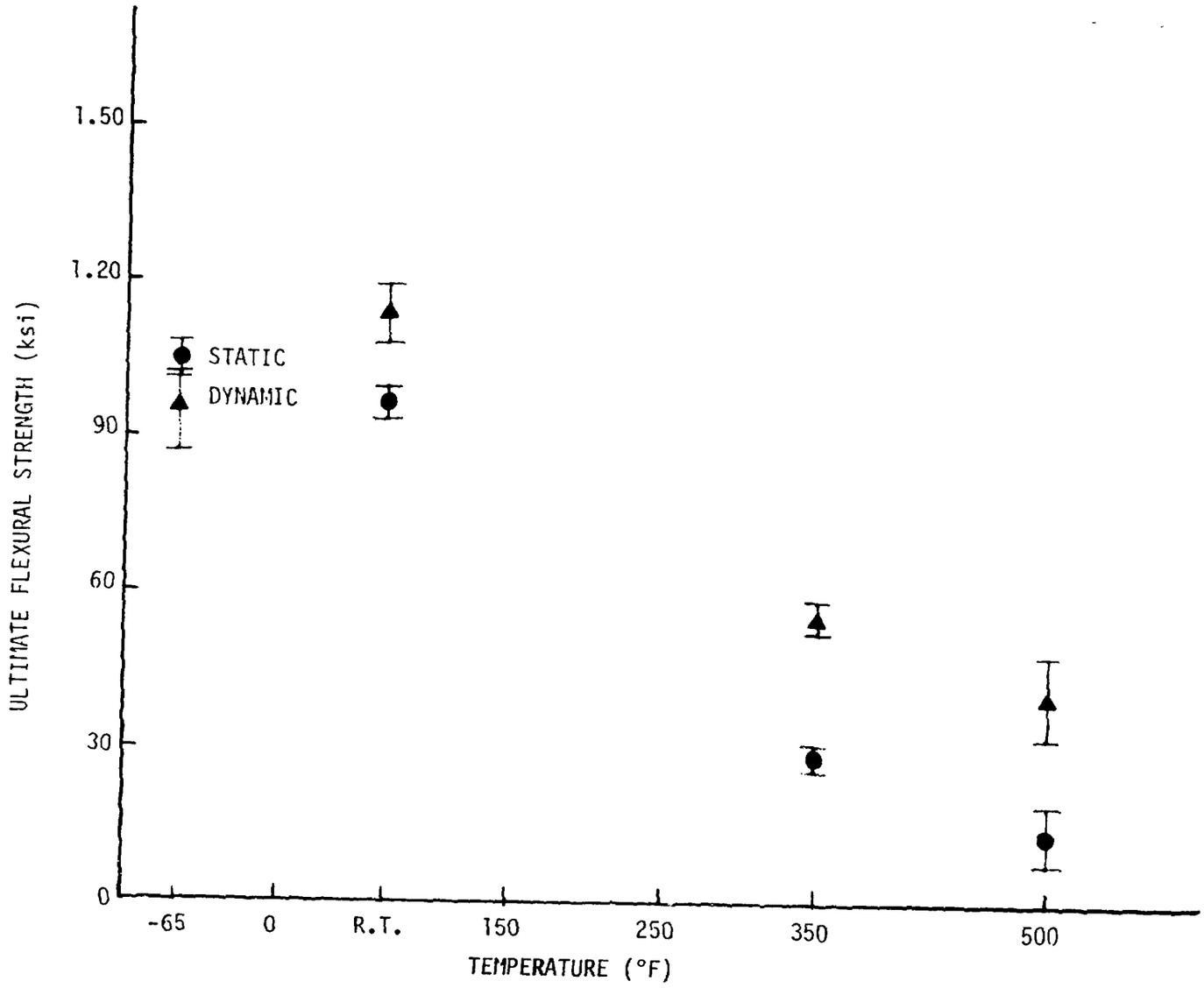

Figure 45. Ultimate Flexural Strength vs. Temperature-Quartz Polyimide Warp Direction.

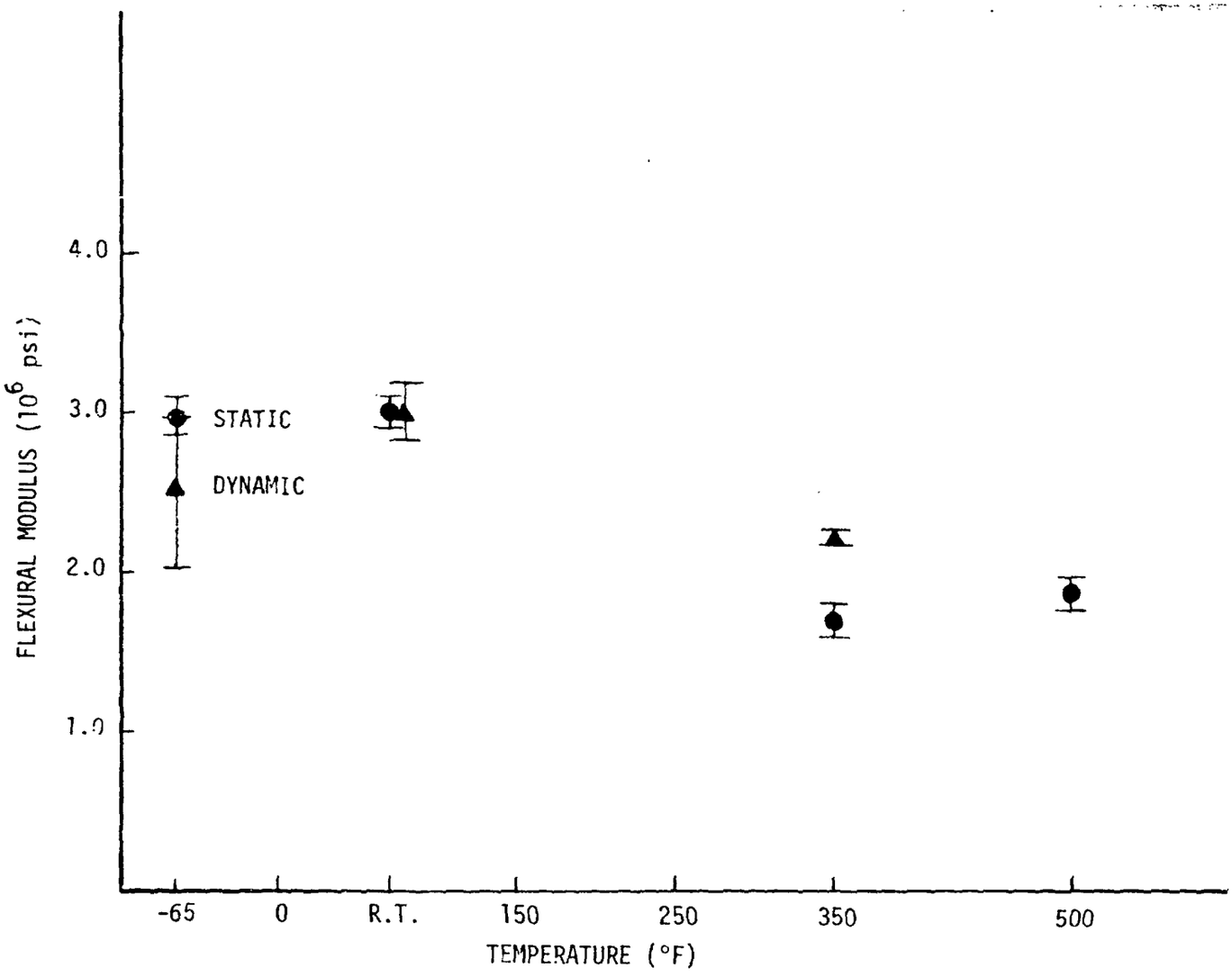

Figure 46. Flexural Modulus vs. Temperature-Quartz Polyimide, Warp Direction.

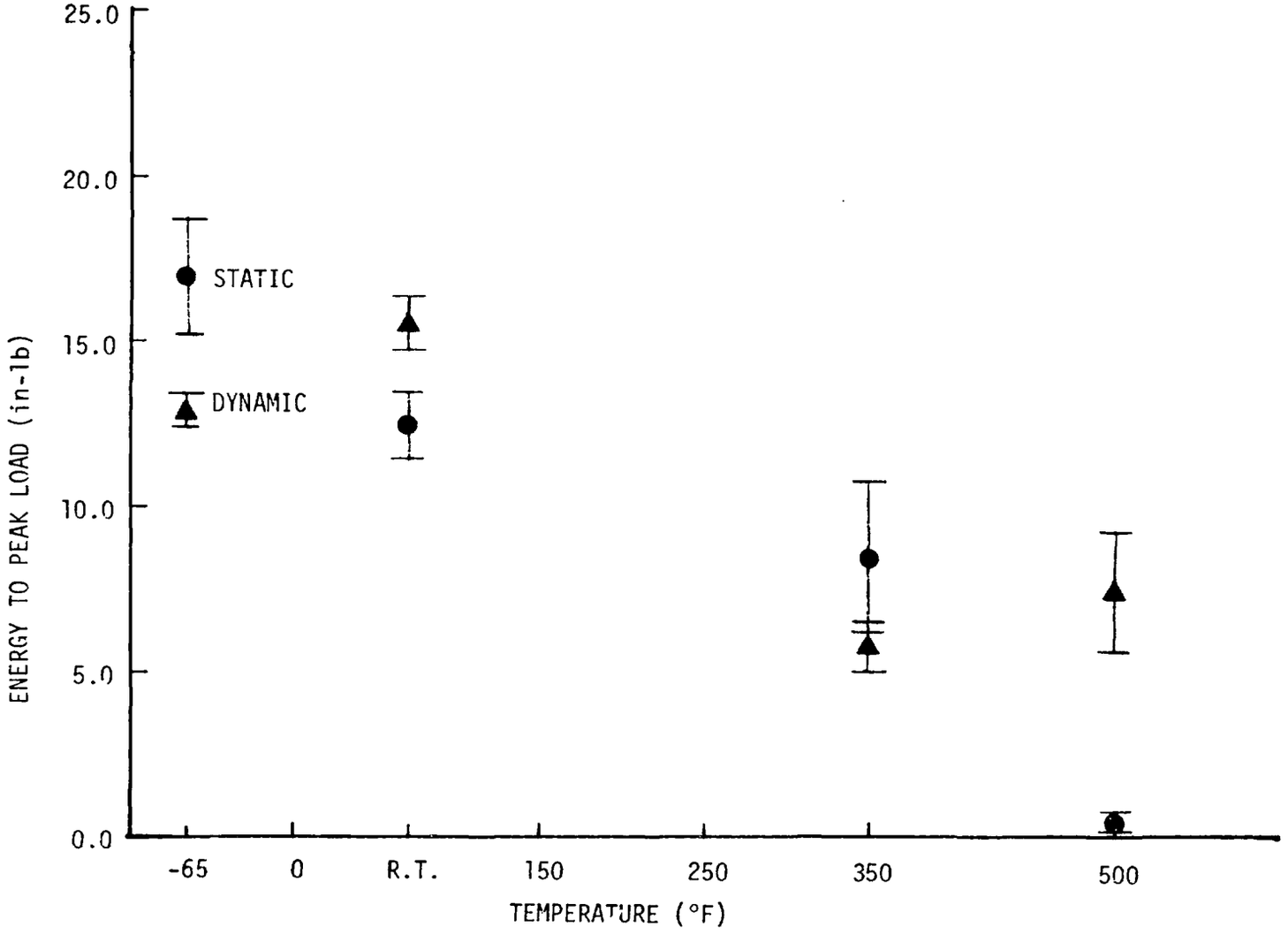

Figure 47. Energy to Peak Load vs. Temperature for Quartz Polyimide, Warp Direction.

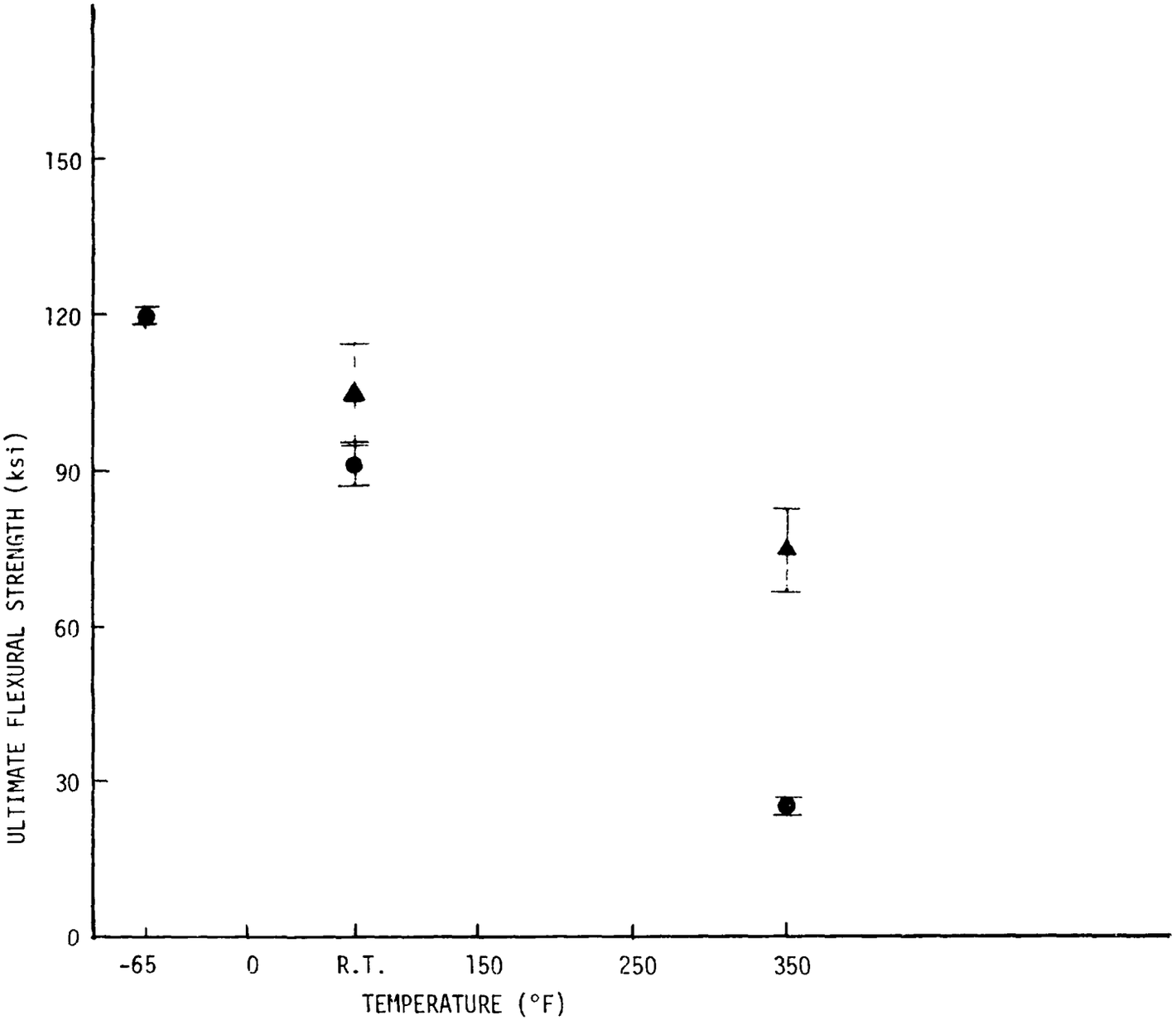

Figure 48. Ultimate Flexural Strength vs. Temperature-Quartz Polyimide-Fill Direction.

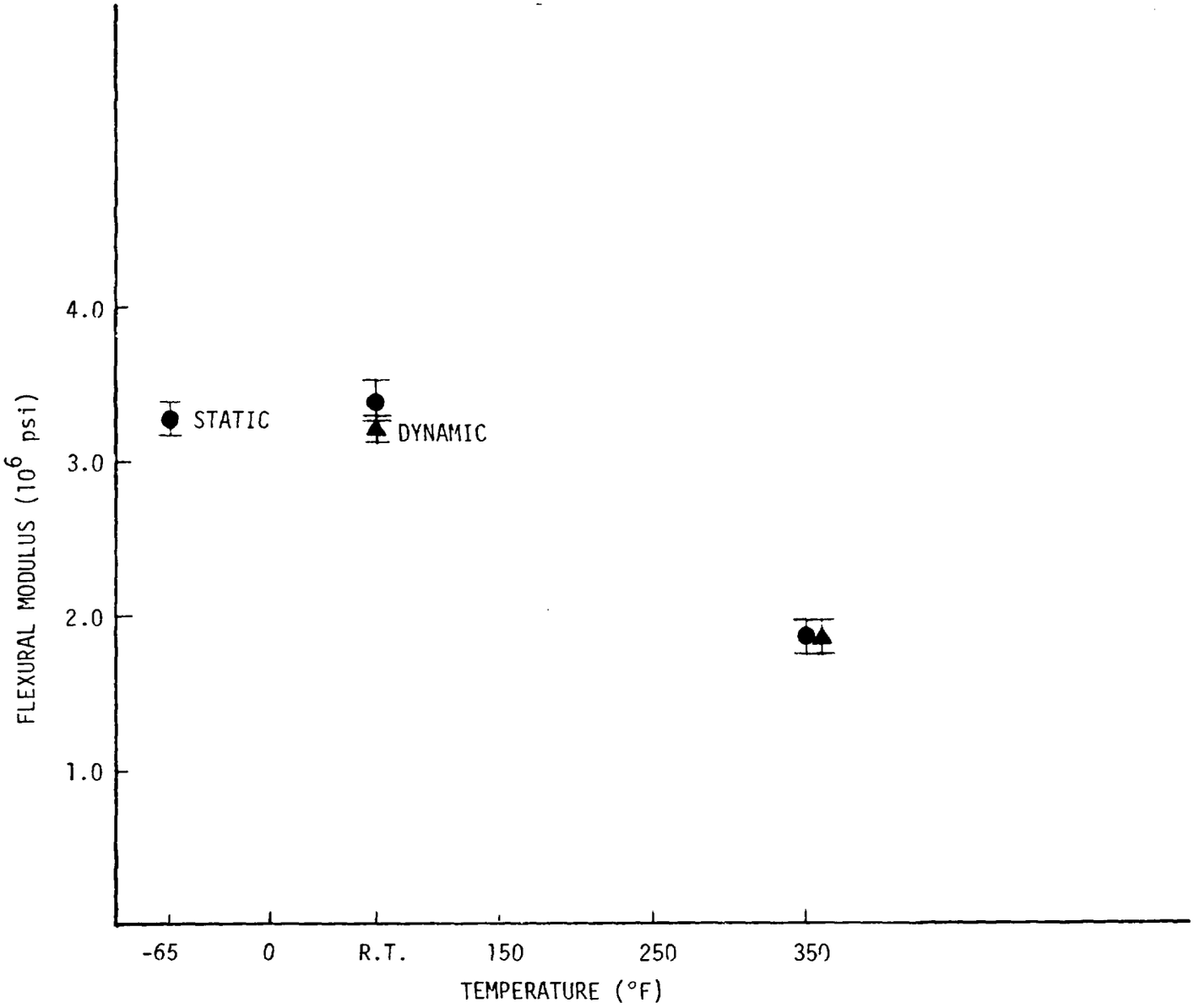

Figure 49. Flexural Modulus vs. Temperature-Quartz Polyimide, Fill Direction.

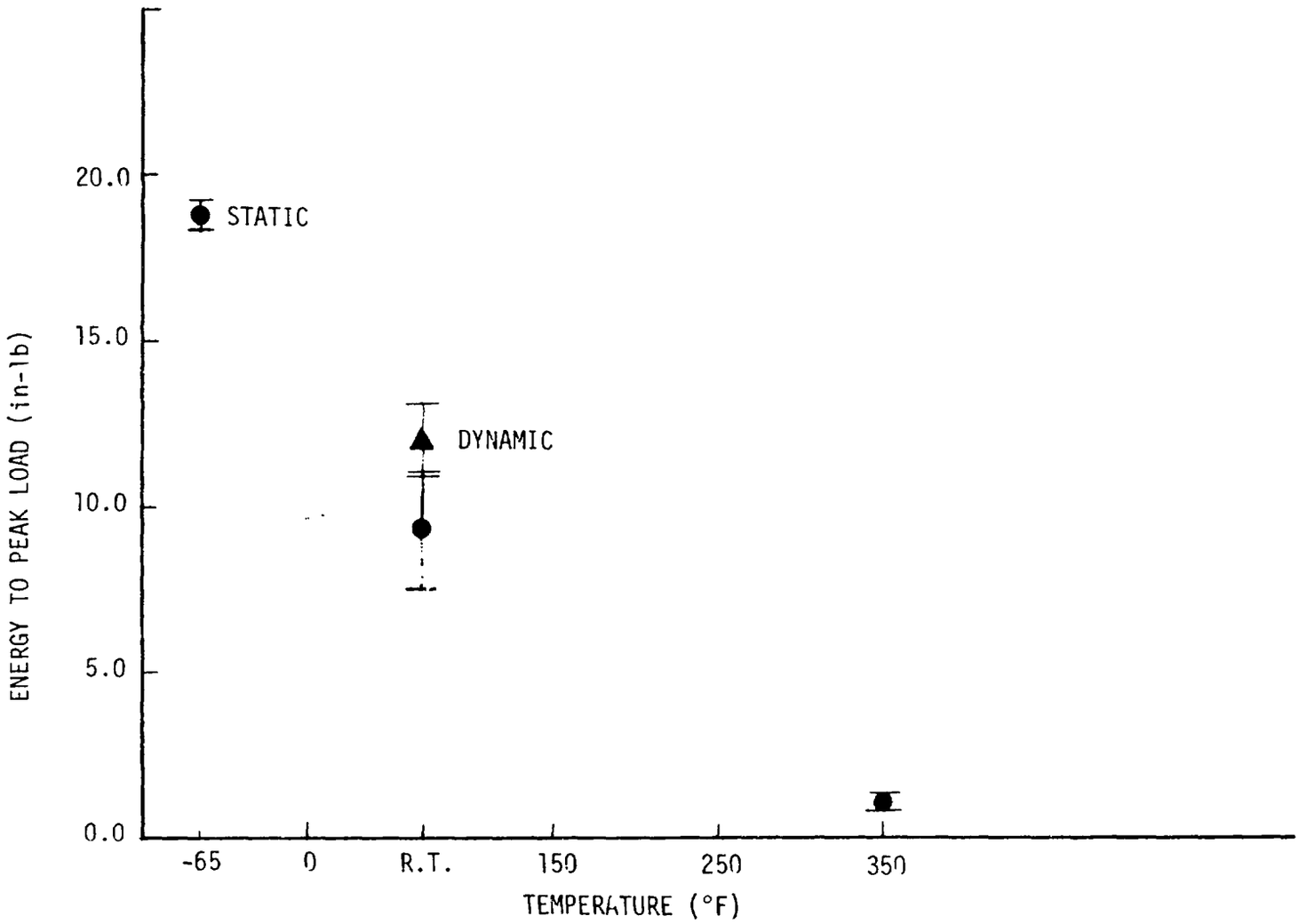

Figure 50. Energy to Peak Load vs. Temperature for Quartz Polyimide, Fill Direction.

Table 13. Properties of Quartz Polyimide, Warp Direction

	Hexcel Aerospace			Experimental Static			Experimental Dynamic		
	R.T.	350°F*	500°F*	R.T.	350°F	500°F	RT	350°F	500°F
Flexural Strength (10^3 psi)	85.0	65.0	56.0	97.6±3	281±1.4	13.7±4	114±5	55.3±2.2	40.6±8
Flexural Modulus (10^6 psi)	3.6	3.2	3.1	3.0±1	1.7±.1	1.9±.1	2.97±.2	2.2±.02	N.A.

*Specimens maintained at temperature for 1/2 hour prior to testing

side indicated a maximum temperature of 650°F. Thermocouple measurements on the rear surface indicated an average temperature of 318°F. Thermocouple temperature data for specimen E4 which was to have been subjected to a temperature above cure temperature have not yet been received. Three point bend specimens were cut from each flat and most of the thermal protective coating was removed.

One region of specimen E3 exhibited a severe delamination between layers of quartz fabric, not between the quartz polyimide and the cork bond as might be expected. No such delamination occurred on specimen E4 which should have experienced a higher thermal gradient than specimen E3. This leads one to question the integrity of the resin in the delaminated region of E3 and to speculate that a fabrication defect might have been responsible for the delamination. No specimens from the delaminated region were tested in the three point bend configuration.

The results of testing degraded specimens from flats E3 and E4 are compared to virgin specimen results in Table 14. Quasistatically there were no differences in ultimate flexural strength and flexural modulus values for the virgin and degraded material. However, the energy to peak load is higher for the degraded material than for the virgin material. Dynamically the flexural strength and energy to peak load were higher for the degraded material than the virgin while there was no significant difference in modulus. Property differences between specimens E3 and E4 were apparent only in the energy to peak load. Specimen E4, which was exposed at the higher temperature, absorbed less energy than E3.

Table 14. Comparison of Virgin and Thermal Flash Specimen Test Results for Quartz Polyimide

$\dot{\varepsilon}$	Specimen	Ultimate Flexural Strength (10^3psi)	Energy to Peak Load (in lb.)	Flexural Modulus (10^6psi)
Static	Virgin	97.6 ± 3.1	12.4 ± 1.0	3.00 ± .1
Static	E3 - UCSI	97.4 ± 1.1	16 5 ± 1.1	2.9 ± .2
Static	E3 - CSI	102.9 ± 2.1	16.8 ± .4	2.4 ± .3
Static	E4 - UCSI	98.9 ± .76	14.0 ± 1.1	2.72 ± .75
Static	E4 - CSI	99.3 ± 2.7	14.6 ± .5	2.7 ± .02
Dynamic	Virgin	114.0 ± 4.8	15.5 ± .8	3.0 ± .2
Dynamic	E3 - UCSI	136.2 ± 16.5	19.8 ± 1.2	N.A.
Dynamic	E3 - CSI	125.8 ± 6.3	18.66 ± 1.6	3.2*
Dynamic	E4 - UCSI	128.7 ± 9.3	17.0 ± 1.7	3.2*
Dynamic	E4 - CSI	127.2 ± 3.83	16.9 ± 2.8	3.18*

* calculation done for one specimen only

UCSI - Uncoated side impacted

CSI - Coated side impacted

6.0 DISCUSSION OF TEST RESULTS

6.1 DYNAMIC PROPERTIES AND QUASISTATIC

The results of this program do indeed show that these materials are strain rate sensitive, and that such sensitivity is a function of temperature. The intent of the program was not to demonstrate that dynamically derived material properties should be used rather than static, but that they are different and each is appropriate for assessing performance capabilities in various parts of an aircraft mission scenario. For these two materials, the use of static properties will lead to an ultra-conservative design for the dynamic overpressure environment because the material is stronger dynamically than would be indicated by quasistatic properties. This difference is most dramatic at elevated temperatures where the graphite epoxy, under dynamic loads, continues to act almost as if at room temperature. While the quasistatic level results in lower strengths at elevated temperatures, it also shows a change in damage mode from a tensile side fracture to a compressive side shear buckling failure as shown in Figure 51. At the same temperatures, the high strain rate test samples continued to fail on the tension side of the specimen. Again, this does not say that one set of properties or the other is superior. The only intent is to demonstrate that the results can be substantially different and that whichever set of properties is used must be chosen in light of the system requirements and constraints for the conditions of interest.

6.2 CORRELATIONS

At the beginning of the program, it was intended to perform a limited correlation by using both dynamically and quasistatically derived data as inputs to a code such as NOVA/DEPROP and also to an orthotropic model in place of DEPROP to show the differences in predictions, both in the same material model and in two different models. As the

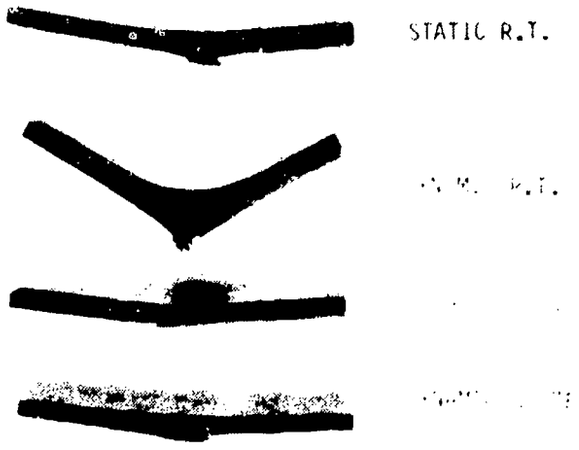

AS/3501-6
$[\pm 45/0/90]_{2S}$

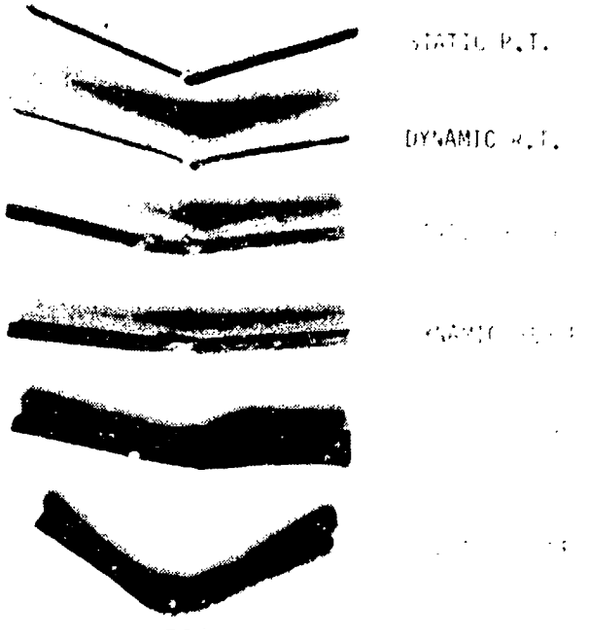

F178/581
QUARTZ POLYIMIDE

Figure 51. Failure Modes of 3 Point Bend Specimens

state of the art survey and assessment progressed, however, it became evident that such an effort was undesirable. There are any number of analytic correlation studies that have been performed to show that using dynamic properties can make a difference, or that using quasistatic properties under assumptions of various boundary conditions can make a difference. The test program showed that the dynamic properties are different than the quasistatic in ultimate strengths, energy absorbed to fracture and modulus, all of which implies that using dynamic and quasistatically derived properties in the same model will result in different response predictions for a structural component such as a panel. But, without experimental data to correlate with, such as a blast loaded panel, the different predictions only confirm what has been known all along - there are different answers for different inputs. To select which approach is appropriate requires additional structural response data, and then an application of Occam's razor.

6.3 VALIDITY OF STATIC FIELD ASSUMPTIONS

The four samples with strain gages were tested to investigate the sample response independent of the tup strain gage measured load-time trace. The assumption in the test is that action-reaction fundamentals apply, so that whatever load the tup experiences, the sample experiences. Then by comparing beam vibration frequencies with the test frequency or duration, it is possible to determine that the static field beam displacement equation is most likely to describe the maximum outer fiber strain that the sample experiences. As has been seen, the strain gage readings on both the specimen and the tup are in good agreement as to linearity. The conclusion is that the tup and the sample remain in contact during the impact event. Further, from the correlation it can be seen that the agreement between measured and calculated strain is in agreement. There were two tests that yielded questionable data. One was for a sample that was hit off center relative to the strain gage. While in principle it is possible to relate the measured off-center strains to fracture area strains, in practice this is difficult due to the finite size of the

gage and the fracture region. The other questionable data trace had an anomaly on the load-time record. At about the midway point in deflection there appears to be a slope change recorded by both the tup and sample strain gages. There is no explanation for this behavior at this time. In general, however, it is possible to state that the strain gage instrumented samples validate using the static displacement equations for data reduction purposes to calculate maximum strain, strain rates and moduli.

6.4 DESIGN IMPLICATIONS

One of the questions originally posed was that since dynamic properties are generally different from static or quasistatic, what results could occur in performing hardness assessments, or in designing hardened aircraft, if dynamic properties were to be used rather than static or quasistatic? There are three possible outcomes of a dynamic test, of course, relative to static. One is that the results are the same. This result, depending upon the strain rate range, would generally hold for metals in the strain rate range investigated in this program, unless elevated temperatures are also included. Reference 7 contains an interesting plot for aluminum that shows strain rate effects that become quite pronounced at elevated temperatures. Figure 52, taken from that report, shows those data.

The results from this program also show an increase in strength with strain rate, and that at moderate strain rates, and at temperatures up to cure, these two materials are stronger than would be calculated using quasistatic properties. For these two materials. AS/3501-6 graphite epoxy and F178/581 quartz polyimide, the main impact of the dynamic properties will be in establishing failure criteria. Both maximum flexural strength and energy to peak load increased with strain rate, and significantly so at elevated temperatures. The implication is that the materials can absorb more punishment under high strain rate loadings than would

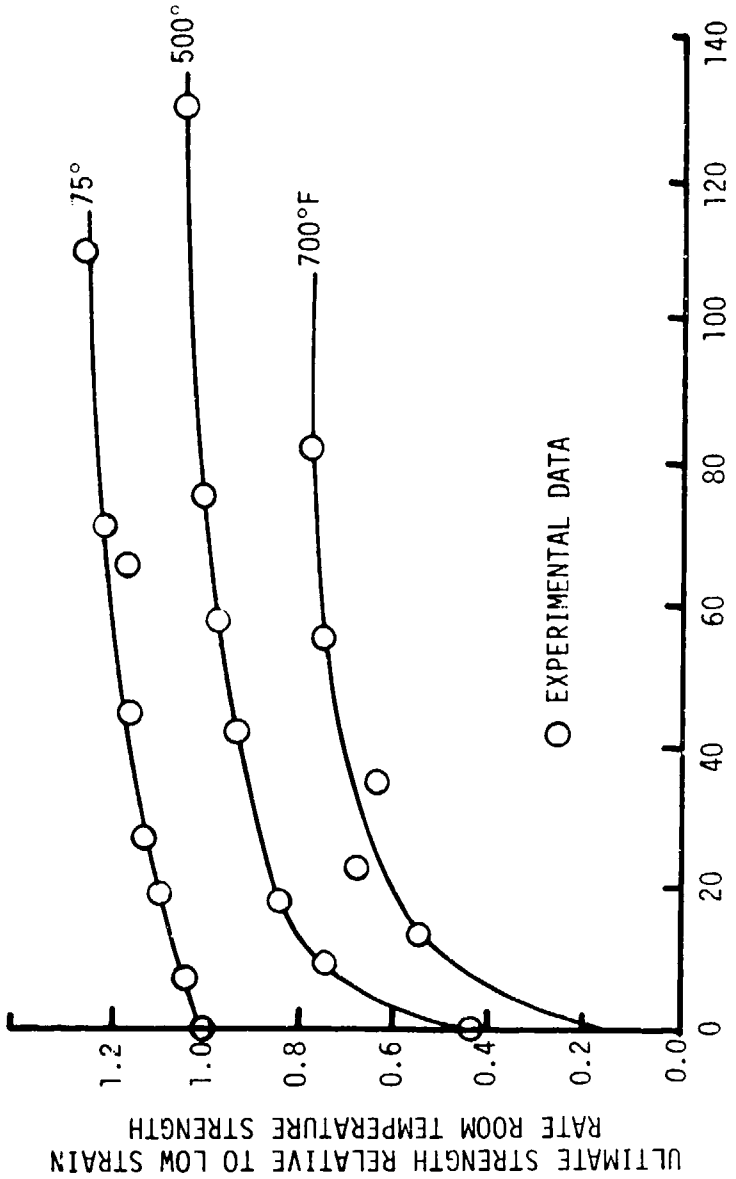

Figure 52. Effect of Strain Rate on Ultimate Strength of Aluminum Alloy 6061-T6.

be predicted based upon quasistatic properties. For example, in the preceding program[1], the potential effects of dynamic properties on aircraft weights were studied. For a bending stress design criterion, the allowable static stress can be expressed as

$$\sigma_{s_{all}} = f \text{ (geometry)} \frac{P_s}{t_s^2}$$

where P_s = static load and t_s = thickness. Similarly, under dynamic loading conditions

$$\sigma_{all} = F \text{ (geometry)} \frac{kP_o}{t_d^2}$$

where P is the dynamic overpressure, and k is the dynamic amplification factor. The structural weight is

$$W = \rho A t$$

where ρ is the material density, A is surface area and t is thickness. Combining these three equations yields

$$\frac{W_d}{W_s} = \left(\frac{kP_o}{P_s}\right)^{1/2} \cdot \left(\frac{\sigma_d}{\sigma_s}\right)^{-1/2}$$

which can be plotted as shown in Figure 53. For overpressure loadings and conditions such as would be experienced by an aircraft in a nuclear burst environment, a load ratio on the order of 1.5 would be reasonable. With this load ratio, $W_d/W_s = 1.22$ when $\sigma_{d_{all}}/\sigma_{s_{all}} = 1$, as shown by (1) in the figure. Therefore by assuming the material has the same allowable stress under dynamic and static load conditions, a 22% weight penalty must be paid to survive the dynamic encounter environment due

to the amplification. If the material was weaker under dynamic loading due to a change in material fracture mode for example, such that σ_d/σ_s decreased to less than 1, an even greater weight penalty results. In this program, the materials were always stronger dynamically so $\sigma_{d_{all}}/\sigma_{s_{all}}$ is always greater than 1. For the $[\pm 45/0/90]_{2s}$ graphite epoxy at room temperature, $\sigma_d/\sigma_s = 1.2$. The intersection with the load ratio curve is shown as (2). At this point, the weight ratio is 1.12, or a 12% weight penalty. If the design were based upon quasistatic properties ($\sigma_d = \sigma_s$), a minimum 22% weight penalty would be paid to survive the environment. By using dynamic properties only a 12% weight penalty had to be paid. This 10% savings is then the cost benefit, in this example, for using dynamic properties data.

The elevated temperature properties provide an even more striking example. At 350°F, the resin cure temperature, $\sigma_d/\sigma_s = 1.5$ shown at point (3). It can be seen that $W_d/W_s = 1$; the material strength under dynamic loads at elevated temperature compensates for the load ratio amplification, which results in a 22% weight savings over using the elevated temperature quasistatic properties. In principle, whatever properties are required for design can be obtained at the correct loading rate to determine if a weight penalty actually needs to be paid for survival in hostile environments.*

*Reference 11 documents tests that were performed to acquire static and dynamic tests on several composites, including a CE-9006/GY70 graphite epoxy. For that material, $\sigma_{s_{all}} = 96$ ksi and $\sigma_{d_{all}} = 70$ ksi, so $\sigma_d/\sigma_s = .78$. This means that $W_d/W_s = 1.39$, i.e., a 17% greater penalty than for $\sigma_d/\sigma_s = 1$. In this case, use of quasistatic properties is non-conservative. Under dynamic load conditions, the design safety margin would be less than expected.

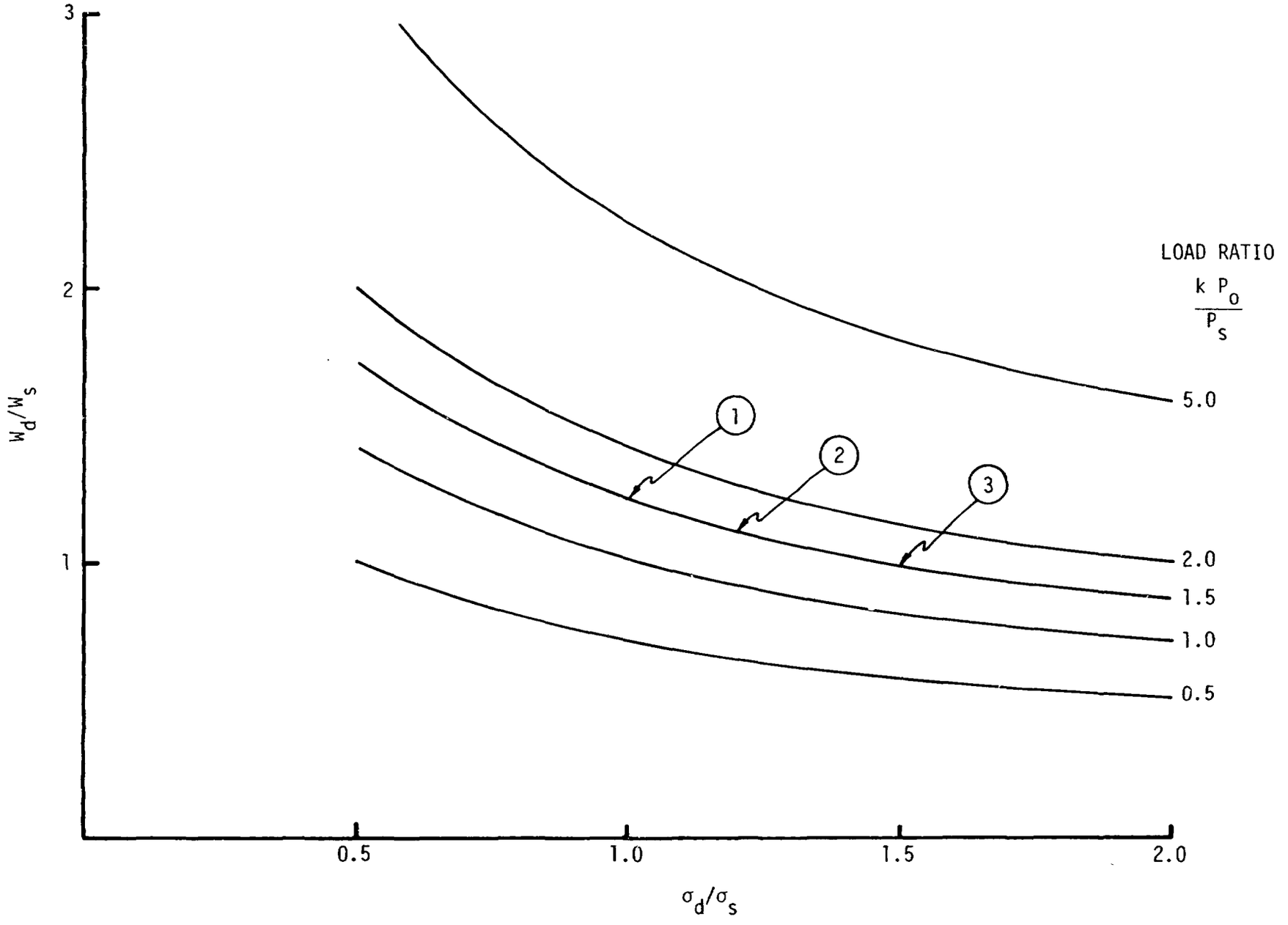

Figure 53. Dynamic and Static Weight Ratio vs. Flexural Strength Ratio

7.0 CONCLUSIONS AND RECOMMENDATIONS

7.1 CONCLUSIONS

Based upon the studies performed in this program, the following are the more significant results:

1. The AS/3501-6 graphite epoxy and F178/581 quartz polyimide materials are strain rate sensitive over the range of operational temperatures.

2. The dynamically obtained strengths indicate that these two materials are harder in a dynamic overpressure environment than would be predicted based upon quasistatically generated properties data.

3. There were no fatigue effects found after 10^6 bend cycles at 20% ultimate load on the graphite epoxy.

4. The samples exposed in the AFML Thermal Flash Facility, and subsequently tested dynamically at room temperature, showed no reduction in strength or modulus.

5. The static field displacement analysis used for data reduction to obtain dynamic modulus and strain rates is valid.

6. Reliable hardness assessments of composite aircraft will necessarily be more dependent upon tests conducted at the appropriate loading conditions, and on analyses utilizing material properties based upon consideration of these loading conditions, than has historically been the case. The responses of composite materials under hostile environment loadings are not yet fully understood, and unexpected responses leading to system failure will be the price for incomplete considerations of pertinent variables such as strain rates and

heating rates.

7. The current capability for performing hardness assessments on aircraft containing substantial amounts of composite material is not clear. There have been an insufficient number of studies to indicate whether the test or analytic techniques are adequate to determine aircraft response in various environments.

7.2 RECOMMENDATIONS

There are two recommendations that arise as a result of having performed this program.

1. Further material characterization should be undertaken on a broader range of composite materials as used in aircraft. This is especially appropriate if both strategic and tactical scenarios are included. This implies consideration of all nuclear generated environments, not only blast and thermal.

2. Correlation studies need to be initiated based upon a careful consideration of types and sequence of environments. This should include tests on structures as large as practical using current composite material design technology, and corresponding analyses, including orthotropic material considerations. The structures tested should account for unique composite aircraft design practices so that appropriate geometries are used.

REFERENCES

1. Globus, R., Green, J., Parisse, R., "Vulnerability Assessment of Non-Metallic Aircraft", Final Report, DNA 4151, Effects Technology, Incorporated, 15 June 1976.

2. Borgart, Peter, "The Vulnerability of the Manned Airborne Weapon System; Part 2: Probability of a Kill", International Defense Review, 5/1977, pp. 860-866.

3. AFWL-TR-74-91, KC-135A Nuclear Hardness Study, April 1974.

4. DNA 2048H-2, Handbook for Analysis of Nuclear Weapon Effects on Aircraft, Vol. 1, 18 March 1976.

5. Spring, R., et al, Structural Response to Simulated Nuclear Overpressure: A Test Program for Evaluating Present and Future Analytical Techniques, Draft Final, February 1977 (no DNA report number assigned at time.)

6. Private communication with E. Criscione at Kaman Avidyne.

7. Wilson, D. M., "A Summary of Methods for Computing the Degradation of Structural Elements Due to the Thermal and Thermal-Blast Effect of Nuclear Weapons", NSWC/WOL/TR 75-134, 26 March 1976, pp. A1-A14.

8. Whitney, J. M., Browning, C. E., and Mair, A., "Analysis of the Flexure Test for Laminated Composite Materials", in Composite Materials: Testing and Design (Third Conference), ASTM STP 546, 1974.

9. Tsai, S.W., "A Test Method for the Determination of Shear Modulus and Shear Strength," AFML-TR-66-372.

10. Waddoups, M. E., Eisenmann, J. R. and Kaminski, B. E., "Macroscopic Fracture Mechanics of Advanced Composite Materials", Journal of Composite Materials, Vol. 5, October, 1971.

11. Mallick, P. K. and Broutman, L. J., "Static and Impact Properties of Laminated Hybrid Composites", Journal of Testing and Evaluation, Vol. 5, No. 3, May 1977, pp. 190-200.

APPENDIX A

TEST MATRIX

Tables A-1 through A-5 show, by type of test, the experiments that were performed. The numbers in the individual matrices refer to the number of samples tested in that configuration. In all, a total of 342 tests were run.

Table A-1. Summary of Three Point Bend Tests - Total = 242

AS/350/-6 Graphite Epoxy

$\dot{\varepsilon}$ (sec^{-1}) / T'(of)	Static			2.9		
	0°	45°	90°	0°	45°	90°
R.T.	3	3	3	4		
250	6	3	3			

8-ply $[\pm 45/9/90]_s$

$\dot{\varepsilon}$ (sec^{-1}) / T'(of)	Static		2.9	
	0°	90°	0°	90°
R.T.	3	3	3	3
250	3	3	3	3

16 ply Unidirectional

$\dot{\varepsilon}$ (sec^{-1}) / T'(of)	Static			5.7		
	0°	45°	90°	0°	45°	90°
R.T.	4	6	4	6	6	3
250	3	3	3	3	3	3
350	3	3	4	3	3	3

16 ply $[\pm 45/0/90]_{2s}$

$\dot{\varepsilon}$ (sec^{-1}) / T(of)	Static		5.7		17.9
	0°	90°	0°	90°	0°
-65	3	3	3	3	
R.T.	3	3	3	3	3
250	6	3	3	3	
350	3	3	3	3	
425	3		3		

Table A-1. Summary of Three Point Bend Tests (Continued)

AS/3501-5 Graphite Epoxy

$[\pm 45/0/90]_{4S}$

$\dot{\varepsilon}$ (sec^{-1}) / T(°F)	Static		12	
	0°	90°	0°	90°
R.T.	3	3	3	3
250	3		3	
350	3		3	

F178/581 Quartz Polyimide

$\dot{\varepsilon}$ (sec^{-1}) / T(°F)	Static		18.1			
	Warp	Fill	Warp	Fill	Warp	Fill
-65	3	3	3			
R.T.	3	3	3	3	3	
350	3	3	3	4		
500	3		3			

Table A-2. Summary of Shear Plug Tests - Total = 31

AS/3501-6 Graphite Epoxy

8 PLY UNIDIRECTIONAL

$\dot{\varepsilon}$ (sec^{-1}) / T(F)	Static	Dynamic
R.T.	3	
250	3	

16 PLY UNIDIRECTIONAL

$\dot{\varepsilon}$ (sec^{-1}) / T(F)	Static	Dynamic
R.T.	3	7
250	3	

16 PLY $[\pm 45/0/90]_{2S}$

$\dot{\varepsilon}$ (sec^{-1}) / T(F)	Static	Dynamic
R.T.	3	6
250	3	

Table A-3. Summary of Fatigue Tests - Total = 9

AS/3501-6 Graphite Epoxy
16 ply $[\pm 45/0/90]_{2s}$

Deflection / Specimen	Static Failure	.04-in.	.08-in.	Break
#1	1			
#2	1			
#3		1		
#4			1	
#5			1	
#6		1	1	1
#7				1

Table A-4. Summary of Low Blow Tests - Total = 12

AS/3501-6 Graphite Epoxy
16 ply $[\pm 45/0/90]_{2s}$

Deflection / Specimen	.04-in	.08-in	Break
#1	1	1	1
#2	1		
#3		1	
#4	3	3	1

Table A-5. Summary of Three Point Bend Tests on Samples Exposed in Thermal Flash Facility - Total = 48

AS/3501-6 Graphite Epoxy
16 ply $[\pm 45/0/90]_{2s}$

F178/581
Quartz Polyimide

$\dot{\varepsilon}$ (sec^{-1}) / T (°F)	Static		5.7	
	Front[2]	Back[2]	Front[2]	Back[2]
<350	3	3	3	3
>350	3	3	3	3

$\dot{\varepsilon}$ (sec^{-1}) / T (°F)	Static		5.7	
	Front[2]	Back[2]	Front[2]	Back[2]
<475	3	3	3	3
>475	3	3	3	3

[1] Temperature of specimens in Thermal Flash Facility

[2] 'Front' denotes that non-exposed side was in tension.
'Back' denotes that exposed side was in tension.

DISTRIBUTION LIST

DEPARTMENT OF DEFENSE

Assistant to the Secretary of Defense
Atomic Energy
ATTN: Executive Assistant

Defense Documentation Center
12 cy ATTN: DD

Defense Nuclear Agency
ATTN: SPAS
ATTN: DDST
ATTN: STSP
4 cy ATTN: TITL

Field Command
Defense Nuclear Agency
ATTN: FCPR

Livermore Division, Fld. Command, DNA
Lawrence Livermore Laboratory
ATTN: FCPRL

Commandant
NATO School (SHAPE)
ATTN: U.S. Documents Officer

Under Secy. of Def. for Rsch. & Engrg.
ATTN: Strategic & Space Systems (OS)

DEPARTMENT OF ARMY

Harry Diamond Laboratories
Department of the Army
ATTN: DELHD-N-NP
ATTN: DELHD-N-P, J. Gwaltney

U.S. Army Ballistic Research Labs.
ATTN: DRXBR-BLE, W. Taylor
ATTN: DRDAR-BLV, J. Meszaros

U.S. Army Materiel Dev. & Readiness Cmd.
ATTN: DRCDE-D, L. Flynn

U.S. Army Nuclear & Chemical Agency
ATTN: Library

DEPARTMENT OF THE NAVY

Naval Material Command
ATTN: MAT 08T-22

Naval Research Laboratory
ATTN: Code 2627, Tech. Lib.

Naval Surface Weapons Center
ATTN: K. Caudle

Naval Weapons Evaluation Facility
ATTN: L. Oliver

Office of Naval Research
ATTN: Code 464

Strategic Systems Project Office
ATTN: NSP-272

DEPARTMENT OF THE AIR FORCE

Aeronautical Systems Division, AFSC
ATTN: ENFT, R. Bachman
4 cy ATTN: ENFTV, D. Ward

Air Force Materials Laboratory
ATTN: MBE, G. Schmitt

Air Force Weapons Laboratory
ATTN: DYV, A. Sharp
ATTN: SUL
ATTN: DYV, G. Campbell

Foreign Technology Division, AFSC
ATTN: PDBF, Mr. Spring

Strategic Air Command/XPFS
Department of the Air Force
ATTN: XPFS, B. Stephan

DEPARTMENT OF DEFENSE CONTRACTORS

Aerospace Corp.
ATTN: W. Barry

Avco Research & Systems Group
ATTN: J. Patrick
ATTN: P. Grady

Boeing Co.
ATTN: R. Dyrdahl
ATTN: S. Strack
ATTN: E. York

Boeing Wichita Co.
ATTN: R. Syring

Calspan Corp.
ATTN: M. Dunn

Effects Technology, Inc.
ATTN: E. Bick
ATTN: R. Parisse
ATTN: R. Wengler
ATTN: P. Van Blaricum

General Dynamics Corp.
ATTN: R. Shemensky

General Electric Co.-TEMPO
Center for Advanced Studies
ATTN: DASIAC

General Research Corp.
ATTN: T. Stathacopoulos

Kaman AviDyne
Division of Kaman Sciences Corp.
ATTN: N. Hobbs
ATTN: R. Ruetenik
ATTN: E. Criscione

Kaman Sciences Corp.
ATTN: D. Sachs

DEPARTMENT OF DEFENSE CONTRACTORS (Continued)

McDonnell Douglas Corp.
ATTN: J. McGrew

Prototype Development Associates, Inc.
ATTN: C. Thacker
ATTN: J. McDonald

R & D Associates
ATTN: C. MacDonald
ATTN: J. Carpenter
ATTN: F. Field

Rockwell International Corp.
ATTN: R. Sparling

DEPARTMENT OF DEFENSE CONTRACTORS (Continued)

Sandia Laboratories
ATTN: Doc. Con. for A. Lieber

Science Applications, Inc.
ATTN: D. Hove

SRI International
ATTN: G. Abrahamson